ABSTRACT

Adaptive Methods for the Helmholtz Equation with Discontinuous Coefficients at an Interface

James W. Rogers, Jr., Ph.D.

Advisor: Qin Sheng, Ph.D.

In this dissertation, we explore highly efficient and accurate finite difference methods for the numerical solution of variable coefficient partial differential equations arising in electromagnetic wave applications. We are particularly interested in the Helmholtz equation due to its importance in laser beam propagation simulations. The single lens environments we consider involve physical domains with subregions of differing indices of refraction. Coefficient values possess jump discontinuities at the interface between subregions. We construct novel numerical solution methods that avoid computational instability and maintain high accuracy near the interface.

The first class of difference methods developed transforms the differential equation problem to a new boundary value problem for which a numerical solution can be readily computed on rectangular subregions with constant wavenumbers. The second class of numerical methods implemented combines adaptive domain transformation with coefficient smoothing to yield a boundary value problem well-suited for numerical solution on a uniform grid in the computational space. The resulting finite difference schemes do not have treat the grid points near the interface as a special case. A novel matrix analysis technique is implemented to examine the stability of these new methods. Computational verifications are carried out.

Adaptive Methods for the Helmholtz Equation with Discontinuous Coefficients at an Interface

by

James W. Rogers, Jr., B.S.

A Dissertation

Approved by the Department of Mathematics

_____

Lance L. Littlejohn, Ph.D., Chairperson

Submitted to the Graduate Faculty of
Baylor University in Partial Fulfillment of the
Requirements for the Degree
of
Doctor of Philosophy

Approved by the Dissertation Committee

_____

Qin Sheng, Ph.D., Chairperson

_____

John M. Davis, Ph.D.

_____

Johnny L. Henderson, Ph.D.

_____

Klaus Kirsten, Ph.D.

_____

Ian A. Gravagne, Ph.D.

Accepted by the Graduate School
December 2007

_____

J. Larry Lyon, Ph.D., Dean

Page bearing signatures is kept on file in the Graduate School.

TABLE OF CONTENTS

LIST OF FIGURES

ACKNOWLEDGMENTS

I would like to thank my advisor Qin Sheng for his invaluable insight and direction throughout the dissertation process, and I look forward to continuing our collaboration long into the future. I am very grateful to Johnny Henderson for the crucial support, encouragement, and excellent instruction he provided me during my time at Baylor University. I would also like to express my appreciation to Brian Raines for a unique assistantship opportunity he made available to me, to the members of my committee for their time and effort, and to all of the Baylor mathematics professors and instructors from whom I learned so much. The interaction with my fellow graduate students, especially Curtis Kunkel and Mariette Maroun, has been a valuable resource to me during my graduate studies. In addition, this work has been supported in part by research grants from Baylor University Offices as well as General Dynamics Information Technology and the U.S. Air Force.

CHAPTER ONE

Introduction

1.1 Interface Problems

Interface problems are boundary value problems where the partial differential equation has one or more coefficients that are discontinuous at some internal curve or surface, called an interface. These type of problems arise when modeling a wide variety of physical processes, such as heat conduction through layers of materials with differing thermal conductivities, magnetic imaging of tissue structures with regions of differing magnetic permeability, geophysical electromagnetic surveying, and multiphase fluid flow in petroleum or groundwater reservoirs with sediment layers of differing porosity or permeability [22, 33, 38]. The problem on which we will focus originates in the modeling of a laser beam propagating from air into and out of a single curved lens, air and lens being layers of media with differing indices of refraction.

Since many existing strategies for the numerical solution of partial differential equations were developed for equations with smooth or even constant coefficients, interface problems may pose insurmountable difficulties for conventional numerical methods. In particular, the accuracy of derivative approximations can suffer significantly if they are based on a set of points that straddle an interface, and instability can be introduced into the solution procedure if a coefficient of the equation varies too greatly between sample points in a discretization.

1.2 Paraxial Wave Optics

In order to facilitate optical wave modeling, several approximations have traditionally been employed. The global properties of axially symmetric optical systems are described in terms of *paraxial* or *Gaussian* optics, where only rays close to and making small angles with the axis of symmetry are considered [73]. The focal point of

these paraxial rays is referred to as the principle focus of the system, while deviations from the Gaussian image point are classified as abberations. The paraxial approximation is obtained by replacing the trigonometric functions sine, cosine and tangent by the first term of their Taylor expansions, *i.e.* $\sin\theta = \theta$, $\cos\theta = 1$, and $\tan\theta = \theta$. For the equation of motion of electromagnetic waves in a linear homogeneous medium, the substitution results in a wave equation approximation that is parabolic in form.

Parabolic wave equation approximations are employed in a number of applications, including acoustics, seismology, geophysical sensing, plasma physics and aerodynamics, microwave signal transmission, as well as optics [17]. Paraxial models are also used extensively in microbeam optoelectronics applications. The approximation is useful both in improving computational efficiency, and reducing the complexity of the model to selectively eliminate certain wave properties, such as reflection [4].

While the paraxial wave approximation is primarily used for modeling waves traveling at small angles to the direction of propagation of the system, several authors have proposed extending it to larger fields and apertures by using higher order differential equations, systems of differential equations, or a generalized set of extended paraxial coordinates [4, 5, 35].

1.2.1 The Helmholtz Equation

Unlike conventional optical light, radiation from lasers is approximately monochromatic, with precise phase and amplitude variations in the first-order approximation, and are thus described most accurately by Maxwell's wave equations [16]. Maxwell's wave equations are derived from Maxwell's four field equations,

$$\nabla \cdot \mathbf{E} = \frac{\rho}{\varepsilon_0}, \tag{1.1}$$

$$\nabla \cdot \mathbf{B} = 0, \tag{1.2}$$

$$\nabla \times \mathbf{E} = -\frac{\partial \mathbf{B}}{\partial t}, \tag{1.3}$$

$$\nabla \times \mathbf{B} = \mu_0 \mathbf{J} + \mu_0 \varepsilon_0 \frac{\partial \mathbf{E}}{\partial t}, \tag{1.4}$$

where $\mathbf{E}$ is the electric field, $\mathbf{B}$ is the magnetic field, $\mathbf{J}$ is the current density, ρ is the electric charge density, ε_0 is the permittivity of free space, μ_0 is the magnetic permeability of free space, $\nabla\cdot$ is the divergence operator, and $\nabla\times$ is the curl operator.

Maxwell's field equations are coupled first-order differential equations not well suited for use in boundary value problems [56]. For this, we may observe that when the first-order equations are decoupled, we obtain the wave equation, or the time-dependent vector Helmholtz equation

$$\nabla^2 E - \frac{1}{c^2}\frac{\partial^2 E}{\partial t^2} = 0,$$

where $E = E(x, y, z)$ is the electric field intensity in volts/meter,

$$\nabla^2 = \frac{\partial^2}{\partial x^2} + \frac{\partial^2}{\partial y^2} + \frac{\partial^2}{\partial z^2},$$

is the Laplacian operator, and c is the *phase velocity*, or the speed of light in a particular medium.

Monochromatic waves can be accurately described by a complex wavefunction U satisfying

$$U(x, y, z, t), = U(x, y, z) \exp(i2\pi\nu t) \tag{1.5}$$

where $|U(x, y, z)|$ and $\arg\left(U(x, y, z)\right)$ are the amplitude and phase of the wave respectively, ν is the frequency in Hz, and $U(x, y, z, t)$ satisfies the scalar wave equation

$$\nabla^2 U - \frac{1}{c^2}\frac{\partial^2 U}{\partial t^2} = 0. \tag{1.6}$$

By substituting (1.5) into (1.6), we obtain the Helmholtz equation

$$\left(\nabla^2 + k^2\right) U(x, y, z) = 0, \tag{1.7}$$

where $k = \dfrac{2\pi\nu}{c} = \dfrac{2\pi}{\lambda}$ is called the *wavenumber*. The value $\lambda = \dfrac{c}{\nu}$ is the *wavelength*.

Let $\varphi(x, y, z)$ represent the phase of the wavefunction at point (x, y, z). The surfaces of equal phase for the wavefunction, where $\varphi(x, y, z)$ is constant, are called *wavefronts*. The wavefront normal at (x, y, z) is parallel to the gradient vector $\nabla\varphi(x, y, z)$ and represents the direction at which the rate of change of the phase is maximum [57].

We consider wavefunctions with complex amplitudes described by the equation

$$U(x, y, z) = u(x, y, z) \exp(-ikz) \tag{1.8}$$

where $i = \sqrt{-1}$, the complex function $u(x, y, z)$ is called the *complex envelope*, and the z axis is taken to be in the direction of the first wavefront normal. If the variation of $u(x, y, z)$ is slow in the z-direction, then we have a wave such that the wavefront normals make small angles with z, a so-called *paraxial wave*.

We substitute (1.8) into the Helmholtz equation (1.7) and factor out $\exp(-ikz)$ to obtain

$$\nabla_T^2 u(x, y, z) - 2ik\frac{\partial u(x, y, z)}{\partial z} + \frac{\partial^2 u(x, y, z)}{\partial z^2} = 0, \tag{1.9}$$

where

$$\nabla_T^2 = \frac{\partial^2}{\partial x^2} + \frac{\partial^2}{\partial y^2}$$

is the transverse Laplacian operator.

Because $u(x, y, z)$ varies relatively slowly in the z-direction, for large wavenumbers k we can assume that within a wavelength of the propagation distance, the change in u is small compared to $|u|$ [54]. We have

$$\left|\frac{\partial^2 u}{\partial z^2}\right| \ll |k^2 u|$$

thus

$$\frac{\partial^2 u}{\partial z^2} \approx 0.$$

We obtain an approximation of (1.9)

$$\nabla_T^2 u(x, y, z) - 2ik\frac{\partial u(x, y, z)}{\partial z} = 0, \tag{1.10}$$

which is called the *slowly varying envelope approximation* of the Helmholtz equation, or simply the *paraxial Helmholtz equation* [6, 57].

Next we let

$$r = (x^2 + y^2)^{\frac{1}{2}} \geq 0, \quad \phi = \arctan \frac{y}{x}.$$

Then (1.10) can be written in polar coordinates as

$$\left(\frac{1}{r} \frac{\partial}{\partial r} + \frac{\partial^2}{\partial r^2} + \frac{1}{r^2} \frac{\partial^2}{\partial \phi^2} - 2ik \frac{\partial}{\partial z} \right) u(x, y, z) = 0, \tag{1.11}$$

Equation (1.11) is considered sufficiently accurate for laser propagation applications in multi-layer media [30, 31, 66].

In our discussions, we consider the partial differential equation (1.11) in a spherical lens environment. In the case of a cylindrically symmetric domain, we assume

$$\frac{\partial^2 u}{\partial \phi^2} \equiv 0$$

and simplify the polar paraxial equation (1.11) to yield

$$2iku_z(z, r) = u_{rr}(z, r) + \frac{1}{r} u_r(z, r). \tag{1.12}$$

Without loss of generality, we may assume that $0 \leq r \leq R_1 \ll \infty$.

1.2.2 Initial and Boundary Conditions

We employ Neumann boundary conditions

$$u_r(z, 0) = u_r(z, R_1) = 0, \quad z > 0, \tag{1.13}$$

at the bottom, $r = 0$ and top, $r = R_1$ of the rectangular domain.

For the initial solution of boundary value problem (1.12), (1.13), we use the following approximation of a Gaussian beam with point source [21]

$$u(z, r) = \frac{1}{1 + iZ} \exp \left(ikz - \frac{r^2}{\beta^2 (1 + iZ)} \right), \tag{1.14}$$

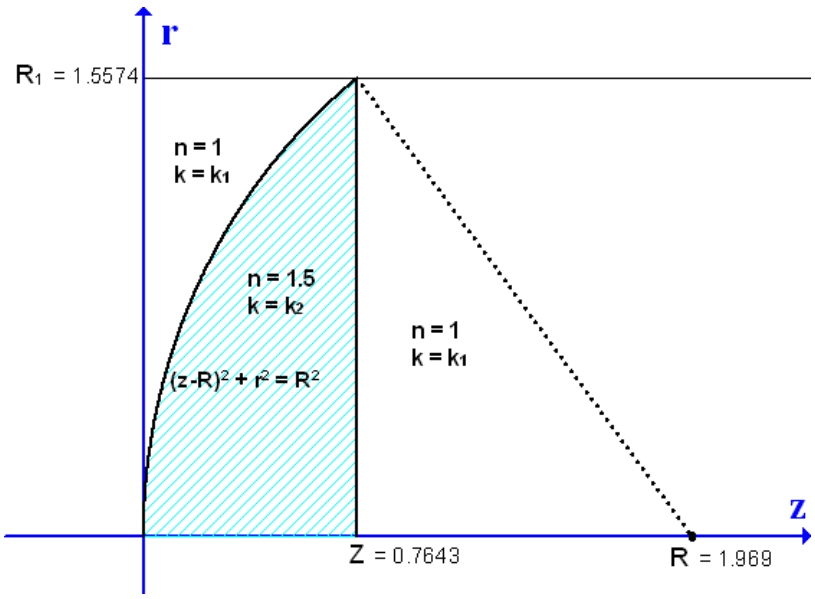

Figure 1.1. The domain.

where β_0 is the Gaussian beam width, while Z, β and A are parameters such that

$$Z = \frac{2z}{\beta^2 k}, \quad \frac{1}{\beta^2} = \frac{1}{\beta_0^2} + \frac{ik}{2z_0}, \quad A = e^{ikz_0}.$$

We also need to know the boundary conditions of the wavefunction at the interface. From Maxwell's equations and the associated constitutive relations for media, it is possible to show that as a monochromatic wave propagates through media of different refractive indices, its frequency remains the same, but we have the following relations for phase velocity c, wavelength λ and wavenumber k

$$c = \frac{c_0}{n}, \quad \lambda = \frac{\lambda_0}{n}, \quad k = \frac{2\pi}{\lambda} = \frac{2\pi n}{\lambda_0} = nk_0$$

where c_0, λ_0 and k_0 are the phase velocity, wavelength and wavenumber in a vacuum and n is the index of refraction of the medium.

For our single lens case simulations, we utilize the following high wavenumbers

$$k(z,r) = \begin{cases} k_2 = \dfrac{2\pi n_1}{\lambda} = 9.97543 \times 10^3, & \text{if } (z,r) \text{ is inside lens area,} \\ k_1 = \dfrac{2\pi n_0}{\lambda} = \dfrac{2k_1}{3} = \dfrac{2}{3} \times 9.97543 \times 10^3, & \text{otherwise,} \end{cases} \tag{1.15}$$

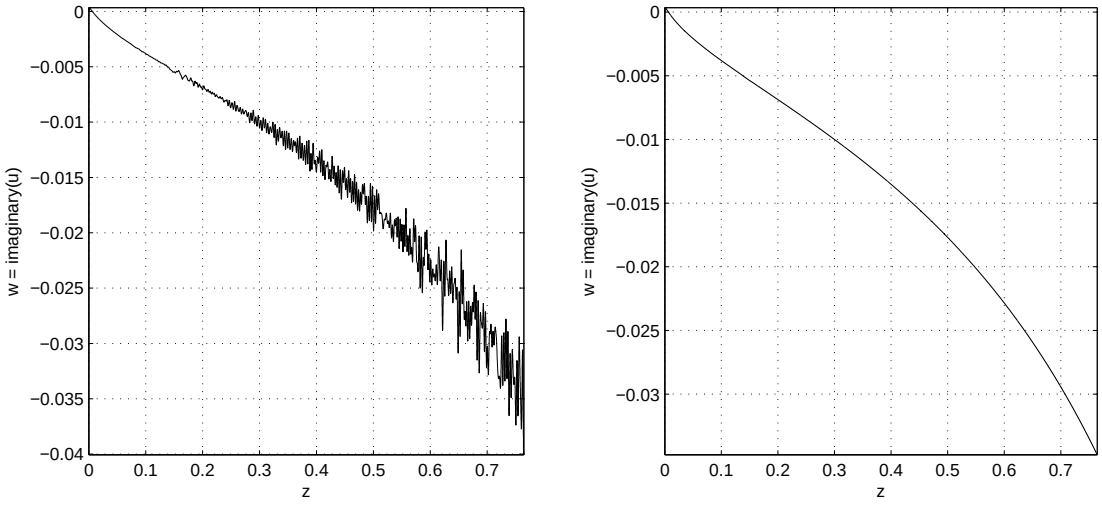

Figure 1.2: Discontinuous coefficients can cause inaccuracy and nonphysical oscillation. Here we see the mid-lens behavior of the imaginary part of a computed solution of Eq. (1.12) for the case of discontinuous and smoothed wavenumber k functions.

which is reasonably consistent with experimental laser beam wavelengths [30, 32]. Clearly, the coefficient function $k(z, r)$ is discontinuous at the lens interface. Mathematically, relation (1.15) introduces a discontinuity in the coefficient of u_z along the boundary between the different media. This adds considerable difficulty to the task of computing the numerical solution of (1.12) [41].

From Maxwell's equations we can deduce that $u(z, r)$, $u_r(z, r)$ and $u_z(z, r)$ are continuous across the curved lens boundary [56, 21]. Then examining (1.12), we can see that $u_{rr}(z, r)$ will have a jump discontinuity at the interface. These jump conditions will be discussed in detail in Section 5.1.

Relation (1.15) represents a single lens situation. We could further consider multiple lens scenarios with additional k values involved.

1.3 Adaptive Grids

There are a variety of well established techniques for the numerical solution of boundary value problems, including the widely used finite difference and finite element methods. The majority of these methods depend upon a discrete grid of points upon

which an approximate solution of the boundary value problem is computed. The grid must include a sufficient number of points in any local region of the domain to accurately represent the solution. For certain problems, especially interface problems, local regions of high variability, shocks or discontinuities will arise, requiring a very fine grid spacing. If the fine resolution necessary in these regions were to be extended over the entire domain of the problem, the amount of data storage and computational cycles required to compute a solution would be far greater than modern computing devices could provide. Practical considerations then, have driven the development of adaptive grid methods.

For the most part, adaptive grid methods fall into two main categories: local grid refinement and grid redistribution [76]. Important early work on local grid refinement was done by Berger and Oliger, who developed the Adaptive Mesh Refinement (AMR) method, a system of successively refined subgrids recursively imposed onto regions of larger, coarser grids [8, 9].

In grid redistribution, often referred to as "moving mesh" methods, the number of points in a grid is fixed, but the positions of these points in the physical space are adjusted via dynamically adaptive transformations so that more points occur in regions where greater accuracy is required. An additional set of differential equations called *mesh generators* are often solved concurrently with the main problem in order to determine efficient grid transformations [24, 39]. A moving mesh method for finite differences was developed by Dorfi and Drury [19].

We will examine the properties of both types of adaptive grid methods in more detail in later sections.

1.3.1 Uniform Cartesian Grids

We wish to employ finite difference methods to find a numerical solution to our interface problem, and we would like to compute that solution on a uniform Cartesian grid, *i.e.* a grid with uniform spacings in each spatial coordinate direction. For two-

level schemes, uniform spacing is not required in the direction of wave propagation.

The advantages of operating on a uniform grid are numerous, with the foremost advantage being the accuracy and simplicity of derivative approximations in such a domain. Examining the Taylor expansion formulas which are the basis for most derivative approximations, we find that when grid spacings are not uniform, we no longer get the cancelation of higher order terms which provides greater order of accuracy for the resulting derivative approximation formulas while using the fewest possible terms. Worse yet, standard difference formulas may not be valid approximations for higher derivatives at all when applied to a nonuniform grid [55, 58].

A uniform grid also facilitates the application of a wide array of well-developed methods, such as fast Poisson solvers and Fast Fourier Transform algorithms, which were originally formulated to use equally spaced sample points [11, 23, 48]. Further, while nonuniform schemes can reduce data array size requirements, this typically comes at the expense of computation time, as well as data space overhead which must be devoted to grid housekeeping. In addition, uniform grid schemes are often much better suited to the optimized vectorization hardware available in modern computer processors, which can provide very significant speed increases for numerical method implementations without the need for specialized programming.

1.3.2 Uniform Grid Numerical Methods

Considering the many advantages of uniform Cartesian grids, it is not surprising that several uniform grid methods have been developed for the numerical solution of partial differential equations with singular or discontinuous coefficients. In 1961, Tikhonov and Samarskii derived second order accurate finite difference approximations of elliptic equations with discontinuous coefficients using Green's function techniques [70, 72]. Mayo developed fast numerical solution methods for Laplace's and biharmonic equations with irregular domains by using integral equation formulations to define discontinuous extensions of the equations to regular, embedding domains.

The solution of the interface problem thus obtained is computed using fast Poisson solvers on a uniform grid, with correction terms applied to the points adjacent to the interface [48]. Mayo and Greenbaum further developed the technique using parallel algorithms [49]. MacKinnon and Carey, and Fornberg and Meyer-Spasche have also utilized the correction term approach to numerically solve interface problems [47, 25].

One of the most significant and widely utilized uniform grid methods for interface problems is the immersed interface method of Li and LeVeque, which is an extension of the earlier immersed boundary method of Peskin [46, 53]. The central idea of the immersed interface method is to employ a conventional finite difference scheme everywhere on a uniform grid except on "irregular" points, *i.e.* points which are adjacent to the interface. For the irregular points, modified finite difference equations are derived using the so-called *jump relations*, which are the relations of the limits of the solution, its derivatives and the coefficient functions as they approach the interface from opposite sides. These jump relations may be obtained from the partial differential equation itself, or by referring to the known behavior of the physical processes being modeled. In the case of an implicit scheme, the modified finite difference equations replace the standard finite difference equations corresponding to the irregular points in the system of equations to be solved.

Various authors have adapted and extended the immersed interface method to additional problems. Zhang applied the method to acoustic wave equations across an interface, [78] while Kreiss and Petersson recently proposed a modified version of the immersed interface method to simplify the derivation of the difference equation coefficients at irregular points for two dimensional second order wave equations [40].

While the immersed interface method retains the advantages of a uniform grid and is particularly effective at forcing the computed solution to behave exactly as we want it to near the interface, there are some drawbacks. With the modification of some of the difference equations, a system of equations may lose certain properties,

such as diagonal dominance or banded structure, becoming considerably more difficult to solve. For example, a tridiagonal system might lose that structure, and thus no longer be solvable using the simple, efficient Thomas algorithm. Perhaps the biggest disadvantage, however, from an implementation standpoint, is the fact that for each interface problem new difference equations must be derived analytically, depending upon the partial differential equation and jump conditions, as well as the properties, position and orientation of the interface. While this process produces excellent results, it is unlikely that it could ever be automated in software.

1.3.3 Goals of an Adaptive Method

We will use domain transformation to map discretization points that are nonuniform in the physical space onto a uniform grid in the computational space. A simple example of this technique is used by Shibayama et. al. [66] and is referred to by the authors as a computational space method. In the aforementioned paper, the physical coordinate space (x, z) is mapped onto coordinate space (u, z) by the mapping

$$x = \alpha \tan(u)$$

where α is a scaling constant. Here the mapping does not depend on z, the direction of propagation coordinate. In contrast, our moving mesh method will use a transverse direction transformation that is dynamically generated at each propagation step.

Our motivation is to produce a numerical method which is flexible enough to adjust to varying interface properties or jump conditions without the need to derive new difference schemes for grid points near the interface. We should not have to determine jump conditions analytically, as long as they are inherent in the partial differential equation and boundary conditions. Ideally, the method should be able to make domain transformation adjustments at a propagation step based solely on the partial differential equation and boundary conditions, the current numerical solution values, and the current dynamically generated transformation function. However, our

current study will focus on methods in which domain transformation is based on the shape of the lens domain segment, or on the location of the interface at the grid lines.

CHAPTER TWO

A Six-Point, Two-Level Finite Difference Scheme

2.1 Derivation

We consider a second-order partial differential equation defined on a domain Ω in the following general form:

$$c_4 u_{rr} + c_3 u_r + c_2 u_z + c_1 u + c_0 = 0, \tag{2.1}$$

where the coefficients $c_i,\ 0 \leq i \leq 4$, are functions of r and z, and the rectangular, two-dimensional domain

$$\Omega = \{(z, r) \mid 0 \leq r \leq R, 0 \leq z \leq Z\}$$

for constants $R > 0$ and $Z > 0$. Let $M, N \in \mathbb{Z}^+$, $h = \dfrac{R}{M}$ and $\tau = \dfrac{Z}{N}$. We define a uniform grid of points

$$\Omega_{\tau,h} = \{(mh, n\tau) \mid 0 \leq m \leq M, 0 \leq n \leq N\} \subset \Omega.$$

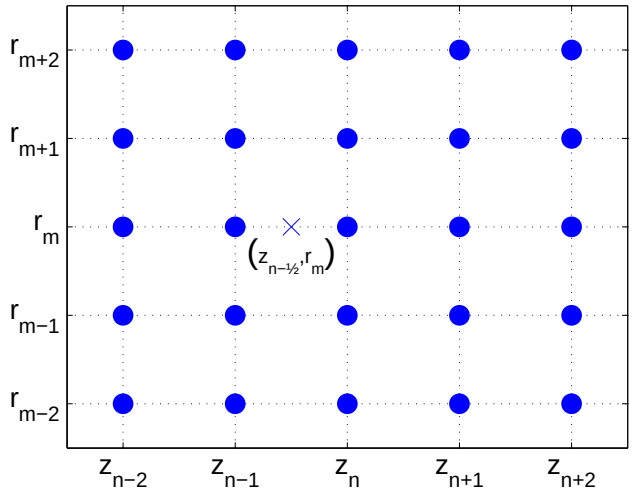

Figure 2.1: Neighborhood of reference point $\left(z_{n-\frac{1}{2}}, r_m\right)$ in a uniform (regularly spaced) grid.

Thus M, N are the number of grid points and h, τ are the discretization parameters or step sizes, in the r and z directions respectively. We will use the notation $r_m = mh$ and $z_n = n\tau$ to represent grid line positions in the r and z directions respectively. We write $z_{n-\frac{1}{2}}$ to specify the non-grid point halfway between z_{n-1} and z_n.

Definition 2.1. Points in Ω at which partial differential equations and finite difference schemes are evaluated and compared may not be in the set $\Omega_{\tau,h}$ We call such points *reference points.*

We use the following Taylor expansions to derive approximations for u_r, u_{rr}, and u_z at reference point $\left(z_{n-\frac{1}{2}}, r_m\right) = \left(\left(n-\frac{1}{2}\right)\tau, mh\right)$:

$$\begin{aligned}
u_{m+1,n} = \; & u_{m,n-\frac{1}{2}} + h\frac{\partial u}{\partial r} + \frac{\tau}{2}\frac{\partial u}{\partial z} + \frac{h^2}{2}\frac{\partial^2 u}{\partial r^2} + \frac{\tau^2}{8}\frac{\partial^2 u}{\partial z^2} + \frac{h\tau}{2}\frac{\partial^2 u}{\partial r \partial z} + \frac{h^3}{6}\frac{\partial^3 u}{\partial r^3} \\
& + \frac{h^2\tau}{4}\frac{\partial^3 u}{\partial r^2 \partial z} + \frac{h\tau^2}{8}\frac{\partial^3 u}{\partial r \partial z^2} + \frac{\tau^3}{48}\frac{\partial^3 u}{\partial z^3} + \frac{h^4}{24}\frac{\partial^4 u}{\partial r^4} + \frac{h^3\tau}{12}\frac{\partial^4 u}{\partial r^3 \partial z} \\
& + \frac{h^2\tau^2}{16}\frac{\partial^4 u}{\partial r^2 \partial z^2} + \frac{h\tau^3}{48}\frac{\partial^4 u}{\partial r \partial z^3} + \frac{\tau^4}{384}\frac{\partial^4 u}{\partial z^4} + O(\tau^5) + O\left(h\tau^4\right) \\
& + O\left(h^2\tau^3\right) + O\left(h^3\tau^2\right) + O\left(h^4\tau\right) + O\left(h^5\right), \qquad (2.2)
\end{aligned}$$

$$u_{m,n} = u_{m,n-\frac{1}{2}} + \frac{\tau}{2}\frac{\partial u}{\partial z} + \frac{\tau^2}{8}\frac{\partial^2 u}{\partial z^2} + \frac{\tau^3}{48}\frac{\partial^3 u}{\partial z^3} + \frac{\tau^4}{384}\frac{\partial^4 u}{\partial z^4} + O(\tau^5), \qquad (2.3)$$

$$\begin{aligned}
u_{m-1,n} = \; & u_{m,n-\frac{1}{2}} - h\frac{\partial u}{\partial r} + \frac{\tau}{2}\frac{\partial u}{\partial z} + \frac{h^2}{2}\frac{\partial^2 u}{\partial r^2} + \frac{\tau^2}{8}\frac{\partial^2 u}{\partial z^2} - \frac{h\tau}{2}\frac{\partial^2 u}{\partial r \partial z} - \frac{h^3}{6}\frac{\partial^3 u}{\partial r^3} \\
& + \frac{h^2\tau}{4}\frac{\partial^3 u}{\partial r^2 \partial z} - \frac{h\tau^2}{8}\frac{\partial^3 u}{\partial r \partial z^2} + \frac{\tau^3}{48}\frac{\partial^3 u}{\partial z^3} + \frac{h^4}{24}\frac{\partial^4 u}{\partial r^4} - \frac{h^3\tau}{12}\frac{\partial^4 u}{\partial r^3 \partial z} \\
& + \frac{h^2\tau^2}{16}\frac{\partial^4 u}{\partial r^2 \partial z^2} - \frac{h\tau^3}{48}\frac{\partial^4 u}{\partial r \partial z^3} + \frac{\tau^4}{384}\frac{\partial^4 u}{\partial z^4} + O(\tau^5) + O\left(h\tau^4\right) \\
& + O\left(h^2\tau^3\right) + O\left(h^3\tau^2\right) + O\left(h^4\tau\right) + O\left(h^5\right), \qquad (2.4)
\end{aligned}$$

$$\begin{aligned}
u_{m+1,n-1} = \; & u_{m,n-\frac{1}{2}} + h\frac{\partial u}{\partial r} - \frac{\tau}{2}\frac{\partial u}{\partial z} + \frac{h^2}{2}\frac{\partial^2 u}{\partial r^2} + \frac{\tau^2}{8}\frac{\partial^2 u}{\partial z^2} - \frac{h\tau}{2}\frac{\partial^2 u}{\partial r \partial z} + \frac{h^3}{6}\frac{\partial^3 u}{\partial r^3} \\
& - \frac{h^2\tau}{4}\frac{\partial^3 u}{\partial r^2 \partial z} + \frac{h\tau^2}{8}\frac{\partial^3 u}{\partial r \partial z^2} - \frac{\tau^3}{48}\frac{\partial^3 u}{\partial z^3} + \frac{h^4}{24}\frac{\partial^4 u}{\partial r^4} - \frac{h^3\tau}{12}\frac{\partial^4 u}{\partial r^3 \partial z} \\
& + \frac{h^2\tau^2}{16}\frac{\partial^4 u}{\partial r^2 \partial z^2} - \frac{h\tau^3}{48}\frac{\partial^4 u}{\partial r \partial z^3} + \frac{\tau^4}{384}\frac{\partial^4 u}{\partial z^4} + O(\tau^5) + O\left(h\tau^4\right) \\
& + O\left(h^2\tau^3\right) + O\left(h^3\tau^2\right) + O\left(h^4\tau\right) + O\left(h^5\right), \qquad (2.5)
\end{aligned}$$

$$u_{m,n-1} = u_{m,n-\frac{1}{2}} - \frac{\tau}{2}\frac{\partial u}{\partial z} + \frac{\tau^2}{8}\frac{\partial^2 u}{\partial z^2} - \frac{\tau^3}{48}\frac{\partial^3 u}{\partial z^3} + \frac{\tau^4}{384}\frac{\partial^4 u}{\partial z^4} + O(\tau^5) \qquad (2.6)$$

$$
\begin{aligned}
u_{m-1,n-1} = \; & u_{m,n-\frac{1}{2}} - h\frac{\partial u}{\partial r} - \frac{\tau}{2}\frac{\partial u}{\partial z} + \frac{h^2}{2}\frac{\partial^2 u}{\partial r^2} + \frac{\tau^2}{8}\frac{\partial^2 u}{\partial z^2} + \frac{h\tau}{2}\frac{\partial^2 u}{\partial r \partial z} - \frac{h^3}{6}\frac{\partial^3 u}{\partial r^3} \\
& - \frac{h^2\tau}{4}\frac{\partial^3 u}{\partial r^2 \partial z} - \frac{h\tau^2}{8}\frac{\partial^3 u}{\partial r \partial z^2} - \frac{\tau^3}{48}\frac{\partial^3 u}{\partial z^3} + \frac{h^4}{24}\frac{\partial^4 u}{\partial r^4} + \frac{h^3\tau}{12}\frac{\partial^4 u}{\partial r^3 \partial z} \\
& + \frac{h^2\tau^2}{16}\frac{\partial^4 u}{\partial r^2 \partial z^2} + \frac{h\tau^3}{48}\frac{\partial^4 u}{\partial r \partial z^3} + \frac{\tau^4}{384}\frac{\partial^4 u}{\partial z^4} + O(\tau^5) + O\left(h\tau^4\right) \\
& + O\left(h^2\tau^3\right) + O\left(h^3\tau^2\right) + O\left(h^4\tau\right) + O\left(h^5\right). \qquad (2.7)
\end{aligned}
$$

It follows that

$$
\begin{aligned}
& \frac{1}{2}\left\{\frac{u_{m+1,n} - u_{m-1,n}}{2h} + \frac{u_{m+1,n-1} - u_{m-1,n-1}}{2h}\right\} \\
& \quad = \frac{1}{4h}\left\{4h\frac{\partial u}{\partial r} + \frac{2h^3}{3}\frac{\partial^3 u}{\partial r^3} + \frac{h\tau^2}{2}\frac{\partial^3 u}{\partial r \partial z^2} + O\left(h^5\right) + O\left(h^3\tau^2\right) + O\left(h\tau^4\right)\right\} \\
& \quad = \frac{\partial u}{\partial r} + \frac{h^2}{6}\frac{\partial^3 u}{\partial r^3} + \frac{\tau^2}{8}\frac{\partial^3 u}{\partial r \partial z^2} + O\left(h^4\right) + O\left(h^2\tau^2\right) + O\left(\tau^4\right) \\
& \quad = \frac{\partial u}{\partial r} + O\left(h^2\right) + O\left(h^2\tau^2\right) + O\left(\tau^2\right), \\
& \frac{1}{2}\left\{\frac{u_{m+1,n} - 2u_{m,n} + u_{m-1,n}}{h^2} + \frac{u_{m+1,n-1} - 2u_{m,n-1} + u_{m-1,n-1}}{h^2}\right\} \\
& \quad = \frac{1}{2h^2}\left\{2h^2\frac{\partial^2 u}{\partial r^2} + \frac{h^4}{6}\frac{\partial^4 u}{\partial r^4} + \frac{h^2\tau^2}{4}\frac{\partial^4 u}{\partial r^2 \partial z^2} + O\left(h^6\right) + O\left(h^2\tau^4\right) + O\left(h^4\tau^2\right)\right\} \\
& \quad = \frac{\partial^2 u}{\partial r^2} + O\left(h^2\right) + O\left(h^2\tau^2\right) + O\left(\tau^2\right), \\
& \frac{u_{m,n} - u_{m,n-1}}{\tau} = \frac{1}{\tau}\left\{\tau\frac{\partial u}{\partial z} + \frac{\tau^3}{24}\frac{\partial^3 u}{\partial z^3} + O\left(\tau^5\right)\right\} = \frac{\partial u}{\partial z} + O\left(\tau^2\right)
\end{aligned}
$$

and

$$
\frac{1}{2}\left\{u_{m,n} + u_{m,n-1}\right\} = \frac{1}{2}\left\{2u_{m,n-\frac{1}{2}} + \frac{\tau^2}{4}\frac{\partial^2 u}{\partial z^2} + \frac{\tau^4}{192}\frac{\partial^4 u}{\partial z^4} + O\left(\tau^6\right)\right\} = u_{m,n-\frac{1}{2}} + O\left(\tau^2\right).
$$

Thus we have

$$
\begin{aligned}
u_r(z_{n-\frac{1}{2}}, r_m) = & \frac{1}{2}\left\{\frac{u_{m+1,n} - u_{m-1,n}}{2h} + \frac{u_{m+1,n-1} - u_{m-1,n-1}}{2h}\right\} \\
& + O\left(h^2\right) + O\left(h^2\tau^2\right) + O\left(\tau^2\right), \qquad (2.8) \\
u_{rr}(z_{n-\frac{1}{2}}, r_m) = & \frac{1}{2}\left\{\frac{u_{m+1,n} - 2u_{m,n} + u_{m-1,n}}{h^2} + \frac{u_{m+1,n-1} - 2u_{m,n-1} + u_{m-1,n-1}}{h^2}\right\} \\
& + O\left(h^2\right) + O\left(h^2\tau^2\right) + O\left(\tau^2\right), \qquad (2.9)
\end{aligned}
$$

$$u_z(z_{n-\frac{1}{2}}, r_m) = \frac{u_{m,n} - u_{m,n-1}}{\tau} + O\left(\tau^2\right), \tag{2.10}$$

$$u(z_{n-\frac{1}{2}}, r_m) = \frac{1}{2}\left\{u_{m,n} + u_{m,n-1}\right\} + O\left(\tau^2\right), \tag{2.11}$$

where all derivatives are evaluated at non-grid point $\left(z_{n-\frac{1}{2}}, r_m\right)$. When $\tau \leq Ch$ for some constant C, we have

$$u_r(z_{n-\frac{1}{2}}, r_m) = \frac{1}{2}\left\{\frac{u_{m+1,n} - u_{m-1,n}}{2h} + \frac{u_{m+1,n-1} - u_{m-1,n-1}}{2h}\right\} + O\left(h^2\right), \tag{2.12}$$

$$u_{rr}(z_{n-\frac{1}{2}}, r_m) = \frac{1}{2}\left\{\frac{u_{m+1,n} - 2u_{m,n} + u_{m-1,n}}{h^2} + \frac{u_{m+1,n-1} - 2u_{m,n-1} + u_{m-1,n-1}}{h^2}\right\} + O\left(h^2\right). \tag{2.13}$$

Substituting the approximations (2.8)-(2.11) into Equation (2.1) yields a six-point, two-level, Crank-Nicholson type scheme

$$\begin{aligned}
&\frac{c_4}{2h^2}\left[u_{m+1,n} - 2u_{m,n} + u_{m-1,n} + u_{m+1,n-1} - 2u_{m,n-1} + u_{m-1,n-1}\right] \\
&\quad + \frac{c_3}{4h}\left[u_{m+1,n} - u_{m-1,n} + u_{m+1,n-1} - u_{m-1,n-1}\right] \\
&\quad + \frac{c_2}{\tau}[u_{m,n} - u_{m,n-1}] + \frac{c_1}{2}\left[u_{m,n} + u_{m,n-1}\right] + c_0 = 0.
\end{aligned} \tag{2.14}$$

To facilitate stability and consistency analysis, we rewrite (2.14) in the following implicit form

$$\begin{aligned}
&\left(\frac{c_4}{2h^2} + \frac{c_3}{4h}\right)u_{m+1,n} + \left(-\frac{c_4}{h^2} + \frac{c_2}{\tau} + \frac{c_1}{2}\right)u_{m,n} + \left(\frac{c_4}{2h^2} - \frac{c_3}{4h}\right)u_{m-1,n} \\
&= -\left(\frac{c_4}{2h^2} + \frac{c_3}{4h}\right)u_{m+1,n-1} + \left(\frac{c_4}{h^2} + \frac{c_2}{\tau} - \frac{c_1}{2}\right)u_{m,n-1} - \left(\frac{c_4}{2h^2} - \frac{c_3}{4h}\right)u_{m-1,n-1} + c_0.
\end{aligned} \tag{2.15}$$

Next, we will derive additional finite difference approximations for the Neumann boundary conditions $u_r(z, 0) = 0$ and $u_r(z, R_1) = 0$. We have

$$u_r(z, 0) = \frac{u_{1,n} - u_{-1,n}}{2h} + O\left(h^2\right) = 0.$$

Then

$$u_{-1,n} = u_{1,n} + O(h). \tag{2.16}$$

We consider the finite difference scheme (2.15) at the boundary $r = 0$

$$\left(\frac{c_4}{2h^2} + \frac{c_3}{4h}\right) u_{1,n} + \left(-\frac{c_4}{h^2} + \frac{c_2}{\tau} + \frac{c_1}{2}\right) u_{0,n} + \left(\frac{c_4}{2h^2} - \frac{c_3}{4h}\right) u_{-1,n}$$
$$= -\left(\frac{c_4}{2h^2} + \frac{c_3}{4h}\right) u_{1,n-1} + \left(\frac{c_4}{h^2} + \frac{c_2}{\tau} - \frac{c_1}{2}\right) u_{0,n-1} - \left(\frac{c_4}{2h^2} - \frac{c_3}{4h}\right) u_{-1,n-1} + c_0.$$

Substituting (2.16) into the above, we obtain

$$\frac{c_4}{h^2} u_{1,n} + \left(-\frac{c_4}{h^2} + \frac{c_2}{\tau} + \frac{c_1}{2}\right) u_{0,n}$$
$$= -\frac{c_4}{h^2} u_{1,n-1} + \left(\frac{c_4}{h^2} + \frac{c_2}{\tau} - \frac{c_1}{2}\right) u_{0,n-1} + c_0. \tag{2.17}$$

Similarly, at $r = R_1$ we have

$$u_r(z, R_1) = \frac{u_{M+1,n} - u_{M-1,n}}{2h} + O\left(h^2\right) = 0,$$

thus

$$u_{M+1,n} = u_{M-1,n} + O\left(h\right). \tag{2.18}$$

We consider the finite difference scheme (2.15) at the boundary $r = R_1$

$$\left(\frac{c_4}{2h^2} + \frac{c_3}{4h}\right) u_{M+1,n} + \left(-\frac{c_4}{h^2} + \frac{c_2}{\tau} + \frac{c_1}{2}\right) u_{M,n} + \left(\frac{c_4}{2h^2} - \frac{c_3}{4h}\right) u_{M-1,n}$$
$$= -\left(\frac{c_4}{2h^2} + \frac{c_3}{4h}\right) u_{M+1,n-1} + \left(\frac{c_4}{h^2} + \frac{c_2}{\tau} - \frac{c_1}{2}\right) u_{M,n-1} - \left(\frac{c_4}{2h^2} - \frac{c_3}{4h}\right) u_{M-1,n-1} + c_0.$$

Substituting (2.18) into the above, we obtain

$$\frac{c_4}{h^2} u_{M+1,n} + \left(-\frac{c_4}{h^2} + \frac{c_2}{\tau} + \frac{c_1}{2}\right) u_{M,n}$$
$$= -\frac{c_4}{h^2} u_{M+1,n-1} + \left(\frac{c_4}{h^2} + \frac{c_2}{\tau} - \frac{c_1}{2}\right) u_{M,n-1} + c_0. \tag{2.19}$$

2.2 Consistency

Definition 2.2. We say that the finite difference equation $P_{\tau,h} v = f$ is *consistent* with the partial differential equation $Pu = f$ if for any smooth function $\phi(z, r)$

$$P_{\tau,h}\phi - P\phi \to 0 \text{ as } \tau, h \to 0,$$

the convergence being pointwise at each reference point (z, r).

Usage of the term "truncation error" can vary somewhat according to source material. The fundamental idea is to provide a measure of the extent to which an exact solution of a differential equation fails to satisfy a difference equation. In this dissertation we will utilize definitions convenient for a Crank-Nicholson type scheme.

Definition 2.3. Let $\phi(z,r)$ be a smooth function. Then the difference $P_{\tau,h}\phi - P\phi$, where $P_{\tau,h}\phi$ and $P\phi$ are evaluated on reference point (z,r), is called the *local truncation error* of finite difference scheme $P_{\tau,h}v = 0$ with respect to partial differential equation $Pu = 0$.

Definition 2.4. A scheme $P_{\tau,h}v = 0$ is *accurate of order* p in the z direction and q in the r direction if for any smooth function $\phi(z,r)$,

$$P_{\tau,h}\phi - P\phi = O\left(\tau^p\right) + O\left(h^q\right), \tag{2.20}$$

where $P_{\tau,h}\phi$ and differential equation $P\phi$ are evaluated at reference point (z,r). We say that the scheme has *local order of accuracy* (p,q).

Recall (2.1). For the theorems and remarks to follow, let P be the linear differential operator such that

$$Pu = c_4 u_{rr} + c_3 u_r + c_2 u_z + c_1 u + c_0 \tag{2.21}$$

where $c_i,\ 0 \le i \le 4$, are functions of r and z. Further, let $P_{\tau,h}$ be the difference operator

$$\begin{aligned} P_{\tau,h}u = &\left(\frac{c_4}{2h^2} + \frac{c_3}{4h}\right) u_{m+1,n} + \left(-\frac{c_4}{h^2} + \frac{c_2}{\tau} + \frac{c_1}{2}\right) u_{m,n} + \left(\frac{c_4}{2h^2} - \frac{c_3}{4h}\right) u_{m-1,n} \\ &+ \left(\frac{c_4}{2h^2} + \frac{c_3}{4h}\right) u_{m+1,n-1} + \left(-\frac{c_4}{h^2} - \frac{c_2}{\tau} + \frac{c_1}{2}\right) u_{m,n-1} + \left(\frac{c_4}{2h^2} - \frac{c_3}{4h}\right) u_{m-1,n-1} \\ &+ c_0, \end{aligned} \tag{2.22}$$

where h and τ are the grid step-sizes, m and n the grid indices for the r and z directions, respectively.

Theorem 2.1. *The finite difference equation $P_{\tau,h}v = 0$ has a local truncation error of order $O(\tau^2) + O(h^2)$ with respect to $Pu = 0$.*

Proof. Let $u(z, r)$ be a smooth function. By substituting the Taylor expansions (2.2)-(2.7) into (2.22) and gathering terms, we see that

$$\begin{aligned}
P_{\tau,h}u &= c_4\left[\frac{\partial^2 u}{\partial r^2} + \frac{h^2}{12}\frac{\partial^4 u}{\partial r^4} + \frac{\tau^2}{8}\frac{\partial^4 u}{\partial r^2 \partial z^2} + O\left(h^4\right) + O\left(h^2\tau^2\right) + O\left(\tau^4\right)\right] \\
&\quad + c_3\left[\frac{\partial u}{\partial r} + \frac{h^2}{6}\frac{\partial^3 u}{\partial r^3} + \frac{\tau^2}{8}\frac{\partial^3 u}{\partial r \partial z^2} + O\left(h^4\right) + O\left(h^2\tau^2\right) + O\left(\tau^4\right)\right] \\
&\quad + c_2\left[\frac{\partial u}{\partial z} + \frac{\tau^2}{24}\frac{\partial^3 u}{\partial z^3} + O\left(\tau^4\right)\right] + c_1\left[u_{m,n-\frac{1}{2}} + \frac{\tau^2}{8}\frac{\partial^2 u}{\partial z^2} + \frac{\tau^4}{384}\frac{\partial^4 u}{\partial z^4} + O\left(\tau^6\right)\right] + c_0 \\
&= c_4\frac{\partial^2 u}{\partial r^2} + c_3\frac{\partial u}{\partial r} + c_2\frac{\partial u}{\partial z} + c_1 u_{m,n-\frac{1}{2}} + c_0 + c_4\left[\frac{h^2}{12}\frac{\partial^4 u}{\partial r^4} + \frac{\tau^2}{8}\frac{\partial^4 u}{\partial r^2 \partial z^2}\right] \\
&\quad + c_3\left[\frac{h^2}{6}\frac{\partial^3 u}{\partial r^3} + \frac{\tau^2}{8}\frac{\partial^3 u}{\partial r \partial z^2}\right] + c_2\left[\frac{\tau^2}{24}\frac{\partial^3 u}{\partial z^3}\right] + c_1\left[\frac{\tau^2}{8}\frac{\partial^2 u}{\partial z^2}\right] + O\left(h^4\right) \\
&\quad + O\left(h^2\tau^2\right) + O\left(\tau^4\right) \\
&= Pu + c_4\left[\frac{h^2}{12}\frac{\partial^4 u}{\partial r^4} + \frac{\tau^2}{8}\frac{\partial^4 u}{\partial r^2 \partial z^2}\right] + c_3\left[\frac{h^2}{6}\frac{\partial^3 u}{\partial r^3} + \frac{\tau^2}{8}\frac{\partial^3 u}{\partial r \partial z^2}\right] + c_2\left[\frac{\tau^2}{24}\frac{\partial^3 u}{\partial z^3}\right] \\
&\quad + c_1\left[\frac{\tau^2}{8}\frac{\partial^2 u}{\partial z^2}\right] + O\left(h^4\right) + O\left(h^2\tau^2\right) + O\left(\tau^4\right).
\end{aligned}$$

Thus the truncation error

$$\begin{aligned}
P_{\tau,h}u - Pu &= c_4\left[\frac{h^2}{12}\frac{\partial^4 u}{\partial r^4} + \frac{\tau^2}{8}\frac{\partial^4 u}{\partial r^2 \partial z^2}\right] + c_3\left[\frac{h^2}{6}\frac{\partial^3 u}{\partial r^3} + \frac{\tau^2}{8}\frac{\partial^3 u}{\partial r \partial z^2}\right] + c_2\left[\frac{\tau^2}{24}\frac{\partial^3 u}{\partial z^3}\right] \\
&\quad + c_1\left[\frac{\tau^2}{8}\frac{\partial^2 u}{\partial z^2}\right] + O\left(h^4\right) + O\left(h^2\tau^2\right) + O\left(\tau^4\right) \\
&= O\left(\tau^2\right) + O\left(h^2\right).
\end{aligned}$$

This completes our proof. □

Corollary 2.1. *The scheme $P_{\tau,h}v = 0$ has local order of accuracy $(2, 2)$.*

Proof. By Theorem 2.1,

$$P_{\tau,h}u - Pu = O\left(\tau^2\right) + O\left(h^2\right).$$

Thus $P_{\tau,h}v = 0$ has local order of accuracy $(2, 2)$ with respect to $Pu = O$. □

Theorem 2.2. *The scheme $P_{\tau,h}v = 0$ is consistent with differential equation $Pu = 0$.*

Proof. By Theorem 2.1

$$P_{\tau,h}u - Pu = O\left(\tau^2\right) + O\left(h^2\right) \to 0$$

as $\tau, h \to 0$. Thus the scheme $P_{\tau,h}v = 0$ is consistent with differential equation $Pu = 0$. □

Now let $Q_{\tau,h}$ be the difference operator such that

$$\begin{aligned} Q_{\tau,h}u = &\left(\frac{c_{h,4}}{2h^2} + \frac{c_{h,3}}{4h}\right) u_{m+1,n} + \left(-\frac{c_{h,4}}{h^2} + \frac{c_{h,2}}{\tau} + \frac{c_{h,1}}{2}\right) u_{m,n} + \left(\frac{c_{h,4}}{2h^2} - \frac{c_{h,3}}{4h}\right) u_{m-1,n} \\ &+ \left(\frac{c_{h,4}}{2h^2} + \frac{c_{h,3}}{4h}\right) u_{m+1,n-1} + \left(-\frac{c_{h,4}}{h^2} - \frac{c_{h,2}}{\tau} + \frac{c_{h,1}}{2}\right) u_{m,n-1} \\ &+ \left(\frac{c_{h,4}}{2h^2} - \frac{c_{h,3}}{4h}\right) u_{m-1,n-1} + c_{h,0}, \end{aligned}$$

where $c_{h,i}, 0 \le i \le 4$, are functions of r, z and h such that $c_{h,i} \to c_i$ as $h \to 0$, and h and τ are the grid intervals, m and n the grid indices for the r and z directions respectively.

Theorem 2.3. *The scheme $Q_{\tau,h}v = 0$ has a truncation error of*

$$\begin{aligned} &\left(c_{h,4} - c_4\right) \frac{\partial^2 u}{\partial r^2} + \left(c_{h,3} - c_3\right) \frac{\partial u}{\partial r} + \left(c_{h,2} - c_2\right) \frac{\partial u}{\partial z} \\ &+ \left(c_{h,1} - c_1\right) u_{m,n-\frac{1}{2}} + c_{h,0} - c_0 + O\left(\tau^2\right) + O\left(h^2\right) \end{aligned}$$

with respect to $Pu = 0$.

Proof. Let $u(z, r)$ be a smooth function. By Theorem 2.1,

$$P_{\tau,h}u - Pu = O\left(\tau^2\right) + O\left(h^2\right).$$

Thus we have

$$\begin{aligned} Q_{\tau,h}u - Pu &= Q_{\tau,h}u - P_{\tau,h}u + P_{\tau,h}u - Pu \\ &= \left(c_{h,4} - c_4\right) \frac{\partial^2 u}{\partial r^2} + \left(c_{h,3} - c_3\right) \frac{\partial u}{\partial r} + \left(c_{h,2} - c_2\right) \frac{\partial u}{\partial z} \\ &+ \left(c_{h,1} - c_1\right) u_{m,n-\frac{1}{2}} + c_{h,0} - c_0 + O\left(\tau^2\right) + O\left(h^2\right). \end{aligned}$$

This completes our proof. □

Theorem 2.4. *The scheme $Q_{\tau,h}v = 0$ is consistent with $Pu = 0$.*

Proof. Let $u(z, r)$ be a smooth function. By Theorem 2.3,

$$Q_{\tau,h}u - Pu = (c_{h,4} - c_4)\frac{\partial^2 u}{\partial r^2} + (c_{h,3} - c_3)\frac{\partial u}{\partial r} + (c_{h,2} - c_2)\frac{\partial u}{\partial z} + (c_{h,1} - c_1)\, u_{m,n-\frac{1}{2}} + c_{h,0} - c_0 + O\left(\tau^2\right) + O\left(h^2\right).$$

Since

$$|c_{h,i} - c_i| \to 0,\ 0 \le i \le 4, \quad \text{as} \quad h \to 0,$$

we have

$$Q_{\tau,h}u - Pu \to 0 \quad \text{as} \quad \tau, h \to 0.$$

We conclude that $Q_{\tau,h}v = 0$ is consistent with $Pu = 0$. □

2.3 A Stability Analysis Method

While we were able to demonstrate consistency for the general form of our scheme when the coefficients are taken from any partial differential equation of the form (2.1), stability of the scheme when applied to a specific problem will have to be established for each case.

Definition 2.5. A finite difference scheme may be written as a system of linear equations:

$$B\mathbf{u}_n = C\mathbf{u}_{n-1},$$

or

$$\mathbf{u}_n = B^{-1}C\mathbf{u}_{n-1},$$

where vector $\mathbf{u}_n = \{u_{k,n}\}_{k=0}^{M}$ and the difference operators $B, C \in \mathbb{C}^{M\times M}$ are coefficient matrices. Let $E = B^{-1}C$. If there exists a constant $K > 0$ independent of n, h and τ such that $\|E^n\| \le K$ for some norm $\|\cdot\|$, we say that the scheme is *stable in the Lax-Richtmyer sense* [42, 51].

In the above definition and in much of the literature, the matrix $B^{-1}C$ is assumed to be constant with respect to the direction of propagation, in other words, $B^{-1}C$ is the same at each z-step. However, in several schemes we wish to explore, $B^{-1}C$ is dependent on z. We must return to the fundamental concepts of stability of an iterative finite difference scheme and formulate a definition of stability suitable for our purposes.

Consider a finite difference scheme written in the form

$$\mathbf{u}_n = A_n \mathbf{u}_{n-1} + \mathbf{f}_{n-1}$$

where the right-hand side matrix A_n can vary with each propagation step. The solution at propagation level n can be obtained by applying the relation recursively to the initial solution $\mathbf{u}_0$, *i.e.*

$$\mathbf{u}_n = \left(\prod_{k=1}^{n} A_k\right)\mathbf{u}_0 + \left(\prod_{k=2}^{n} A_k\right)\mathbf{f}_0 + \left(\prod_{k=3}^{n} A_k\right)\mathbf{f}_1 + \ldots + A_n\mathbf{f}_{n-2} + \mathbf{f}_{n-1}. \tag{2.23}$$

If we perturb the vector $\mathbf{u}_0$ of initial values to $\tilde{\mathbf{u}}_0$, the solution at propagation step n will be

$$\tilde{\mathbf{u}}_n = \left(\prod_{k=1}^{n} A_k\right)\tilde{\mathbf{u}}_0 + \left(\prod_{k=2}^{n} A_k\right)\mathbf{f}_0 + \left(\prod_{k=3}^{n} A_k\right)\mathbf{f}_1 + \ldots + A_n\mathbf{f}_{n-2} + \mathbf{f}_{n-1}. \tag{2.24}$$

Let $\mathbf{e}_n$ be the error vector at propagation step n defined as $\mathbf{e}_n = \tilde{\mathbf{u}}_n - \mathbf{u}_n$. Then by (2.23) and (2.24),

$$\mathbf{e}_n = \tilde{\mathbf{u}}_n - \mathbf{u}_n = \left(\prod_{k=1}^{n} A_k\right)(\tilde{\mathbf{u}}_0 - \mathbf{u}_0) = \left(\prod_{k=1}^{n} A_k\right)\mathbf{e}_0. \tag{2.25}$$

Let $\rho(A)$ be the spectral radius of matrix A. If

$$\rho(A_n) \leq 1$$

for all $0 < n\tau < Z$ and any transverse direction step size $0 < h < \epsilon$ for some $\epsilon > 0$, then $\| \prod_{k=1}^{n} A_k \| \leq 1$.

By (2.25), this stability condition will guarantee that the perturbations will not increase exponentially with n. However, it does not always guarantee convergence. Additional parameter constraints may need to be determined.

To facilitate our analysis of the stability of our schemes, some preliminary results concerning matrices must be established.

Definition 2.6. An $n \times n$ Hermitian matrix A is said to be *positive definite* if

$$\mathbf{x}^* A\mathbf{x} > 0 \text{ , for all nonzero } \mathbf{x} \in \mathbb{C}^n.$$

Definition 2.7. An $n \times n$ Hermitian matrix A is said to be *positive semidefinite* if

$$\mathbf{x}^* A\mathbf{x} \geq 0 \text{ , for all nonzero } \mathbf{x} \in \mathbb{C}^n.$$

Note: While the definitions of positive definite and positive semidefinite are sometimes extended to include non-Hermitian matrices, we will limit our usage to the Hermitian case, as do Horn and Johnson [36, 37].

Definition 2.8. A matrix $A \in \mathbb{C}^{n\times n}$ is said to be *positive semistable* if the real part of every eigenvalue of A is nonnegative.

Lemma 2.1. *Let $A, B, C \in \mathbb{C}^{n\times n}$ be such that*

$$B = dI + A, \quad C = dI - A,$$

where $d \in \mathbb{R}$, $d > 0$. Then every eigenvector $\mathbf{v} \in \mathbb{C}^n$ of any of the three matrices is also an eigenvector of the other two, i.e. $A\mathbf{v} = \lambda_A\mathbf{v}$, $B\mathbf{v} = \lambda_B\mathbf{v}$ and $C\mathbf{v} = \lambda_C\mathbf{v}$, for $\lambda_A, \lambda_B, \lambda_C \in \mathbb{C}$ with the following relationship between the corresponding eigenvalues:

$$\lambda_B = d + \lambda_A = 2d - \lambda_C,$$

$$\lambda_C = d - \lambda_A = 2d - \lambda_B.$$

Proof. *Let* $A, B, C \in \mathbb{C}^{n\times n}$ as above. Clearly, each of the matrices commutes with the other two, and thus by a well known result in matrix theory, they share a common basis of eigenvectors. To show the eigenvalue relations, let $\mathbf{v} \in \mathbb{C}^n$ be an eigenvector of A with corresponding eigenvalue λ_A, i.e, $A\mathbf{v} = \lambda_A \mathbf{v}$. Then

$$C\mathbf{v} = (dI - A)\,\mathbf{v} = dI\mathbf{v} - A\mathbf{v} = d\mathbf{v} - \lambda_A\mathbf{v} = (d - \lambda_A)\,\mathbf{v}$$

and thus $\lambda_C = d - \lambda_A$. Also,

$$B\mathbf{v} = (dI + A)\,\mathbf{v} = dI\mathbf{v} + A\mathbf{v} = d\mathbf{v} + \lambda_A\mathbf{v} = (d + \lambda_A)\,\mathbf{v}$$

and we have $\lambda_B = d + \lambda_A$. □

Theorem 2.5. *Let* $A, B, C \in \mathbb{C}^{n\times n}$ *be such that*

$$B = dI + A, \quad C = dI - A,$$

where $d \in \mathbb{R}$, $d > 0$. *Then the difference scheme defined by*

$$B\boldsymbol{u}_n = C\boldsymbol{u}_{n-1}$$

is stable if and only if matrix A *is positive semistable.*

Proof. Let $A, B, C \in \mathbb{C}^{n\times n}$ be such that

$$B = dI + A, \quad C = dI - A,$$

where $d \in \mathbb{R}$, $d > 0$. Then by Lemma 2.1, any eigenvalue λ of the matrix $B^{-1}C$ is of the form

$$\lambda = \frac{d - \lambda_A}{d + \lambda_A},$$

where λ_A is an eigenvalue of A. It follows that

$$|\lambda| = \frac{|d - \lambda_A|}{|d + \lambda_A|} = \frac{(d - \mathrm{Re}(\lambda_A))^2 + \mathrm{Im}^2(\lambda_A)}{(d + \mathrm{Re}(\lambda_A))^2 + \mathrm{Im}^2(\lambda_A)} = 1 - \frac{4d\mathrm{Re}(\lambda_A)}{(d + \mathrm{Re}(\lambda_A))^2 + \mathrm{Im}^2(\lambda_A)}.$$

Case 1: $\mathrm{Re}(\lambda_A) < 0$

$$|\lambda| = 1 + \left| \frac{4d\mathrm{Re}(\lambda_A)}{(d + \mathrm{Re}(\lambda_A))^2 + \mathrm{Im}^2(\lambda_A)} \right| > 1.$$

Case 2: $\mathrm{Re}(\lambda_A) = 0$

$$|\lambda| = 1 + \frac{4d \cdot 0}{(d + \mathrm{Re}(\lambda_A))^2 + \mathrm{Im}^2(\lambda_A)} = 1 + 0 = 1.$$

Case 3: $\mathrm{Re}(\lambda_A) > 0$

$$|\lambda| = 1 - \left| \frac{4d\mathrm{Re}(\lambda_A)}{(d + \mathrm{Re}(\lambda_A))^2 + \mathrm{Im}^2(\lambda_A)} \right| < 1.$$

Thus we see that for an arbitrary eigenvalue λ of $B^{-1}C$, $|\lambda| \leq 1$ if and only if the real parts of the eigenvalues of A are nonnegative. Therefore $\rho(B^{-1}C) \leq 1$ if and only if the real parts of all eigenvalues of A are nonnegative. We conclude that our scheme is stable if and only if A is positive semistable. □

Consider the general form of our six-point, two-level Crank-Nicholson type scheme (2.15) with $c_0 = 0$. We multiply through by $\dfrac{2\tau}{c_2}$ to obtain

$$\begin{aligned}
&\frac{\tau}{c_2}\left(\frac{c_4}{h^2} + \frac{c_3}{2h}\right) u_{m+1,n} + \left(2 - \frac{\tau}{c_2}\left(\frac{2c_4}{h^2} - c_1\right)\right) u_{m,n} + \frac{\tau}{c_2}\left(\frac{c_4}{2h^2} - \frac{c_3}{4h}\right) u_{m-1,n} \\
&= -\frac{\tau}{c_2}\left(\frac{c_4}{h^2} + \frac{c_3}{2h}\right) u_{m+1,n-1} + \left(2 + \frac{\tau}{c_2}\left(\frac{2c_4}{h^2} - c_1\right)\right) u_{m,n-1} - \frac{\tau}{c_2}\left(\frac{c_4}{h^2} - \frac{c_3}{2h}\right) u_{m-1,n-1}.
\end{aligned}$$

This can be expressed in matrix form

$$B\mathbf{u}_n = C\mathbf{u}_{n-1}$$

with

$$B = 2I + A, \quad C = 2I - A,$$

and

$$A = \begin{bmatrix} a_1 & q_1 & 0 & \cdots & 0 \\ b_2 & a_2 & q_2 & 0 & \cdots \\ 0 & b_3 & a_3 & q_3 & 0 \\ & \cdots & & & \\ & & \cdots & & \\ & & & \cdots & \\ \cdots & 0 & b_{N-1} & a_{N-1} & q_{N-1} \\ 0 & \cdots & 0 & b_N & a_N \end{bmatrix}$$

where

$$a_m = -\frac{\tau}{c_2(z,mh)}\left(\frac{2c_4(z,mh)}{h^2} - c_1(z,mh)\right),$$
$$b_m = \frac{c_4(z,mh)}{2h^2} - \frac{c_3(z,mh)}{4h},\ q_m = \frac{c_4(z,mh)}{2h^2} + \frac{c_3(z,mh)}{4h}.$$

Theorem 2.6. *Our six-point, two-level Crank-Nicholson type scheme is stable for a partial differential equation of form* (2.1) *if and only if the corresponding matrix A as defined above is positive semistable.*

Proof. It follows immediately from Theorem 2.5. □

2.4 Homogeneous Paraxial Helmholtz Scheme

We derive a Crank-Nicholson scheme for the paraxial Helmholtz equation for the case of homogeneous media. Recall Equation (1.12), the paraxial Helmholtz equation in a radially symmetric polar domain

$$2iku_z(z,r) = u_{rr}(z,r) + \frac{1}{r}u_r(z,r).$$

First, we identify the coefficients of the paraxial Helmholtz equation which correspond to the coefficients c_0 through c_4 of equation (2.1) given in Section 2.1

$$c_4 = 1,\ c_3 = \frac{1}{r},\ c_2 = -2ik,,\ c_1 = 0,\ c_0 = 0.$$

Then we substitute these specific coefficients into the implicit form general finite difference scheme (2.15) to obtain

$$\begin{aligned} &-\left(\frac{1}{2h^2}+\frac{1}{4rh}\right)u_{m+1,n}+\left(\frac{1}{h^2}+\frac{2ik}{\tau}\right)u_{m,n}-\left(\frac{1}{2h^2}-\frac{1}{4rh}\right)u_{m-1,n} \\ =&\left(\frac{1}{2h^2}+\frac{1}{4rh}\right)u_{m+1,n-1}+\left(-\frac{1}{h^2}+\frac{2ik}{\tau}\right)u_{m,n-1}+\left(\frac{1}{2h^2}-\frac{1}{4rh}\right)u_{m-1,n-1}. \end{aligned} \tag{2.26}$$

By substituting the relation $r = mh$ and $\alpha = \dfrac{-\tau i}{2kh^2}$, we can rewrite this as

$$\begin{aligned} &-\alpha\left(1+\frac{1}{2m}\right)u_{m+1,n}+(2+2\alpha)\,u_{m,n}-\alpha\left(1-\frac{1}{2m}\right)u_{m-1,n} \\ =&\alpha\left(1+\frac{1}{2m}\right)u_{m+1,n-1}+(2-2\alpha)\,u_{m,n-1}+\alpha\left(1-\frac{1}{2m}\right)u_{m-1,n-1}. \end{aligned} \tag{2.27}$$

Using the same method as above, we use (2.17) and (2.19) to derive finite difference equations associated with the boundary conditions of our scheme.

$$-2\alpha u_{1,n}+(2+2\alpha)\,u_{0,n}=2\alpha u_{1,n-1}+(2-2\alpha)\,u_{0,n-1}$$

and

$$(2+2\alpha)\,u_{M,n}-2\alpha u_{M-1,n}=(2-2\alpha)\,u_{M,n-1}+2\alpha u_{M-1,n-1}.$$

2.5 Stability of Homogeneous Paraxial Helmholtz Scheme

Lemma 2.2. *Let $A \in \mathbb{R}^{n\times n}$ be tridiagonal with all sub and super-diagonal elements positive, or all sub and super-diagonal elements negative. Then there exists a diagonal matrix D such that $D^{-1}AD$ is a real symmetric matrix.*

Proof. We proceed as in Smith [67]. Let $A \in \mathbb{R}^{N\times N}$ such that

$$A = \begin{bmatrix} a_1 & c_1 & 0 & \cdots & 0 \\ b_2 & a_2 & c_2 & 0 & \cdots \\ 0 & b_3 & a_3 & c_3 & 0 \\ & \cdots & & & \\ & & \cdots & & \\ & & & \cdots & \\ \cdots & 0 & b_{N-1} & a_{N-1} & c_{N-1} \\ 0 & \cdots & 0 & b_N & a_N \end{bmatrix}$$

where $b_i > 0$, $2 \le i \le N$ and $c_i > 0$, $1 \le i \le N-1$. Let $D \in \mathbb{C}^{N\times N}$ be a real diagonal matrix with diagonal elements $d_1, d_2, ..., d_N$. Then

$$DAD^{-1} = \begin{bmatrix} a_1 & \frac{c_1 d_1}{d_2} & 0 & \cdots & 0 \\ \frac{b_2 d_2}{d_1} & a_2 & \frac{c_2 d_2}{d_3} & 0 & \cdots \\ 0 & \frac{b_3 d_3}{d_2} & a_3 & \frac{c_3 d_3}{d_4} & 0 \\ & \cdots & & & \\ & & \cdots & & \\ & & & \cdots & \\ \cdots & 0 & \frac{b_{N-1} d_{N-1}}{d_{N-2}} & a_{N-1} & \frac{c_{N-1} d_{N-1}}{d_N} \\ 0 & \cdots & 0 & \frac{b_N d_N}{d_{N-1}} & a_N \end{bmatrix}$$

Set $d_1 = 1$ and $d_i = \sqrt{\frac{c_{i-1}}{b_i}} d_{i-1}$ for $2 \le i \le N$. Since c_{i-1} and b_i have the same sign, all d_i will be positive. Then

$$\frac{c_{i-1} d_{i-1}}{d_i} = \frac{b_i d_i}{d_{i-1}},\ 2 \le i \le N.$$

We see that $D^{-1}AD$ is a real symmetric matrix. For the case of negative off-diagonal elements, substitute $-A$ for A above. □

Lemma 2.3. *Let $A \in \mathbb{R}^{n\times n}$ be tridiagonal with all sub and super-diagonal elements positive, or all sub and super-diagonal elements negative. Then all eigenvalues of A are real.*

Proof. Let A be as above. By Lemma 2.2 there exists a diagonal matrix D such that $D^{-1}AD$ is a real symmetric matrix. Then A is similar to a real symmetric matrix, which has only real eigenvalues. Thus A has only real eigenvalues. □

Theorem 2.7. *Let the wavenumber k be a constant. Then the homogeneous paraxial Helmholtz finite difference scheme is stable.*

Proof. Let the wavenumber k be a constant. Consider the finite difference scheme (2.27) in matrix form

$$B\mathbf{u}_n = C\mathbf{u}_{n-1}.$$

We have $B = 2I + A$, $C = 2I - A$, and $A = \alpha H$, where

$$H = \begin{bmatrix} 2 & -2 & 0 & \cdots & 0 \\ -\left(1-\frac{1}{2(1)}\right) & 2 & -\left(1+\frac{1}{2(1)}\right) & 0 & \cdots \\ & \cdots & & & \\ & & \cdots & & \\ & & & \cdots & \\ \cdots & 0 & -\left(1-\frac{1}{2(M-1)}\right) & 2 & -\left(1+\frac{1}{2(M-1)}\right) \\ 0 & \cdots & 0 & -2 & 2 \end{bmatrix}.$$

Observe that α is purely imaginary and that matrix H is a real tridiagonal matrix with all off-diagonal elements negative. Then by Lemma 2.3, H has real eigenvalues. Thus A has purely imaginary eigenvalues and is therefore positive semistable. By Theorem 2.5, we can conclude that homogeneous paraxial Helmholtz finite difference scheme is stable. □

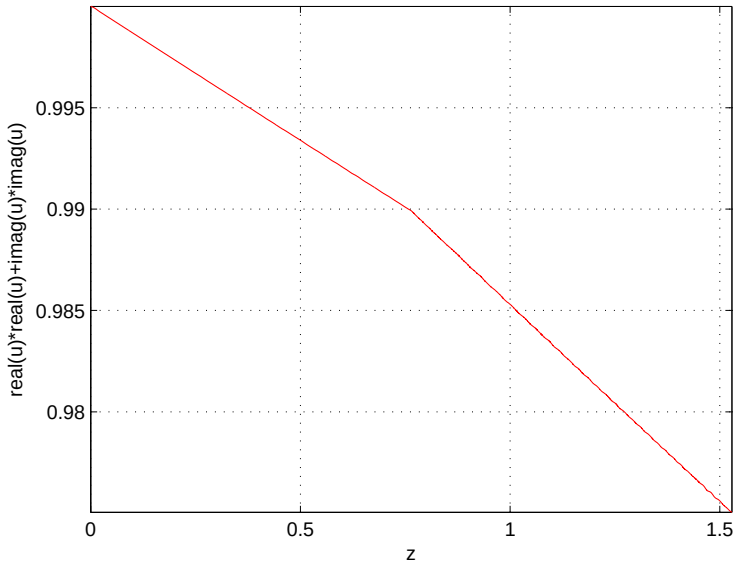

Figure 2.2: Simulation using the two-level, six-point scheme with discontinuous coefficient: intensity of the computed solution near the z-axis. No focusing is observed.

2.6 Coefficient Smoothing

To facilitate the use of conventional numerical techniques for partial differential equations with discontinuous coefficients at an interface, several methods have been proposed that replace the discontinuous coefficient functions with continuous functions derived through harmonic averaging of the coefficient function values near the interface [2, 14, 72]. We shall explore a somewhat different approach to coefficient function smoothing.

The consistency result of Theorem 2.4 implies that we may replace a discontinuous coefficient function c_i in a partial differential equation of form (2.1) with a continuous function $c_{h,i}$ of h that approaches c_i as $h \to 0$ to derive our scheme and still maintain consistency. However, the truncation error will no longer be $O(h^2)$, but will now be proportional to $\max_{0 \le i \le 4} |c_{h,i} - c_i|$ near the interface. Brown demonstrated that for a piecewise continuous wave equation with coefficient functions approximated by continuous functions, the accuracy with which the amplitude is computed is dependent on the accuracy with which the interface conditions are approximated [14].

We once again consider Equation (1.12), the paraxial Helmholtz equation in a radially symmetric polar domain

$$2iku_z(z,r) = u_{rr}(z,r) + \frac{1}{r}u_r(z,r).$$

Let $\eta(z) = \sqrt{R^2 - (z-R)^2}$ be the function which gives the position of the interface (the point of discontinuity of the wavenumber, k) with respect to the r axis. The k parameter can be expressed as

$$k(z,r) = \begin{cases} k_2, & r < \eta(z), \\ k_1, & r \geq \eta(z). \end{cases} \tag{2.28}$$

We construct a continuous function k_h that approximates k,

$$k(z,r) \approx k_h(z,r) = k_2 + (k_1 - k_2)\,\sigma_h(z,r), \tag{2.29}$$

where $\sigma_h(z,r)$ is monotonically increasing with respect to r, $\sigma_h(z,0) = 0$, $\sigma_h(z,R_1) = 1$ for $0 \leq z \leq Z$, and

$$\sigma_h(z,r) \approx \begin{cases} 0, & r < \eta(z), \\ 1, & r > \eta(z). \end{cases}$$

A candidate for our σ_h function is

$$\sigma_h(z,r) = \frac{\tanh\left(\frac{r-\eta(z)}{h}\right) - \tanh\left(\frac{-\eta(z)}{h}\right)}{\tanh\left(\frac{R_1-\eta(z)}{h}\right) - \tanh\left(\frac{-\eta(z)}{h}\right)},$$

which is the hyperbolic tangent function with a steepness factor of $\frac{1}{h}$, centered at $\eta(z)$, and normalized so that $\sigma(z,0) = 0$, $\sigma(z,R_1) = 1$ for $0 \leq z \leq Z$.

Then

$$\sigma_{lim}(z,r) = \lim_{h\to 0} \sigma_h(z,r) = \begin{cases} 0, & r < \eta(z), \\ \frac{1}{2}, & r = \eta(z), \\ 1, & r > \eta(z). \end{cases} \tag{2.30}$$

and

$$k_{lim}(z,r) = \lim_{h\to 0} k_h(z,r) = \begin{cases} k_1, & r < \eta(z), \\ k_1 + \frac{1}{2}(k_2 - k_1), & r = \eta(z), \\ k_2, & r > \eta(z). \end{cases} \tag{2.31}$$

We see that $k_{lim}(z,r) = k(z,r)$ except at $r = \eta(z)$. For convenience, we modify our model by replacing k with k_{lim} to obtain

$$2ik_{lim}u_z(z,r) = u_{rr}(z,r) + \frac{1}{r}u_r(z,r) \tag{2.32}$$

and further replace k_{lim} with k_h, to obtain a smoothed-coefficient model from which we will derive a finite difference scheme consistent with (2.32).

$$2ik_h u_z(z,r) = u_{rr}(z,r) + \frac{1}{r}u_r(z,r). \tag{2.33}$$

We form the six-point, two-level finite difference scheme with

$$c_{h,0} = 0, \quad c_{h,1} = 0, \quad c_{h,2} = 2ik_h, \quad c_{h,3} = -\frac{1}{r} \quad \text{and} \quad c_{h,4} = -1$$

in implicit form

$$\begin{aligned} &-\left(\frac{1}{2h^2} + \frac{1}{4rh}\right)u_{m+1,n} + \left(\frac{1}{h^2} + \frac{2ik_h}{\tau}\right)u_{m,n} - \left(\frac{1}{2h^2} - \frac{1}{4rh}\right)u_{m-1,n} \\ &= \left(\frac{1}{2h^2} + \frac{1}{4rh}\right)u_{m+1,n-1} + \left(-\frac{1}{h^2} + \frac{2ik_h}{\tau}\right)u_{m,n-1} + \left(\frac{1}{2h^2} - \frac{1}{4rh}\right)u_{m-1,n-1} \end{aligned} \tag{2.34}$$

or on the grid lines $r = mh$

$$\begin{aligned} &-\frac{\alpha}{k_h}\left(1 + \frac{1}{2m}\right)u_{m+1,n} + \left(2 + 2\frac{\alpha}{k_h}\right)u_{m,n} - \frac{\alpha}{k_h}\left(1 - \frac{1}{2m}\right)u_{m-1,n} \\ &= \frac{\alpha}{k_h}\left(1 + \frac{1}{2m}\right)u_{m+1,n-1} + \left(2 - 2\frac{\alpha}{k_h}\right)u_{m,n-1} + \frac{\alpha}{k_h}\left(1 - \frac{1}{2m}\right)u_{m-1,n-1} \end{aligned} \tag{2.35}$$

where $\alpha = \dfrac{-\tau i}{2h^2}$.

As in the homogeneous case, we substitute the specific coefficient c_i values into (2.17) and (2.19) to obtain difference equations for the boundary conditions. At $r = 0$ we have

$$-2\frac{\alpha}{k_h}u_{1,n} + \left(2 + 2\frac{\alpha}{k_h}\right)u_{0,n} = 2\frac{\alpha}{k_h}u_{1,n-1} + \left(2 - 2\frac{\alpha}{k_h}\right)u_{0,n-1} \tag{2.36}$$

and at $r = R_1$

$$\left(2 + 2\frac{\alpha}{k_h}\right) u_{M,n} - 2\frac{\alpha}{k_h} u_{M-1,n} = \left(2 - 2\frac{\alpha}{k_h}\right) u_{M,n-1} + 2\frac{\alpha}{k_h} u_{M-1,n-1}. \tag{2.37}$$

2.7 Stability of Smoothed Case

We need further results concerning matrix properties, especially the eigenvalues of tridiagonal matrices.

Definition 2.9. Let $A \in \mathbb{C}^{N\times N}$. We define the functions $\iota_+ : C^{N\times N} \to \mathbb{Z}$, $\iota_- : C^{N\times N} \to \mathbb{Z}$ and $\iota_0 : C^{N\times N} \to \mathbb{Z}$ as follows

$\iota_+(A)$: the number of eigenvalues of A, including multiplicities, with positive real part.

$\iota_-(A)$: the number of eigenvalues of A, including multiplicities, with negative real part.

$\iota_0(A)$: the number of eigenvalues of A, including multiplicities, with zero real part.

The row vector $\iota(A) := [\iota_+(A), \iota_-(A), \iota_0(A)]$ is called the *inertia* of A.

Lemma 2.4 (Horn [37]). *Let $A, B \in \mathbb{C}^{N\times N}$ with B Hermitian and $A + A^*$ positive definite. Then $\iota(AB) = \iota(B)$.*

Theorem 2.8. *Let $A, B \in \mathbb{C}^{N\times N}$ with B Hermitian, A diagonal and $A + A^*$ positive semidefinite. Then $\iota_-(AB) \le \iota_-(B)$.*

Proof. Let $A, B \in \mathbb{C}^{N\times N}$ with B Hermitian, A diagonal and $A + A^*$ positive semidefinite. We have

$$A + A^* = \operatorname{diag}\left\{2\mathrm{Re}(a_{11}), 2\mathrm{Re}(a_{22}), \ldots, 2\mathrm{Re}(a_{NN})\right\},$$

with $\mathrm{Re}(a_{mm}) \ge 0,\ 1 \le m \le N$. Choose real $\epsilon > 0$. Then $\mathrm{Re}(a_{mm}) + \epsilon > 0,\ 1 \le m \le N$ and

$$(A + \epsilon I) + (A + \epsilon I)^* = \operatorname{diag}\left\{2\mathrm{Re}(a_{11}) + 2\epsilon, 2\mathrm{Re}(a_{22}) + 2\epsilon, \ldots, 2\mathrm{Re}(a_{NN}) + 2\epsilon\right\}.$$

Thus, $(A+\epsilon I)+(A+\epsilon I)^*$ is positive definite. By Lemma 2.4, it follows that

$$i\left((A+\epsilon I)B\right) = \iota(B) \text{ for all } \epsilon > 0. \tag{2.38}$$

Assume $\iota_-(AB) > \iota_-(B)$. Since $\lim_{\epsilon\to 0}(A+\epsilon I)B = AB$ and eigenvalues are a continuous function of the elements of a matrix, there must exist some $\epsilon_0 > 0$ such that $\iota_-\left((A+\epsilon I)B\right) = \iota_-\left(AB\right) > \iota_-(B)$ for all $\epsilon < \epsilon_0$. This contradicts (2.38). Thus $\iota_-(AB) \leq \iota_-(B)$. □

Theorem 2.9. *Let $S \in \mathbb{C}^{N\times N}$ and $H \in \mathbb{R}^{N\times N}$. If*

(*i*) *S is diagonal;*

(*ii*) *$S + S^*$ is positive semidefinite;*

(*iii*) *H is tridiagonal with all off-diagonal elements positive or all off-diagonal elements negative,*

then $\iota_-(SH) \leq \iota_-(H)$.

Proof. Let S and H be as above. Then by Theorem 2.2, there exists a diagonal matrix D such that $D^{-1}HD$ is a real symmetric matrix, thus Hermitian. By Lemma 2.8, $\iota_-(SD^{-1}HD) \leq \iota_-(D^{-1}HD)$. Since D^{-1} and S are diagonal, they commute. Then $SD^{-1}HD = D^{-1}SHD$. Then

$$\iota_-(SH) = \iota_-(D^{-1}SHD) = \iota_-(SD^{-1}HD) \leq \iota_-(D^{-1}HD) = \iota_-(H).$$

□

Theorem 2.10. *The finite difference scheme* (2.35), (2.36), (2.37) *is stable.*

Proof. Consider the finite difference scheme (2.35) in the form of a matrix equation:

$$B\mathbf{u}_n = C\mathbf{u}_{n-1}$$

with $B = 2I + A$, $C = 2I - A$, and $A = \alpha H$, where

$$H = \begin{bmatrix} \frac{2}{k_0} & -\frac{2}{k_0} & 0 & \cdots & 0 \\ -\frac{1}{k_1}\left(1 - \frac{1}{2(1)}\right) & \frac{2}{k_1} & -\frac{1}{k_1}\left(1 + \frac{1}{2(1)}\right) & 0 & \cdots \\ & \cdots & & & \\ & & \cdots & & \\ & & & \cdots & \\ \cdots & 0 & -\frac{1}{k_{M-1}}\left(1 - \frac{1}{2(M-1)}\right) & \frac{2}{k_{M-1}} & -\frac{1}{k_{M-1}}\left(1 + \frac{1}{2(M-1)}\right) \\ 0 & \cdots & 0 & -\frac{2}{k_M} & \frac{2}{k_M} \end{bmatrix}$$

with $k_m = k_h(mh)$, for $0 \leq m \leq M$.

As in the case of the homogeneous scheme, α is purely imaginary, and since $k_m > 0$ for all $0 \leq m \leq M$, matrix H is a real tridiagonal matrix with all off-diagonal elements negative. Then by Lemma 2.3, H has real eigenvalues. Thus A has purely imaginary eigenvalues, and is therefore positive semistable. Then by Theorem 2.5, the smoothed coefficient scheme is stable. □

CHAPTER THREE

z-Stretching Domain Transformation

In this chapter we explore domain segmentation and transformation. We first use properties of the solution consistent with the slowly varying envelope approximation to derive an efficient approximation method for our model boundary value problem. Then we examine further applications.

3.1 Stretching in the z direction

If the pre-lens, lens and post-lens segments of the domain were successive rectangular areas along the direction of propagation, we would be able to use conventional finite difference techniques to solve the paraxial Helmholtz equation for a constant k on each segment. We could achieve this scenario by "stretching" each segment by a 1-1 coordinate transformation onto a rectangular area and transforming the partial differential equation for the new coordinate system.

By shifting the z-coordinate (propagation direction) values for the points of a domain segment, while keeping the transverse r-coordinate values constant, we can obtain rectangular subdomains such that the solution computed at the rightmost edge of each segment would become the initial condition of the next segment. We will call this type of transformation *z-stretching*.

We are looking for a solution of the form

$$u(x(z,r), y(z,r))$$

which satisfies the boundary value problem

$$\begin{aligned} 2iku_z(x(z,r), y(z,r)) &= u_{rr}(x(z,r), y(z,r)) + \frac{1}{r}u_r(x(z,r), y(z,r)), \\ u_r(x(z,0), y(z,0)) &= 0, \\ u_r(x(z,R_1), y(z,R_1)) &= 0. \end{aligned}$$

We find the derivatives with respect to the transformed coordinates

$$\begin{aligned}
\frac{\partial u}{\partial r} &= \frac{\partial u}{\partial y}\frac{\partial y}{\partial r} + \frac{\partial u}{\partial x}\frac{\partial x}{\partial r}, \\
\frac{\partial u}{\partial z} &= \frac{\partial u}{\partial y}\frac{\partial y}{\partial z} + \frac{\partial u}{\partial x}\frac{\partial x}{\partial z}, \\
\frac{\partial^2 u}{\partial r^2} &= \frac{\partial u}{\partial y}\frac{\partial^2 y}{\partial r^2} + \frac{\partial^2 u}{\partial y^2}\left(\frac{\partial y}{\partial r}\right)^2 + 2\frac{\partial^2 u}{\partial y \partial x}\frac{\partial y}{\partial r}\frac{\partial x}{\partial r} + \frac{\partial u}{\partial x}\frac{\partial^2 x}{\partial r^2} + \frac{\partial^2 u}{\partial x^2}\left(\frac{\partial x}{\partial r}\right)^2.
\end{aligned}$$

Our transformed partial differential equation is

$$\begin{aligned}
2ik\left(\frac{\partial u}{\partial y}\frac{\partial y}{\partial z} + \frac{\partial u}{\partial x}\frac{\partial x}{\partial z}\right) &= \frac{\partial u}{\partial y}\frac{\partial^2 y}{\partial r^2} + \frac{\partial^2 u}{\partial y^2}\left(\frac{\partial y}{\partial r}\right)^2 + 2\frac{\partial^2 u}{\partial y \partial x}\frac{\partial y}{\partial r}\frac{\partial x}{\partial r} \\
&+ \frac{\partial u}{\partial x}\frac{\partial^2 x}{\partial r^2} + \frac{\partial^2 u}{\partial x^2}\left(\frac{\partial x}{\partial r}\right)^2 + \frac{1}{r}\left(\frac{\partial u}{\partial y}\frac{\partial y}{\partial r} + \frac{\partial u}{\partial x}\frac{\partial x}{\partial r}\right).
\end{aligned}$$

Collecting terms we can write the above as

$$\begin{aligned}
\left(2ik\frac{\partial x}{\partial z} - \frac{\partial^2 x}{\partial r^2} - \frac{1}{r}\frac{\partial x}{\partial r}\right)u_x &= \left(-2ik\frac{\partial y}{\partial z} + \frac{\partial^2 y}{\partial r^2} + \frac{1}{r}\frac{\partial y}{\partial r}\right)u_y \\
&+ \left(\frac{\partial y}{\partial r}\right)^2 u_{yy} + 2\left(\frac{\partial y}{\partial r}\frac{\partial x}{\partial r}\right)u_{yx} + \left(\frac{\partial x}{\partial r}\right)^2 u_{xx}. \qquad (3.1)
\end{aligned}$$

In this method, rather than derive a difference scheme for the pre-lens segment we will evaluate the input beam equation at the lens surface and use this as the initial solution for the simulation of the lens segment. The solution at the right edge of the lens segment becomes the initial solution of the post-lens segment, which we simulate using the homogeneous scheme described earlier.

We wish to map the lens area $\Omega : 0 \le z \le Z$, $(z-R)^2 + r^2 \le R^2$, $r \ge 0$, onto the rectangular area $\Omega_1 : 0 \le x \le Z$, $0 \le y \le R_1$ using z-stretching. A natural choice is the following one-to-one transformation

$$x(z,r) = \frac{z - \left(R - \sqrt{R^2 - r^2}\right)}{Z - \left(R - \sqrt{R^2 - r^2}\right)}Z, \quad y(z,r) = r,$$

with inverse transformation

$$z(x,y) = R - \sqrt{R^2 - y^2} + \frac{x}{Z}\left[Z - \left(R - \sqrt{R^2 - y^2}\right)\right], \quad r(x,y) = y.$$

We have

$$\frac{\partial y}{\partial r}=1,\quad \frac{\partial^2 y}{\partial r^2}=0,\quad \frac{\partial y}{\partial z}=0,$$

$$\frac{\partial x}{\partial r}=\frac{rZ\left(z-Z\right)}{\sqrt{R^2-r^2}\left(Z-\left(R-\sqrt{R^2-r^2}\right)\right)^2},$$

$$\frac{\partial^2 x}{\partial r^2}=-\frac{Z\left(-R^3+\left(Z+\sqrt{R^2-r^2}\right)R^2+2r^2\sqrt{R^2-r^2}\right)\left(Z-z\right)}{\left(R^2-r^2\right)^{3/2}\left(Z-\left(R-\sqrt{R^2-r^2}\right)\right)^3},$$

and

$$\frac{\partial x}{\partial z}=\frac{Z}{Z-\left(R-\sqrt{R^2-r^2}\right)},\quad \frac{\partial z}{\partial y}=\frac{y}{\sqrt{R^2-r^2}}\left(1-\frac{x}{Z}\right).$$

We define functions

$$\phi(x,y):=\frac{\partial x}{\partial r}\left(r\left(x,y\right),z\left(x,y\right)\right)=\frac{\left(x-Z\right)y}{\sqrt{R^2-y^2}\left[Z-\left(R-\sqrt{R^2-y^2}\right)\right]},$$

$$\psi(x,y):=\frac{\partial^2 x}{\partial r^2}\left(r\left(x,y\right),z\left(x,y\right)\right)=\frac{\left(x-Z\right)\left[R^3-\sqrt{R^2-y^2}\left(R^2+2y^2\right)-Z\right]}{\left(R^2-y^2\right)^{\frac{3}{2}}\left[Z-\left(R-\sqrt{R^2-y^2}\right)\right]^2},$$

$$\theta(x,y):=\frac{\partial x}{\partial z}\left(r\left(x,y\right),z\left(x,y\right)\right)=\frac{Z}{Z-\left(R-\sqrt{R^2-y^2}\right)}.$$

Equation (3.1) becomes

$$\left(2ik\theta-\psi-\frac{1}{y}\phi\right)u_x=\frac{1}{y}u_y+u_{yy}+2\phi u_{xy}+\phi^2 u_{xx}. \tag{3.2}$$

Theorem 3.1. *The slowly varying envelope approximation implies that the term $\phi^2 u_{xx}$ in* (3.2) *is negligible.*

Proof. For a fixed value of y in the transformed lens segment, $|u_{xx}|$ is bounded by the value of $|u_{xx}|$ at $x=0$. Equivalently in the physical space, for a fixed value of r, $|u_{xx}|$ is bounded by the value of $|u_{xx}|$ at the lens surface $z=R-\sqrt{R^2-r^2}$. Clearly, $|u_{xx}|$ is monotonically increasing with respect to y. Because we are stretching along the direction of propagation, we have the relation

$$u_{xx}=\frac{\left(Z-\left(R-\sqrt{R^2-r^2}\right)\right)}{Z}u_{zz},$$

where the derivative term on the left is evaluated at a point in the computational space, and the derivative term on the right is evaluated at the corresponding point in the physical space. We find that

$$\phi^2|u_{xx}| \leq \frac{R_1^2 Z}{(R^2 - R_1^2)\left(Z - \left(R - \sqrt{R^2 - R_1^2}\right)\right)}|u_{zz}|$$

for all points in the lens segment.

Thus in a typical lens where the slowly varying envelope approximation is applicable, neglecting $\phi^2 u_{xx}$, the last term on the righthand side of equation (3.2), will not decrease the accuracy of the approximation. □

Solely for the purpose of analysis, we will first assume that the cross derivative u_{zr} is also negligible. With this assumption, by a similar argument to above we can demonstrate that the term $2\phi u_{xy}$ is negligible as well.

Within the lens segment, our transformed equation can be simplified to

$$\left(2ik\theta - \psi - \frac{1}{y}\phi\right) u_x = \frac{1}{y}u_y + u_{yy}. \tag{3.3}$$

The coefficients of our simplified equation are

$$c_4 = 1, \quad c_3 = \frac{1}{y}, \quad c_2 = -\left(2ik\theta - \psi - \frac{1}{y}\phi\right), \quad c_1 = 0, \quad c_0 = 0.$$

Substituting the specific coefficient c_i values into (2.15) we obtain the scheme

$$\left(\frac{1}{2h^2} + \frac{1}{4hy}\right) u_{m+1,n} + \left(-\frac{1}{h^2} - \frac{1}{\tau}\left[2ik\theta - \psi - \frac{1}{y}\phi\right]\right) u_{m,n}$$

$$+ \left(\frac{1}{2h^2} - \frac{1}{4hy}\right) u_{m-1,n} = -\left(\frac{1}{2h^2} + \frac{1}{4hy}\right) u_{m+1,n-1}$$

$$+ \left(\frac{1}{h^2} - \frac{1}{\tau}\left[2ik\theta - \psi - \frac{1}{y}\phi\right]\right) u_{m,n-1} - \left(\frac{1}{2h^2} - \frac{1}{4hy}\right) u_{m-1,n-1}.$$

On the grid lines $y = mh$, we can write the above as

$$-\alpha\gamma\left(1 + \frac{1}{2m}\right) u_{m+1,n} + (2 + 2\alpha\gamma)\, u_{m,n} - \alpha\gamma\left(1 - \frac{1}{2m}\right) u_{m-1,n}$$

$$= \alpha\gamma \left(1 + \frac{1}{2m}\right) u_{m+1,n-1} + (2 - 2\alpha\gamma)\, u_{m,n-1} + \alpha\gamma \left(1 - \frac{1}{2m}\right) u_{m-1,n-1}$$

where

$$\alpha = \frac{\tau}{h^2}, \quad \gamma(x, y) = \frac{1}{2ik\theta - \psi - \frac{1}{y}\phi}.$$

For the boundary condition at $y = 0$ and $y = R_1$ we have

$$u_y(x, 0) = u_z z_y(x, 0) + u_r r_y(x, 0) = u_z \cdot 0 + u_r(x, 0) = 0,$$

and

$$u_y(x, R_1) = u_z z_y(x, R_1) + u_r r_y(x, R_1) = u_z \cdot 0 + u_r(x, R_1) = 0.$$

Substituting the specific coefficient values into the general form for the boundary value difference equations, we obtain

$$-2\alpha\gamma u_{1,n} + (2 + 2\alpha\gamma)\, u_{0,n} = 2\alpha\gamma u_{1,n-1} + (2 - 2\alpha\gamma)\, u_{0,n-1},$$

and

$$(2 + 2\alpha\gamma)\, u_{M,n} - 2\alpha\gamma u_{M-1,n} = (2 - 2\alpha\gamma)\, u_{M,n-1} + 2\alpha\gamma u_{M-1,n-1}.$$

It is interesting to note that for a lens that tapers to a point at the top, the geometric interpretation of this new boundary condition is that the single point (Z, R_1) has been stretched into the upper edge of our transformed rectangular domain, i.e. the upper boundary in the computational space corresponds to the single point (Z, R_1) in the physical space.

Expressing the scheme in matrix form

$$B\mathbf{u}_n = C\mathbf{u}_{n-1},$$

we have

$$B = 2I + A, \quad C = 2I - A,$$

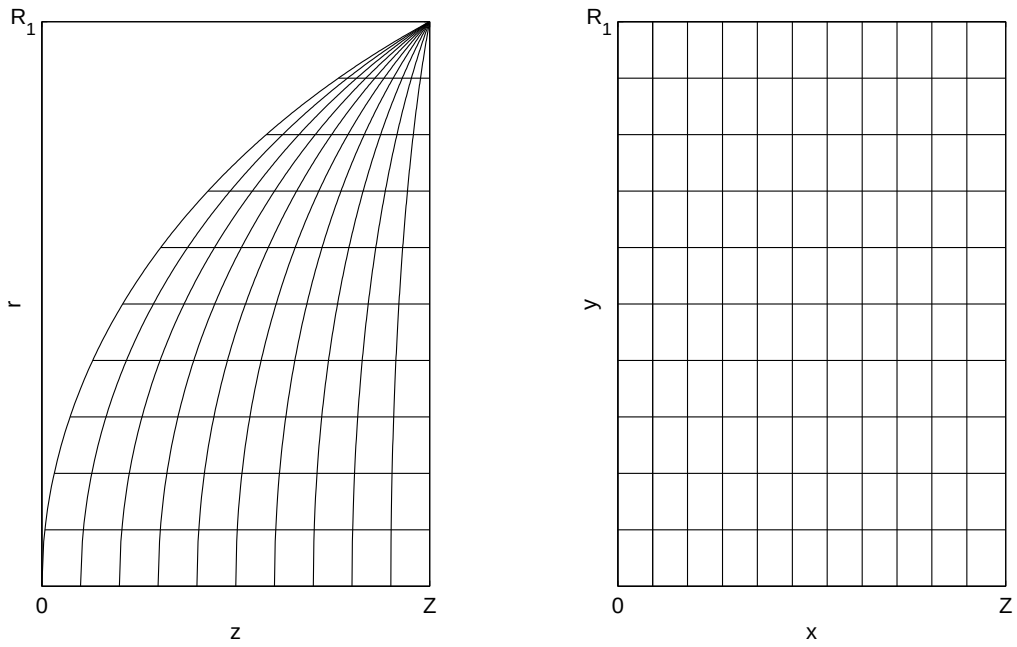

Figure 3.1: LEFT: An in-lens domain before z-stretching. RIGHT: The in-lens domain after z-stretching.

where

$$A = \begin{bmatrix} 2\alpha\gamma_0 & -2\alpha\gamma_0 & 0 & \cdots & 0 \\ -\alpha\gamma_1\left(1+\frac{1}{2(1)}\right) & 2\alpha\gamma_1 & -\alpha\gamma_1\left(1-\frac{1}{2(1)}\right) & 0 & \cdots \\ & \cdots & & & \\ & & \cdots & & \\ & & & \cdots & \\ \cdots & 0 & -\alpha\gamma_{M-1}\left(1+\frac{1}{2(M-1)}\right) & 2\alpha\gamma_{M-1} & -\alpha\gamma_{M-1}\left(1-\frac{1}{2(M-1)}\right) \\ 0 & \cdots & 0 & -2\alpha\gamma_M & 2\alpha\gamma_M \end{bmatrix}.$$

3.2 z-Stretching Stability

Theorem 3.2. *Let $x_{zr} \approx 0$. Then the z-stretched scheme is stable*

Proof. For the z-stretched scheme, we have $A = \alpha SH$, where $\alpha > 0$,

$$H = \begin{bmatrix} 2 & -2 & 0 & \cdots & 0 \\ -\left(1+\frac{1}{2(1)}\right) & 2 & -\left(1-\frac{1}{2(1)}\right) & 0 & \cdots \\ & \cdots & & & \\ & & \cdots & & \\ & & & \cdots & \\ \cdots & 0 & -\left(1+\frac{1}{2(M-1)}\right) & 2 & -\left(1-\frac{1}{2(M-1)}\right) \\ 0 & \cdots & 0 & -2 & 2 \end{bmatrix}, \; S = \begin{bmatrix} \gamma_0 & 0 & \cdots & 0 \\ 0 & \gamma_1 & 0 & \cdots \\ & \cdots & & \\ & & \cdots & \\ \cdots & 0 & \gamma_{M-1} & 0 \\ 0 & \cdots & 0 & \gamma_M \end{bmatrix}$$

Looking at H row-wise, we see that the Gershgorin circles are centered at 2, and have radius 2. Thus the eigenvalues of H are located on the closed right half of the complex plane, *i.e.* the real parts of the eigenvalues are non-negative. Subsequently,

we have

$$\gamma(x,y) = \frac{1}{2ik\theta(x,y) - \left(\psi(x,y) + \frac{1}{y}\phi(x,y)\right)}$$
$$= \frac{-\left(\psi(x,y) + \frac{1}{y}\phi(x,y)\right) - 2ik\theta(x,y)}{\left(\psi(x,y) + \frac{1}{y}\phi(x,y)\right)^2 + (2k\theta(x,y))^2}.$$

Now we examine the terms of the γ function, beginning with

$$\psi(x,0) = \begin{cases} \frac{-Z(Z-x)}{RZ^2} < 0, & 0 \le x < Z, \\ 0, & x = Z \end{cases}.$$

With respect to y, $\psi(x,y)$ changes sign at asymptote $y = \sqrt{R^2 - (R-Z)^2} = R_1$. We find that $\psi(x,y) < 0$ for $0 \le y < R_1$, $0 \le x < Z$. Next, we have

$$\frac{1}{y}\phi(x,0) = \begin{cases} \frac{-(Z-x)}{RZ} < 0, & 0 \le x < Z, \\ 0, & x = Z \end{cases}.$$

Examining ϕ, we find that $\phi(x,y) < 0$ for $0 \le y < R_1$, $0 \le x < Z$. Thus we can see that

$$\mathrm{Re}\,(\gamma(x,y)) = \frac{-\left(\psi(x,y) + \frac{1}{y}\phi(x,y)\right)}{\left(\psi(x,y) + \frac{1}{y}\phi(x,y)\right)^2 + (2k\theta(x,y))^2} \ge 0, \text{ for } 0 \le y < R_1,\ 0 \le x < Z.$$

Thus matrix S is positive semidefinite.

Consequently by Theorem 2.9, $\iota_-(\alpha HS) = \iota_-(HS) \le \iota_-(H) = 0$. Thus A is positive semistable and we can conclude that the z-stretched scheme is stable. □

3.3 z-Stretching Scheme with Cross Derivative Term

We now discard the assumption that the cross derivative term in the transformed equation (3.2) is negligible. It will be necessary therefore to establish a few results concerning partial differential equations of the form

$$c_5 u_{zr} + c_4 u_{rr} + c_3 u_r + c_2 u_z + c_1 u + c_0 = 0, \tag{3.4}$$

where $c_i,\ 0 \le i \le 5$ are functions of r and z. For the theorems and remarks to follow, let P be the differential operator such that

$$Pu = c_5 u_{zr} + c_4 u_{rr} + c_3 u_r + c_2 u_z + c_1 u + c_0. \tag{3.5}$$

We use the Taylor expansions (2.2)-(2.7) around reference point $\left(z_{n-\frac{1}{2}}, r_m\right)$ to derive

$$u_{zr} = \frac{1}{\tau}\left\{\frac{u_{m+1,n} - u_{m-1,n}}{2h} - \frac{u_{m+1,n-1} - u_{m-1,n-1}}{2h}\right\} + O(h^2). \tag{3.6}$$

We substitute the approximations (2.8)-(2.11) and (3.6) into equation (3.4) to form a six-point, two-level difference scheme as follows

$$\begin{aligned}
&\frac{c_5}{2\tau h}\left[u_{m+1,n} - u_{m-1,n} - u_{m+1,n-1} + u_{m-1,n-1}\right] \\
&+ \frac{c_4}{2h^2}\left[u_{m+1,n} - 2u_{m,n} + u_{m-1,n} + u_{m+1,n-1} - 2u_{m,n-1} + u_{m-1,n-1}\right] \\
&+ \frac{c_3}{4h}\left[u_{m+1,n} - u_{m-1,n} + u_{m+1,n-1} - u_{m-1,n-1}\right] \\
&+ \frac{c_2}{\tau}[u_{m,n} - u_{m,n-1}] + \frac{c_1}{2}\left[u_{m,n} + u_{m,n-1}\right] + c_0 = 0.
\end{aligned}$$

The above can be expressed as a difference operator in implicit form

$$\begin{aligned}
P_{\tau,h}u = &\left(\frac{c_5}{2h\tau} + \frac{c_4}{2h^2} + \frac{c_3}{4h}\right)u_{m+1,n} + \left(-\frac{c_4}{h^2} + \frac{c_2}{\tau} + \frac{c_1}{2}\right)u_{m,n} \\
&+ \left(-\frac{c_5}{2h\tau} + \frac{c_4}{2h^2} - \frac{c_3}{4h}\right)u_{m-1,n} \\
&= -\left(-\frac{c_5}{2h\tau} + \frac{c_4}{2h^2} + \frac{c_3}{4h}\right)u_{m+1,n-1} + \left(\frac{c_4}{h^2} + \frac{c_2}{\tau} - \frac{c_1}{2}\right)u_{m,n-1} \\
&- \left(\frac{c_5}{2h\tau} + \frac{c_4}{2h^2} - \frac{c_3}{4h}\right)u_{m-1,n-1} + c_0
\end{aligned} \tag{3.7}$$

where h and τ are the grid step-sizes, m and n the grid indices for the r and z directions respectively.

For the Neumann boundary conditions

$$u_r(0) = 0, \quad u_r(R_1) = 0$$

as in Section 2.1 we derive difference equations in general form

$$\begin{aligned}
&\frac{c_4}{h^2}u_{1,n} + \left(-\frac{c_4}{h^2} + \frac{c_2}{\tau} + \frac{c_1}{2}\right)u_{0,n} \\
&\quad = -\frac{c_4}{h^2}u_{1,n-1} + \left(\frac{c_4}{h^2} + \frac{c_2}{\tau} - \frac{c_1}{2}\right)u_{0,n-1} + c_0
\end{aligned} \tag{3.8}$$

and

$$\begin{aligned}&\frac{c_4}{h^2}u_{M-1,n}+\left(-\frac{c_4}{h^2}+\frac{c_2}{\tau}+\frac{c_1}{2}\right)u_{M,n}\\&\quad=-\frac{c_4}{h^2}u_{M-1,n-1}+\left(\frac{c_4}{h^2}+\frac{c_2}{\tau}-\frac{c_1}{2}\right)u_{M,n-1}+c_0.\end{aligned}\tag{3.9}$$

Theorem 3.3. *The scheme $P_{\tau,h}v=0$ has a local truncation error of order $O(\tau^2)+O(h^2)$ with respect to $Pu=0$.*

Proof. Let $u(z,r)$ be a smooth function. By substituting the Taylor expansions (2.2)-(2.7) into (3.7) and gathering terms, we see that

$$\begin{aligned}P_{\tau,h}u&=c_5\left[\frac{\partial^2u}{\partial z\partial r}+\frac{h^2}{6}\frac{\partial^4u}{\partial z\partial r^3}+\frac{\tau^2}{24}\frac{\partial^4u}{\partial z^3\partial r}+O\left(h^4\right)+O\left(h^2\tau^2\right)+O\left(\tau^4\right)\right]\\&\quad+c_4\left[\frac{\partial^2u}{\partial r^2}+\frac{h^2}{12}\frac{\partial^4u}{\partial r^4}+\frac{\tau^2}{8}\frac{\partial^4u}{\partial r^2\partial z^2}+O\left(h^4\right)+O\left(h^2\tau^2\right)+O\left(\tau^4\right)\right]\\&\quad+c_3\left[\frac{\partial u}{\partial r}+\frac{h^2}{6}\frac{\partial^3u}{\partial r^3}+\frac{\tau^2}{8}\frac{\partial^3u}{\partial r\partial z^2}+O\left(h^4\right)+O\left(h^2\tau^2\right)+O\left(\tau^4\right)\right]\\&\quad+c_2\left[\frac{\partial u}{\partial z}+\frac{\tau^2}{24}\frac{\partial^3u}{\partial z^3}+O\left(\tau^4\right)\right]+c_1\left[u_{m,n-\frac{1}{2}}+\frac{\tau^2}{8}\frac{\partial^2u}{\partial z^2}+\frac{\tau^4}{384}\frac{\partial^4u}{\partial z^4}+O\left(\tau^6\right)\right]+c_0\\&=c_5\frac{\partial^2u}{\partial z\partial r}+c_4\frac{\partial^2u}{\partial r^2}+c_3\frac{\partial u}{\partial r}+c_2\frac{\partial u}{\partial z}+c_1u_{m,n-\frac{1}{2}}+c_0\\&\quad+c_5\left[\frac{h^2}{6}\frac{\partial^4u}{\partial z\partial r^3}+\frac{\tau^2}{24}\frac{\partial^4u}{\partial z^3\partial r}\right]+c_4\left[\frac{h^2}{12}\frac{\partial^4u}{\partial r^4}+\frac{\tau^2}{8}\frac{\partial^4u}{\partial r^2\partial z^2}\right]\\&\quad+c_3\left[\frac{h^2}{6}\frac{\partial^3u}{\partial r^3}+\frac{\tau^2}{8}\frac{\partial^3u}{\partial r\partial z^2}\right]+c_2\left[\frac{\tau^2}{24}\frac{\partial^3u}{\partial z^3}\right]+c_1\left[\frac{\tau^2}{8}\frac{\partial^2u}{\partial z^2}\right]+O\left(h^4\right)\\&\quad+O\left(h^2\tau^2\right)+O\left(\tau^4\right)\\&=Pu+c_5\left[\frac{h^2}{6}\frac{\partial^4u}{\partial z\partial r^3}+\frac{\tau^2}{24}\frac{\partial^4u}{\partial z^3\partial r}\right]+c_4\left[\frac{h^2}{12}\frac{\partial^4u}{\partial r^4}+\frac{\tau^2}{8}\frac{\partial^4u}{\partial r^2\partial z^2}\right]\\&\quad+c_3\left[\frac{h^2}{6}\frac{\partial^3u}{\partial r^3}+\frac{\tau^2}{8}\frac{\partial^3u}{\partial r\partial z^2}\right]+c_2\left[\frac{\tau^2}{24}\frac{\partial^3u}{\partial z^3}\right]+c_1\left[\frac{\tau^2}{8}\frac{\partial^2u}{\partial z^2}\right]+O\left(h^4\right)\\&\quad+O\left(h^2\tau^2\right)+O\left(\tau^4\right).\end{aligned}$$

Thus the truncation error

$$\begin{aligned} P_{\tau,h} - Pu = c_5 &\left[\frac{h^2}{6}\frac{\partial^4 u}{\partial z \partial r^3} + \frac{\tau^2}{24}\frac{\partial^4 u}{\partial z^3 \partial r}\right] + c_4 \left[\frac{h^2}{12}\frac{\partial^4 u}{\partial r^4} + \frac{\tau^2}{8}\frac{\partial^4 u}{\partial r^2 \partial z^2}\right] \\ &+ c_3 \left[\frac{h^2}{6}\frac{\partial^3 u}{\partial r^3} + \frac{\tau^2}{8}\frac{\partial^3 u}{\partial r \partial z^2}\right] + c_2 \left[\frac{\tau^2}{24}\frac{\partial^3 u}{\partial z^3}\right] + c_1 \left[\frac{\tau^2}{8}\frac{\partial^2 u}{\partial z^2}\right] \\ &+ O\left(h^4\right) + O\left(h^2\tau^2\right) + O\left(\tau^4\right) = O\left(\tau^2\right) + O\left(h^2\right). \end{aligned}$$

This completes our proof. □

Corollary 3.1. *The scheme $P_{\tau,h}v = 0$ has local order of accuracy $(2, 2)$.*

Proof. By Theorem 3.3,

$$P_{\tau,h} - Pu = O\left(\tau^2\right) + O\left(h^2\right).$$

Thus $P_{\tau,h}v = 0$ has local order of accuracy $(2, 2)$ with respect to $Pu = O$. □

Theorem 3.4. *The scheme $P_{\tau,h}v = 0$ is consistent with differential equation $Pu = 0$.*

Proof. By Theorem 3.3

$$P_{\tau,h} - Pu = O\left(\tau^2\right) + O\left(h^2\right) \to 0$$

as $\tau, h \to 0$. Thus the scheme $P_{\tau,h}v = 0$ is consistent with differential equation $Pu = 0$. □

With a non-negligible cross derivative term, our transformed equation (3.2) becomes

$$\left(2ik\theta - \psi - \frac{1}{y}\phi\right) u_x = \frac{1}{y}u_y + u_{yy} + 2\phi u_{xy}. \tag{3.10}$$

The coefficients of our simplified equation with cross derivative term are

$$c_5 = 2\phi, \quad c_4 = 1, \quad c_3 = \frac{1}{y}, \quad c_2 = -\left(2ik\theta - \psi - \frac{1}{y}\phi\right), \quad c_1 = 0, \quad c_0 = 0.$$

Substituting the specific coefficient c_i values into (3.7) we obtain the scheme

$$\left(\frac{2\phi}{2h\tau} + \frac{1}{2h^2} + \frac{1}{4hy}\right) u_{m+1,n} + \left(-\frac{1}{h^2} - \frac{1}{\tau}\left[2ik\theta - \psi - \frac{1}{y}\phi\right]\right) u_{m,n}$$

$$+\left(-\frac{2\phi}{2h\tau}+\frac{1}{2h^2}-\frac{1}{4hy}\right)u_{m-1,n}=-\left(-\frac{2\phi}{2h\tau}+\frac{1}{2h^2}+\frac{1}{4hy}\right)u_{m+1,n-1}$$
$$+\left(\frac{1}{h^2}-\frac{1}{\tau}\left[2ik\theta-\psi-\frac{1}{y}\phi\right]\right)u_{m,n-1}-\left(\frac{2\phi}{2h\tau}+\frac{1}{2h^2}-\frac{1}{4hy}\right)u_{m-1,n-1}.$$

On the grid lines $y=mh$, we can write the above as

$$\begin{aligned}&-\gamma\left[\frac{2\phi}{h}+\alpha\left(1+\frac{1}{2m}\right)\right]u_{m+1,n}+(2+2\alpha\gamma)u_{m,n}-\gamma\left[-\frac{2\phi}{h}+\alpha\left(1-\frac{1}{2m}\right)\right]u_{m-1,n}\\&=\gamma\left[-\frac{2\phi}{h}+\alpha\left(1+\frac{1}{2m}\right)\right]u_{m+1,n-1}+(2-2\alpha\gamma)u_{m,n-1}\\&\quad+\gamma\left[\frac{2\phi}{h}+\alpha\left(1-\frac{1}{2m}\right)\right]u_{m-1,n-1}\end{aligned}\tag{3.11}$$

where

$$\alpha=\frac{\tau}{h^2},\quad \gamma(x,y)=\frac{1}{2ik\theta-\psi-\frac{1}{y}\phi}.$$

Substituting the specific coefficient values into the general form for the boundary value difference equations, we obtain

$$-2\alpha\gamma u_{1,n}+(2+2\alpha\gamma)\,u_{0,n}=2\alpha\gamma u_{1,n-1}+(2-2\alpha\gamma)\,u_{0,n-1},$$

and

$$(2+2\alpha\gamma)\,u_{M,n}-2\alpha\gamma u_{M-1,n}=(2-2\alpha\gamma)\,u_{M,n-1}+2\alpha\gamma u_{M-1,n-1}.$$

3.4 Stability of z-Stretching scheme with Cross Derivative Term

To determine the stability of the z-stretching scheme with the cross derivative term, we will need to establish additional lemmas concerning matrices.

Lemma 3.1. *Let $A\in\mathbb{C}^{n\times n}$ be nonsingular. Then $A+A^*$ is positive definite if and only if $A^{-1}+(A^{-1})^*$ is positive definite.*

Proof. Let $A\in\mathbb{C}^{n\times n}$ such that A is nonsingular and $A+A^*$ is positive definite. Then

$$\mathbf{x}^*\left(A+A^*\right)\mathbf{x}>0\text{ , for all nonzero }\mathbf{x}\in\mathbb{C}^n.$$

Let $\mathbf{x} \in \mathbb{C}^n$. Since A is nonsingular, $\exists \mathbf{y} \in \mathbb{C}^n$ such that $\mathbf{x} = A\mathbf{y}$. Then

$$\begin{aligned}
\mathbf{x}^* \left(A^{-1} + \left(A^{-1}\right)^*\right) \mathbf{x} &= \mathbf{x}^* A^{-1} \mathbf{x} + \mathbf{x}^* \left(A^{-1}\right)^* \mathbf{x} \\
&= (A\mathbf{y})^* A^{-1} A\mathbf{y} + (A\mathbf{y})^* \left(A^{-1}\right)^* A\mathbf{y} \\
&= \mathbf{y}^* A^* \mathbf{y} + \mathbf{y}^* A^* \left(A^*\right)^{-1} A\mathbf{y} \\
&= \mathbf{y}^* A^* \mathbf{y} + \mathbf{y}^* A\mathbf{y} \\
&= \mathbf{y}^* \left(A + A^*\right) \mathbf{y} > 0.
\end{aligned}$$

□

Lemma 3.2. *Let $A, B \in \mathbb{C}^{n\times n}$ with A positive semistable and B nonsingular. Further assume $B + B^*$ is positive definite. Then AB^{-1} is positive semistable.*

Proof. Let $A, B \in \mathbb{C}^{n\times n}$ with A positive semistable, B nonsingular, and $B + B^*$ positive definite. By Lemma 3.1, $B^{-1} + (B^{-1})^*$ is positive definite. By Lemma 2.4, $\iota\left(AB^{-1}\right) = \iota(A)$. Thus AB^{-1} is positive semistable. □

Theorem 3.5. *Let $A, B, C, G \in \mathbb{C}^{n\times n}$ be such that G is nonsingular and*

$$B = G + A, \quad C = G - A.$$

Then the difference scheme defined by

$$B\boldsymbol{u}_n = C\boldsymbol{u}_{n-1}$$

is stable if and only if AG^{-1} is positive semistable.

Proof. Let $A, B, C, \widetilde{B}, \widetilde{C}, G \in \mathbb{C}^{n\times n}$ be such that G is nonsingular and

$$B = G + A, \quad C = G - A, \quad \widetilde{B} = I + AG^{-1}, \quad \widetilde{C} = I - AG^{-1}$$

We note that the matrix $B^{-1}C$ is similar to the matrix $\widetilde{B}^{-1}\widetilde{C}$. Specifically

$$\begin{aligned}
G\left(B^{-1}C\right)G^{-1} &= G\left(G + A\right)^{-1}\left(G - A\right)G^{-1} \\
&= \left((G + A)G^{-1}\right)^{-1}\left(G - A\right)G^{-1} \\
&= \left(I + AG^{-1}\right)^{-1}\left(I - AG^{-1}\right) = \widetilde{B}^{-1}\widetilde{C}.
\end{aligned}$$

Then $\rho(B^{-1}C) = \rho(\widetilde{B}^{-1}\widetilde{C})$, and we see that the difference scheme defined by

$$B\mathbf{u}_n = C\mathbf{u}_{n-1}$$

is stable if and only if the scheme

$$\widetilde{B}\mathbf{u}_n = \widetilde{C}\mathbf{u}_{n-1}$$

is stable. Thus the conclusion follows from Theorem 2.5. □

Theorem 3.6. *Let* $Re\left(\gamma\left(x,y\right)\right) \geq 0$ *for* $0 \leq y < R_1$ *and*

$$\left|\frac{2\gamma\left(x,y\right)\phi\left(x,y\right)}{h}\right| < 1 \text{ for } \ 0 \leq y < R_1, \ \ 0 \leq x < Z.$$

Then scheme (3.11) *is stable.*

Proof. Let $\mathrm{Re}\left(\gamma\left(x,y\right)\right) \geq 0$ for $0 \leq y < R_1$ and

$$\left|\frac{2\gamma\left(x,y\right)\phi\left(x,y\right)}{h}\right| < 1 \text{ for } \ 0 \leq y < R_1, \ \ 0 \leq x < Z.$$

Expressing scheme (3.11) in matrix form

$$B\mathbf{u}_n = C\mathbf{u}_{n-1}$$

we have

$$B = \left(G + A\right), \ \ C = \left(G - A\right)$$

where matrix A is the same as in the z-stretching with no cross derivative scheme, and

$$G = \begin{bmatrix} 2 & 0 & 0 & \cdots & 0 \\ -\frac{\gamma_1\phi_1}{h} & 2 & \frac{\gamma_1\phi_1}{h} & 0 & \cdots \\ & \cdots & & & \\ & & \cdots & & \\ & & & \cdots & \\ \cdots & 0 & -\frac{\gamma_{M-1}\phi_{M-1}}{h} & 2 & \frac{\gamma_{M-1}\phi_{M-1}}{h} \\ 0 & \cdots & 0 & 0 & 2 \end{bmatrix}$$

where $\gamma_m = \gamma(x, mh)$ and $\phi_m = \gamma(x, mh)$.

Then

$$G + G^* = \begin{bmatrix} 2 & \overline{-\frac{\gamma_1\phi_1}{h}} & 0 & \cdots & 0 \\ -\frac{\gamma_1\phi_1}{h} & 2 & \frac{\gamma_1\phi_1}{h} - \overline{\frac{\gamma_2\phi_2}{h}} & 0 & \cdots \\ & \cdots & & & \\ & & \cdots & & \\ & & & \cdots & \\ \cdots & 0 & \overline{\frac{\gamma_{M-2}\phi_{M-2}}{h}} - \frac{\gamma_{M-1}\phi_{M-1}}{h} & 2 & \frac{\gamma_{M-1}\phi_{M-1}}{h} \\ 0 & \cdots & 0 & \overline{\frac{\gamma_{M-1}\phi_{M-1}}{h}} & 2 \end{bmatrix}.$$

We will apply Sylvester's Criterion, which states that a Hermitian matrix A is positive definite if and only if all principal minors of A have a positive determinate [26]. For a tridiagonal matrix, we observe that the determinates of the principle minors can be expressed in recursive form as so

$$\det [A]_{\{k,\ldots,n\}} = a_{n,n} \det [A]_{\{k,\ldots,n-1\}} - a_{n,n-1}a_{n-1,n} \det [A]_{\{k,\ldots,n-2\}} .$$

With our assumptions it is straightforward to demonstrate via induction that all principal minors have positive determinate. Thus $G + G^*$ is positive definite. We demonstrated in the previous case that A is positive semistable, thus by Lemma 3.2, AG^{-1} is positive semistable. Then by Theorem 3.5, we see that our scheme is stable. □

3.5 Numerical Results

Simulation results were obtained using the z-stretching method with cross-derivative term included. Within the lens segment, the grid utilized 5,000 points in the transverse y-direction and 32,000 points in the x-direction of propagation. The function (1.14) approximating a Gaussian beam with point source was used as the initial value, with point source located at $z_0 = 10$ cm., and beam width $\beta_0 = 1.5$ cm.

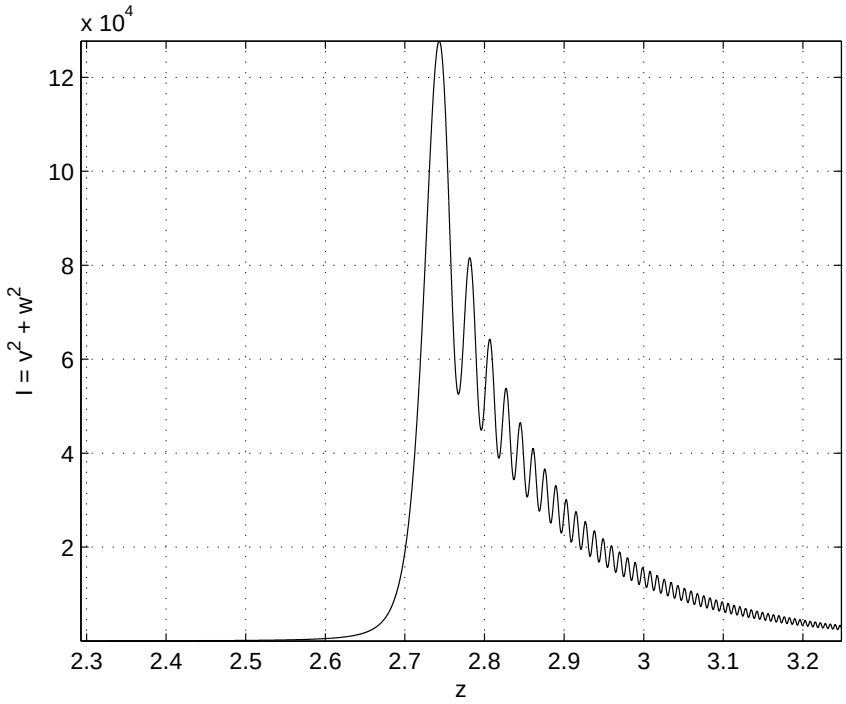

Figure 3.2: z-stretch simulation: intensity of the computed solution near the z-axis, at $r = h$.

The post-peak oscillation in the graph of the solution intensity near the z-axis matches behavior observed in experimental data.

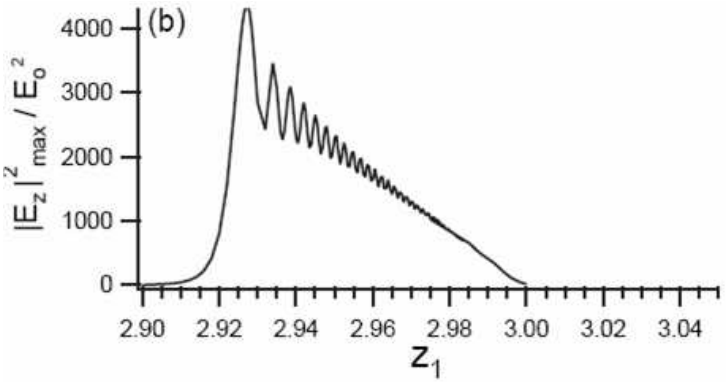

Figure 3.3. Normalized intensity graph of experimental data.

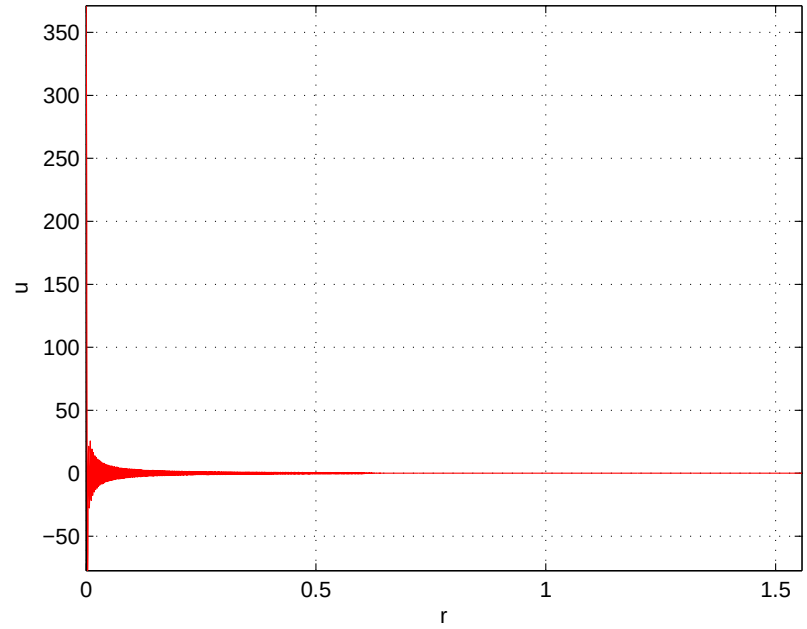

Figure 3.4: z-stretch simulation: real part of the computed solution at the focal point $z = 2.74$ cm.

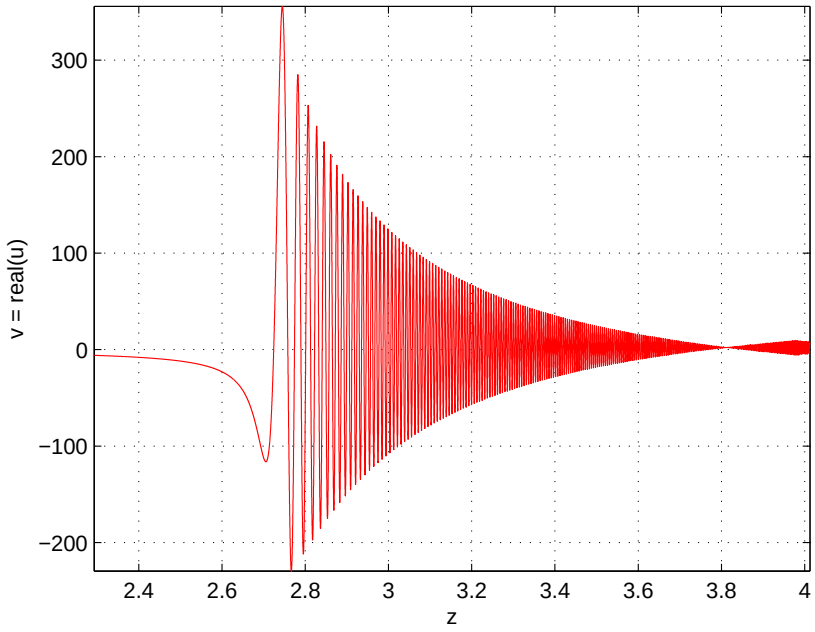

Figure 3.5: z-stretch simulation: amplitude of the real part of the computed solution near the z-axis, at $r = h$.

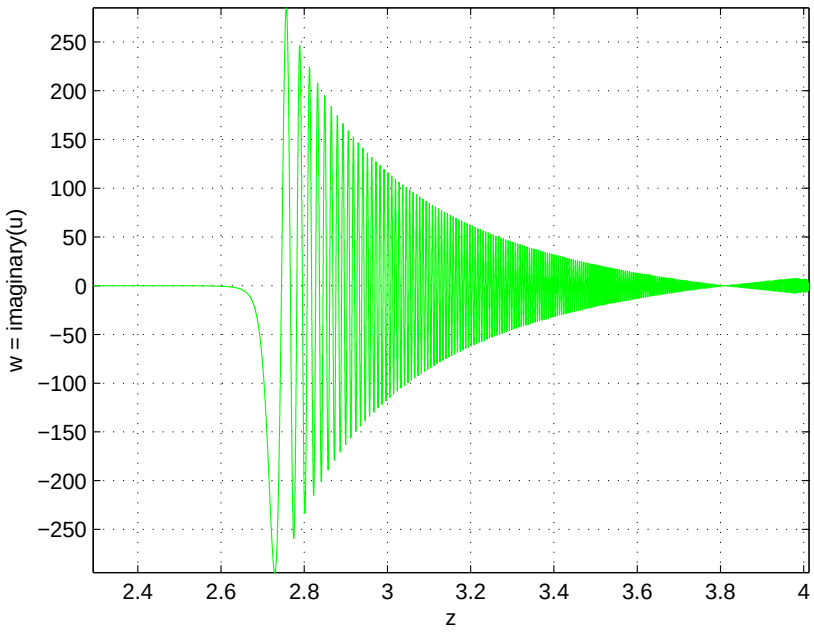

Figure 3.6: z-stretch simulation: amplitude of the imaginary part of the computed solution near the z-axis, at $r = h$.

CHAPTER FOUR

Moving Mesh Methods

4.1 Stretching in the r Direction

We next consider stretching only in the transverse r direction. It will be convenient in this case to formulate our transformation in terms of the mappings from the computational space to the physical space, $r = r(x, y)$ and $z = x$. We see that

$$\frac{\partial z}{\partial x} = 1, \quad \frac{\partial^2 z}{\partial x^2} = 0, \quad \frac{\partial z}{\partial y} = 0, \quad \frac{\partial^2 z}{\partial y^2} = 0.$$

We first derive the transformed derivatives

$$\begin{aligned}
\frac{\partial u}{\partial x} &= \frac{\partial u}{\partial z}\frac{\partial z}{\partial x} + \frac{\partial u}{\partial r}\frac{\partial r}{\partial x} = \frac{\partial u}{\partial z} + \frac{\partial u}{\partial r}\frac{\partial r}{\partial x}, \\
\frac{\partial u}{\partial y} &= \frac{\partial u}{\partial z}\frac{\partial z}{\partial y} + \frac{\partial u}{\partial r}\frac{\partial r}{\partial y} = \frac{\partial u}{\partial r}\frac{\partial r}{\partial y}, \\
\frac{\partial^2 u}{\partial y^2} &= \left(\frac{\partial u}{\partial r}\frac{\partial r}{\partial y}\right)_y = \left(\frac{\partial^2 u}{\partial z \partial r}\frac{\partial z}{\partial y} + \frac{\partial^2 u}{\partial r^2}\frac{\partial r}{\partial y}\right)\frac{\partial r}{\partial y} + \frac{\partial u}{\partial r}\frac{\partial^2 r}{\partial y^2} \\
&= \left(\frac{\partial^2 u}{\partial r^2}\frac{\partial r}{\partial y}\right)\frac{\partial r}{\partial y} + \frac{\partial u}{\partial r}\frac{\partial^2 r}{\partial y^2} = \frac{\partial^2 u}{\partial r^2}\left(\frac{\partial r}{\partial y}\right)^2 + \frac{\partial u}{\partial r}\frac{\partial^2 r}{\partial y^2}.
\end{aligned}$$

Isolating the derivatives in the physical space, we find

$$u_z = u_x - u_y\left(\frac{r_x}{r_y}\right), \quad u_r = \frac{1}{r_y}u_y, \quad u_{rr} = \frac{u_{yy}r_y - u_y r_{yy}}{r_y^3}.$$

Substituting the above into Equation (3.1), we obtain the transformed partial differential equation

$$2ik\left[u_x - u_y\left(\frac{r_x}{r_y}\right)\right] = \frac{u_{yy}r_y - u_y r_{yy}}{r_y^3} + \frac{1}{r r_y}u_y.$$

Collecting derivative terms we can rewrite this as

$$2ikr_y u_x = \frac{1}{r_y}u_{yy} + \left(2ikr_x - \frac{r_{yy}}{r_y^2} + \frac{1}{r}\right)u_y. \tag{4.1}$$

The transformation function r has the properties that

$$r(0) = 0, \quad r(R_1) = R_1, \quad r_y(0) > 0, \quad r_y(R_1) > 0.$$

Then the relation

$$\frac{\partial u}{\partial y} = \frac{\partial u}{\partial z}\frac{\partial z}{\partial y} + \frac{\partial u}{\partial r}\frac{\partial r}{\partial y} = \frac{\partial u}{\partial r}\frac{\partial r}{\partial y}$$

implies the transformed boundary conditions

$$\frac{\partial u}{\partial y}(0) = 0, \quad \frac{\partial u}{\partial y}(R_1) = 0.$$

Next, we define a finite difference scheme by the method described in Section 2.1. Our coefficients are

$$c_{h,0} = 0, \quad c_{h,1} = 0, \quad c_{h,2} = -2ik_h r_y, \quad c_{h,3} = 2ik_h r_x - \frac{r_{yy}}{r_y^2} + \frac{1}{r}, \quad c_{h,4} = \frac{1}{r_y}. \tag{4.2}$$

Substituting these coefficients into (2.15), we obtain the scheme

$$\begin{aligned}
&\left(\frac{1}{2h^2 r_y} + \frac{1}{4h}\left[2ik_h r_x - \frac{r_{yy}}{r_y^2} + \frac{1}{r}\right]\right) u_{m+1,n} + \left(-\frac{1}{h^2 r_y} - \frac{2ik_h r_y}{\tau}\right) u_{m,n} \\
&\quad + \left(\frac{1}{2h^2 r_y} - \frac{1}{4h}\left[2ik_h r_x - \frac{r_{yy}}{r_y^2} + \frac{1}{r}\right]\right) u_{m-1,n} \\
= &\quad -\left(\frac{1}{2h^2 r_y} + \frac{1}{4h}\left[2ik_h r_x - \frac{r_{yy}}{r_y^2} + \frac{1}{r}\right]\right) u_{m+1,n-1} + \left(\frac{1}{h^2 r_y} - \frac{2ik_h r_y}{\tau}\right) u_{m,n-1} \\
&\quad - \left(\frac{1}{2h^2 r_y} - \frac{1}{4h}\left[2ik_h r_x - \frac{r_{yy}}{r_y^2} + \frac{1}{r}\right]\right) u_{m-1,n-1}.
\end{aligned}$$

Setting $\alpha = \dfrac{\tau}{2h^2}$, we rewrite the above as

$$\begin{aligned}
&\frac{i\alpha}{k_h r_y^2}\left(1 + \frac{hr_y}{2}\left[2ik_h r_x - \frac{r_{yy}}{r_y^2} + \frac{1}{r}\right]\right) u_{m+1,n} + \left(-\frac{2i\alpha}{k_h r_y^2} + 2\right) u_{m,n} \\
&\quad + \frac{i\alpha}{k_h r_y^2}\left(1 - \frac{hr_y}{2}\left[2ik_h r_x - \frac{r_{yy}}{r_y^2} + \frac{1}{r}\right]\right) u_{m-1,n} \\
&= -\frac{i\alpha}{k_h r_y^2}\left(1 + \frac{hr_y}{2}\left[2ik_h r_x - \frac{r_{yy}}{r_y^2} + \frac{1}{r}\right]\right) u_{m+1,n-1} + \left(\frac{2i\alpha}{k_h r_y^2} + 2\right) u_{m,n-1} \\
&\quad - \frac{i\alpha}{k_h r_y^2}\left(1 - \frac{hr_y}{2}\left[2ikr_x - \frac{r_{yy}}{r_y^2} + \frac{1}{r}\right]\right) u_{m-1,n-1}.
\end{aligned} \tag{4.3}$$

We likewise substitute the specific coefficient c_i values into (2.17) and (2.19) to form the difference equations for the boundary conditions.

$$\frac{2i\alpha}{k_h r_y^2} u_{1,n} + \left(-\frac{2i\alpha}{k_h r_y^2} + 2\right) u_{0,n} = -\frac{2i\alpha}{k_h r_y^2} u_{1,n-1} + \left(\frac{2i\alpha}{k_h r_y^2} + 2\right) u_{0,n-1} \tag{4.4}$$

and

$$\left(-\frac{2i\alpha}{k_h r_y^2}+2\right)u_{M,n}+\frac{2i\alpha}{k_h r_y^2}u_{M-1,n}=\left(\frac{2i\alpha}{k_h r_y^2}+2\right)u_{M,n-1}-\frac{2i\alpha}{k_h r_y^2}u_{M-1,n-1}. \tag{4.5}$$

Theorem 4.1. *The scheme* (4.3) *has truncation error*

$$2i\left(k_h-k\right)\left(r_y u_x-r_x u_y\right)+O\left(\tau^2\right)+O\left(h^2\right).$$

with respect to the transformed equation (4.1).

Proof. By Theorem 2.3, the truncation error is

$$\begin{aligned}&\left(c_{h,4}-c_4\right)\frac{\partial^2 u}{\partial y^2}+\left(c_{h,3}-c_3\right)\frac{\partial u}{\partial y}+\left(c_{h,2}-c_2\right)\frac{\partial u}{\partial x}\\&+\left(c_{h,1}-c_1\right)u_{m,n-\frac{1}{2}}+c_{h,0}-c_0+O\left(\tau^2\right)+O\left(h^2\right)\end{aligned}$$

Substituting the specific coefficients (4.2) into the above, we obtain a truncation error of

$$2i\left(k_h-k\right)\left(r_y u_x-r_x u_y\right)+O\left(\tau^2\right)+O\left(h^2\right).$$

□

4.2 Stability in the Transformed Space

Theorem 4.2. *Let* $H\in\mathbb{C}^{M\times M}$ *be such that*

$$H=\begin{bmatrix}-2 & 2 & 0 & \cdots & 0\\ 1-\theta_1 & -2 & 1+\theta_1 & 0 & \cdots\\ & \cdots & & & \\ & & \cdots & & \\ & & & \cdots & \\ \cdots & 0 & 1-\theta_{M-1} & -2 & 1+\theta_{M-1}\\ 0 & \cdots & 0 & 2 & -2\end{bmatrix},$$

where

$$\theta_m = \frac{hr_y(mh)}{2}\left[2ik_h(mh)r_x(mh) - \frac{r_{yy}(mh)}{r_y^2(mh)} + \frac{1}{r(mh)}\right]$$

and r is the r-stretching transformation $r = r(x, y)$. Then the difference scheme (4.3), (4.4), (4.5) *is stable if and only if the matrix iH is positive semistable.*

Proof. We can express the scheme (4.3), (4.4), (4.5) in matrix form

$$B\mathbf{u}_n = C\mathbf{u}_{n-1}$$

with

$$B = 2I + A, \quad C = 2I - A, \quad A = i\alpha SH,$$

$$\alpha = \frac{\tau}{h^2}, \quad S = \begin{bmatrix} \varphi_0 & 0 & \cdots & 0 \\ 0 & \varphi_1 & 0 & \cdots \\ & \cdots & & \\ & & \cdots & \\ \cdots & 0 & \varphi_{M-1} & 0 \\ 0 & \cdots & 0 & \varphi_M \end{bmatrix}, \quad \varphi_m = \frac{1}{k_h(mh)r_y^2(mh)},$$

and H is as above. By Theorem 2.5, the scheme is stable if and only if A is positive semistable. Since $k_h(y) > 0$, $r_y(y) > 0$, for all $0 \le y \le R_1$, S is positive definite. Also, $\alpha > 0$, therefore αS is positive definite. Thus $A = (\alpha S)(iH)$ is positive semistable if and only if iH is positive semistable. □

Definition 4.1. A *refinement path* is a sequence of mesh sizes τ and h, both of which tend to zero. We typically specify a relationship between τ and h, for example,

$$\tau \le Ch$$

for some constant C, as a constraint on the refinement path.

For the r-stretching method, as $h \to 0$, the transform function and derivatives are dependent on h. To evaluate stability, we have the following theorem.

Theorem 4.3. *We assume a constraint on the refinement path of*

$$\tau \leq Ch$$

for some constant C. Let the transform function, $r(x, y, h)$, and derivatives of the r-stretching method be such that

$$|\theta_m| \to 0, \text{ as } h \to 0, \text{ for all } 0 \leq m \leq M-1.$$

Then the eigenvalues of iH approach pure imaginary as $h \to 0$.

Proof. As $h \to 0$, $H \to H_0$ where

$$H_0 = \begin{bmatrix} -2 & 2 & 0 & \cdots & 0 \\ 1 & -2 & 1 & 0 & \cdots \\ & \cdots & & & \\ & & \cdots & & \\ & & & \cdots & \\ \cdots & 0 & 1 & -2 & 1 \\ 0 & \cdots & 0 & 2 & -2 \end{bmatrix}.$$

Since the subdiagonal and superdiagonal entries of H_0 are all positive reals, by Lemma 2.3, the eigenvalues of H_0 are real. Eigenvalues are a continuous function of the coefficients of a matrix, thus the eigenvalues of iH approach pure imaginary as $h \to 0$. □

4.3 Adaptive Grid Methods

We will examine previous adaptive grid methods in greater detail, to determine what ideas and methods we can apply to our adaptive techniques.

4.3.1 Adaptive Mesh Refinement

Berger and Oliger introduced the Adaptive Mesh Refinement (AMR) method in 1984, originally applied to hyperbolic partial differential equations [8]. The technique

proceeds as follows: A base grid consisting of one or more component meshes of points with uniform spacing in each coordinate direction and with sufficient resolution for those regions of least variability in the solution is constructed for the entire domain. During computation, smaller subgrids are placed in regions of greater variability. These subgrids are rectangular, possibly rotated with respect to the base grid, and have a finer mesh with uniform grid spacings in each coordinate direction that have the same relative ratios as the grid spacings in the base grid.

The points of the mesh of a subgrid do not have to line up with the points of the base grid in any way. Initial and boundary values for the subgrid are obtained through interpolation from the values calculated on the coarser grid, and a separate solution is then computed for the grid with these boundary values. If the subgrid is rotated with respect to the base grid, the difference equations are transformed onto the rotated coordinates. Successively finer subgrids may be placed on top subgrids recursively.

To generate subgrids, truncation error for points on a coarse grid are estimated using a Richardson extrapolation and a finer subgrid is placed to cover each region where the error estimate is greater than a determined tolerance. Refinement is by an arbitrary even integer ratio, which in numerical examples is typically chosen to be four [10]. Rotation is used if it is desirable that a feature of the solution should be normal or tangent to a coordinate direction. If for some area within a subgrid, error estimates are still too high, finer subgrids are applied in a nested hierarchy.

The Adaptive Mesh Refinement method was applied to several one and two dimensional shock problems and compared to simulations using uniform meshes with the resolution of the finest subgrid. Considerable savings were achieved in computation time and storage requirement, with error estimates being comparable, or in some cases better due to rotation of the subgrids [8].

4.3.2 Grid Redistribution

Grid redistribution or "moving mesh" methods utilize a fixed number of spatial grid points. These grid points are "moved" within the physical space so that a higher concentration of them occur in regions where, because of some local solution feature such as greater variability, more points are needed to represent the solution accurately.

The repositioning of the grid points is achieved via coordinate transformation. Beginning with a uniform grid in a rectangular computational space, a 1-1 mapping is defined from the computational space to the physical space. As the simulation proceeds, the mapping is dynamically adapted to reposition grid points where needed in the physical space at each propagation step.

The study of how to define useful mappings is a well-developed field referred to as *grid generation* or *mesh generation* [24, 39, 71]. An example mapping would be the widely used transformation of cartesian coordinates into polar, cylindrical or spherical coordinates. Such a transformation from a uniform coordinate system onto a general space corresponds directly to the concept of a general *curvilinear coordinate* system for the physical space, as used in differential geometry and other fields. Typically, the boundary of the computational space corresponds to the boundary of physical space. Magnifying a particular subregion in a physical domain via coordinate transformation is functionally equivalent to decreasing the grid spacings in that region.

The numerical computation occurs on the uniform grid in the computational space, sometimes called the *logical space*. The partial differential equations to be solved in the physical space must be transformed into the uniform coordinate system. The mapping must possess certain properties for the transformed equations to be valid.

Definition 4.2. For a coordinate transformation

$$z = z(x, y), \quad r = r(x, y),$$

the matrix

$$\mathfrak{J} = \begin{bmatrix} \frac{\partial z}{\partial x} & \frac{\partial z}{\partial y} \\ \frac{\partial r}{\partial x} & \frac{\partial r}{\partial y} \end{bmatrix}$$

is called the *Jacobian matrix* of the transformation, while the determinate $\mathbf{J} = |\mathfrak{J}|$ is referred to as the *Jacobian*.

The quality of the transformation can be determined by properties of the Jacobian. For instance, for the transformation to be 1-1, the Jacobian must have full rank.

Transformations are often designed to distribute some function, called a *monitor function* evenly throughout the physical domain. Most such techniques are based on the equidistribution principle of de Boor [18].

The calculus of variations is commonly employed to obtain a mesh generating equation. The minimizer of a functional can be used to obtain a partial differential equation which is solved by numerical means to generate transformed grid coordinates. We will use this technique to obtain a mesh generator for our r-stretching method.

4.4 A Mesh Generator

We choose the monitor function

$$g(y) = [r(y) + \sigma_r(r(y))]^2 = ([1 + \sigma_r(r(y))]\, r_y)^2 .$$

Our object is to produce a mesh generator that will concentrate up to half of the grid points in the region of the interface, without increasing the spacing by more than a factor of 2 between points away from the interface.

Theorem 4.4. *For a continuous sigma function $\sigma(r)$, a unique solution of the initial value problem*

$$[1 + R_1\sigma_r\,(r(y))]\, r_y = 2, \tag{4.6}$$

$$r(0) = 0 \tag{4.7}$$

exists and has the following properties:

(*i*) $r(R_1) = R_1$

(*ii*) $\max(r_y) < 2, \quad 0 \le y \le R_1$

(*iii*) $\max(R_1\sigma(y)) = \max(R_1\sigma_r\left(r(y)\right) r_y) < 2, \quad 0 \le y \le R_1$

Proof. Let $f(r) = y = \frac{1}{2}\left(r + R_1\sigma(r)\right)$. Our sigma functions are monotonically increasing and

$$\sigma(0) = 0, \quad \sigma(R_1) = 1.$$

Thus $f(r)$ is monotonically increasing, and

$$f(0) = 0, \quad f(R_1) = \frac{1}{2}\left(R_1 + R_1\sigma(R_1)\right) = R_1.$$

Then we have the inverse function $r(y) = f^{-1}(y)$, which is monotonically increasing, and

$$r_y = \frac{1}{f'\left(f^{-1}(y)\right)} = \frac{2}{1 + R_1\sigma_r\left(r(y)\right)}.$$

Substituting $f^{-1}(y)$ into (4.6), we see that it is a solution.

(*i*) We have $r(R_1) = f^{-1}(R_1) = R_1$.

(*ii*) Assume $r_y \ge 2$. Then $1 + R_1\sigma_r(r(y)) \le 1$ and therefore $R_1\sigma_r(r(y)) \le 0$. Contradicts $R_1 > 0$ and $\sigma(r)$ monotonically increasing. Thus $r_y < 2$.

(*iii*) Assume $R_1\sigma_r\left(r(y)\right) r_y \ge 2$. Then $r(y) \le 0$, which contradicts $r(y)$ monotonically increasing. Thus $R_1\sigma_r\left(r(y)\right) r_y < 2$.

□

Theorem 4.5. *The solution of* (4.6), (4.7) *minimizes the functional*

$$I(r) = \int_0^{R_1} \left(\sigma_r(r(y))r_y + r_y\right)^2 dy$$
$$= \int_0^{R_1} \left\{\left[\sigma_r(r(y)) + 1\right] r_y\right\}^2 dy$$

over the set of admissible functions $r(y)$, *such that*

$$r(y) \in C^2[0, R_1], \quad r(0) = 0, \quad r(R_1) = R_1.$$

Proof. Let $I(r)$ be the functional defined above and $c(y) \in C^2[0, R_1]$ be a function such that

$$c(0) = c(R_1) = 0.$$

Then for any $\varepsilon > 0$, the function $t(y, \varepsilon) = r(y) + \varepsilon c(y)$ is admissible. We define a function of ε,

$$F(\varepsilon) = \int_0^{R_1} \left[(\sigma_t(t(y, \varepsilon)) + 1) (r_y + \varepsilon c_y) \right]^2 dy$$

If $r(y)$ minimizes the functional $I(r)$, we must have a minimum of $F(\varepsilon)$ at $\varepsilon = 0$. We examine the derivative

$$F'(\varepsilon) = \int_0^{R_1} 2 \left\{ \left[(\sigma_t(t(y, \varepsilon)) + 1) t_y \right] \left[c(y) \sigma_{tt}(t(y, \varepsilon)) t_y + c_y (\sigma_t(t(y, \varepsilon)) + 1) \right] \right\} dy$$

at $\varepsilon = 0$,

$$F'(0) = \int_0^{R_1} 2 \left\{ \left[(\sigma_r(r(y)) + 1) r_y \right] \left[c(y) \sigma_{rr}(r(y)) r_y + c_y (\sigma_r(r(y)) + 1) \right] \right\} dy$$

$$= 2 \left\{ \int_0^{R_1} c(y) \left[\sigma_r(r(y)) + 1 \right] \sigma_{rr}(r(y)) r_y^2 dy + \int_0^{R_1} c_y \left[\sigma_r(r(y)) + 1 \right]^2 r_y \right\}$$

$$= 2 \int_0^{R_1} c(y) \left[\sigma_r(r(y)) + 1 \right] \sigma_{rr}(r(y)) r_y^2 dy$$

$$-2 \int_0^{R_1} c(y) \left(2 \left[\sigma_r(r(y)) + 1 \right] r_y^2 \sigma r r(r(y)) + \left[\sigma_r(r(y)) + 1 \right]^2 \right)$$

$$= 2 \int_0^{R_1} c(y) \left\{ - \left[\sigma_r(r(y)) + 1 \right] r_y^2 \sigma_{rr}(r(y)) + \left[\sigma_r(r(y)) + 1 \right]^2 r_{yy} \right\} dy = 0.$$

Since the equation holds for arbitrary $c(y)$, we must have

$$- \left[\sigma_r(r(y)) + 1 \right] r_y^2 \sigma_{rr}(r(y)) + \left[\sigma_r(r(y)) + 1 \right]^2 r_{yy} = 0.$$

We can divide through by $[\sigma_r(r(y)) + 1]$ to simply this equation to

$$- r_y^2 \sigma_{rr}(r(y)) + \left[\sigma_r(r(y)) + 1 \right] r_{yy} = 0.$$

But this is

$$\left[\left[1 + \sigma_r(r(y)) \right] r_y \right]_y = 0$$

which is satisfied by the solution of (4.6). Theorem 4.4 tells us that the solution $r(y)$ of (4.6), (4.7) is admissible. Thus $r(y)$ minimizes the functional $I(r)$ over the set of admissible functions.

□

4.5 A Moving Mesh Method

In the z-stretching example, domain "stretching" was employed simply to put our domain in a convenient rectangular shape. However, we would like to utilize domain transformation to provide computational flexibility. Specifically, we would like to use coefficient smoothing to avoid difficulties at the interface, and employ r-stretching domain transformation to reduce the resulting region of poor accuracy near the interface to an arbitrarily small size.

We could make our sigma functions as steep as we like to make the region of significant truncation error $P_{\tau,h}\phi - P\phi$ as small as we like. However, when discretized, sigma functions that are too steep are indistinguishable from the purely discontinuous functions they are approximating and will likewise cause nonphysical oscillation in the computed solution. Our strategy will be to choose transformations that make the slopes of all coefficient functions less steep in the computational space.

Our moving mesh method proceeds as follows: Begin with the boundary value problem to be solved in (z, r) coordinate space. For each discontinuous coefficient function, substitute a continuous function of sigma, as described in Section 2.6, that approximates the coefficient function. Let the sigma function be sufficiently steep to achieve a desired accuracy in the numerical solution. We then transform the boundary value problem into a uniform (x, y) coordinate space by the mapping

$$z = x, \quad r = r(x, y).$$

The specific transformation $r(x, y)$ will be determined dynamically at each propagation step by our algorithm.

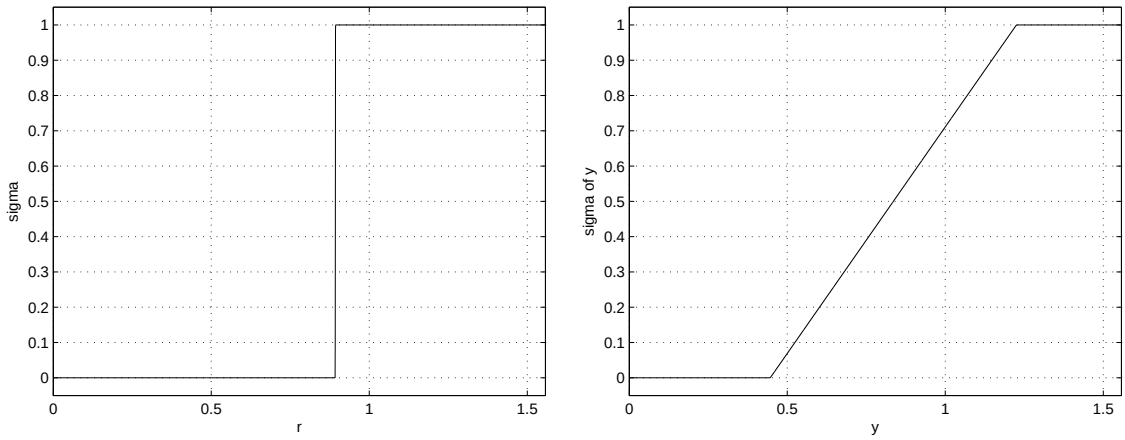

Figure 4.1: Here we see the sigma function in LEFT: r coordinates, and in RIGHT: y coordinates.

Next, formulate a finite difference scheme for the transformed boundary value problem by substituting the specific coefficient functions into the general formula for the six-point, two-level scheme (2.15) described in Chapter 2. We have shown that the r-stretching transformation will not change the general form of the equation. Thus changing the specific transformation will not change the form of the equation or the scheme. In the computational space, the problem is discretized on a uniform grid.

During simulation, our algorithm uses a nonlinear ordinary differential equation to generate a transformation function for the r direction at each propagation step. Based on the relation

$$\sigma_y = \sigma_r r_y$$

we determine an expression for r_y such that $r_y \leq 2$ and $R_1\sigma_y \leq 2$. Specifically, we use the generator derived in the previous section

$$r_y = \frac{2}{1 + \sigma_r\left(r(y)\right)}.$$

We use an explicit fourth order Runge-Katta method to solve the generator equation quickly at each time step. It is neither necessary nor desirable to use the generator function to determine the values of r_y or r_{yy}. Rather we employ the central difference

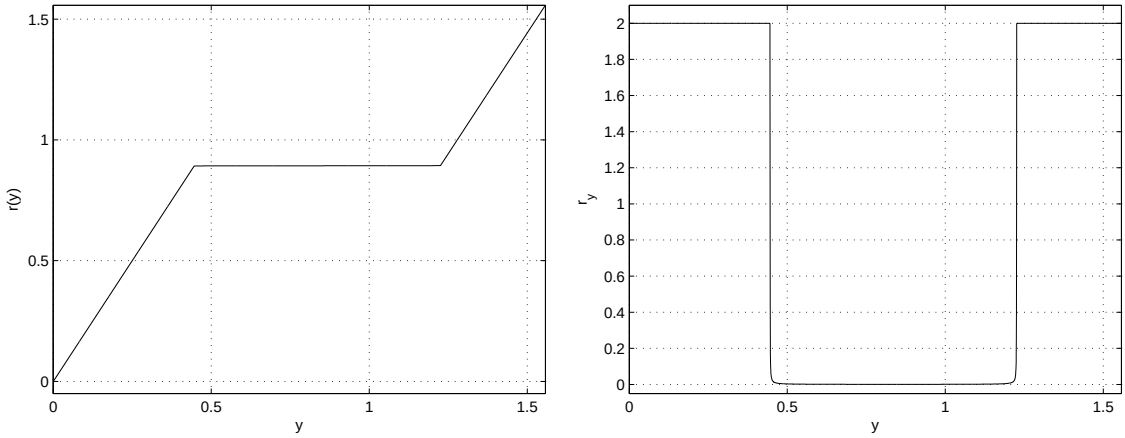

Figure 4.2: LEFT: The r transformation function. RIGHT: The derivative of r with respect to y

formulas

$$r_y(x_n, y_m) = \frac{r(x_n, y_{m+1}) - r(x_n, y_{m-1})}{2h},$$

and

$$r_{yy}(x_n, y_m) = \frac{r(x_n, y_{m+1}) - 2r(x_n, y_m) + 2r(x_n, y_{m-1})}{h^2}.$$

For our scheme, we actually need the derivative values at the reference points $\left(x_{n-\frac{1}{2}}, y_m\right)$, which are halfway between the grid points along the direction of propagation. We define the values of the transformation function $r(x, y)$ between two tranverse grid lines to be a linear combination of the functions at those lines, *i.e.*,

$$r(x_{n-\theta}, y) = (1-\theta)\, r(x_n, y) + \theta r(x_{n-1}, y), \quad 0 \le \theta \le 1.$$

Then we have

$$\frac{\partial r}{\partial y}\left(x_{n-\frac{1}{2}}, y_m\right) = \frac{1}{2}\left(\frac{\partial r}{\partial y}\left(x_n, y_m\right) + \frac{\partial r}{\partial y}\left(x_{n-1}, y_m\right)\right),$$

$$\frac{\partial^2 r}{\partial y^2}\left(x_{n-\frac{1}{2}}, y_m\right) = \frac{1}{2}\left(\frac{\partial^2 r}{\partial y^2}\left(x_n, y_m\right) + \frac{\partial^2 r}{\partial y^2}\left(x_{n-1}, y_m\right)\right),$$

$$r\left(x_{n-\frac{1}{2}}, y_m\right) = \frac{1}{2}\left(r\left(x_n, y_m\right) + r\left(x_{n-1}, y_m\right)\right),$$

$$\frac{\partial r}{\partial x}\left(x_{n-\frac{1}{2}}, y_m\right) = \frac{r\left(x_n, y_m\right) - r\left(x_{n-1}, y_m\right)}{\tau}.$$

Using the central difference formulas to approximate the derivatives of the r transform at the reference point can result in better overall accuracy, since we do not want to have to solve our generating equation to extremely high precision. The transform and derivative values obtained for each reference point can be considered a local coordinate transformation.

Once the solution is computed in the lens region, the solution at the right edge of the lens can be interpolated back onto physical coordinates, or the stretching can be slowly relaxed, and the scheme for the homogeneous case can be used to simulate the behavior of the beam in the post lens segment.

4.6 A Simple Example

In order to illustrate the benefits of r-stretching in combination with coefficient smoothing, we present a very simple example problem. We will solve the equation

$$\frac{\partial u}{\partial r} = \alpha(r)$$

where

$$\alpha(r) = \begin{cases} \frac{4}{\pi}, & 0 \geq r < \frac{\pi}{4}, \\ -\frac{4}{4-\pi}, & \frac{\pi}{4} \leq r \leq 1 \end{cases}$$

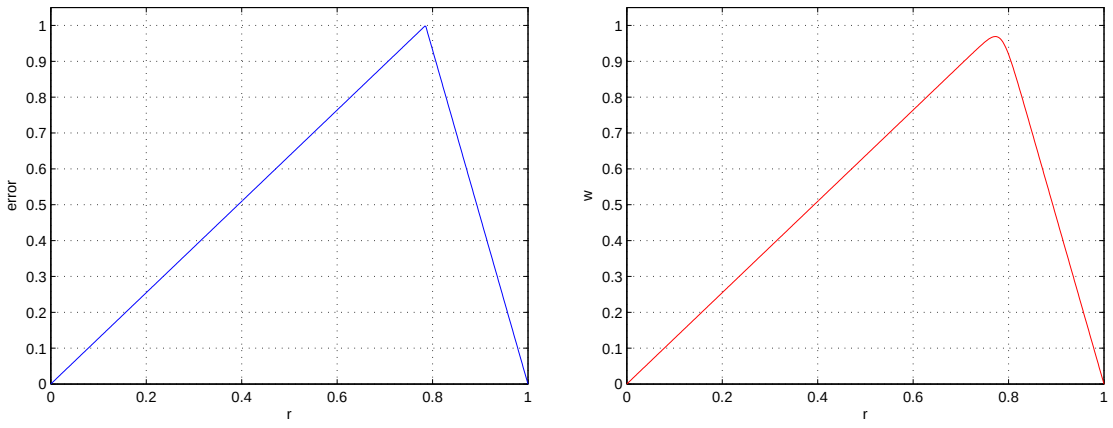

Figure 4.3: LEFT: Analytic, piecewise linear solution. RIGHT: Smoothed coefficient solution, steepness factor $\beta = \frac{1}{10}$.

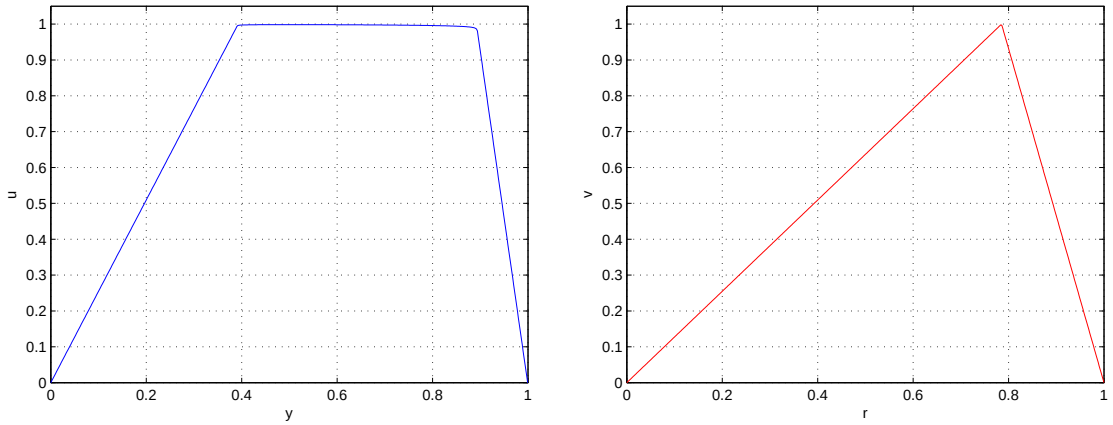

Figure 4.4: LEFT: Solution in r-stretched coordinates, $\beta = \frac{1}{2}$. RIGHT: Solution with $\beta = \frac{1}{2}$, translated back to original coordinates.

with Dirichlet boundary conditions

$$u(0) = 0, \quad u(1) = 0.$$

The analytic solution is piecewise linear. We use the sigma function

$$\sigma_h(r) = \frac{\tanh\left(\beta\frac{r-\eta(z)}{h}\right) - \tanh\left(\beta\frac{-\eta(z)}{\beta h}\right)}{\tanh\left(\beta\frac{1-\eta(z)}{h}\right) - \tanh\left(\beta\frac{-\eta(z)}{\beta h}\right)},$$

where $\eta = \dfrac{\pi}{4}$ and β is a steepness parameter, to create the following continuous

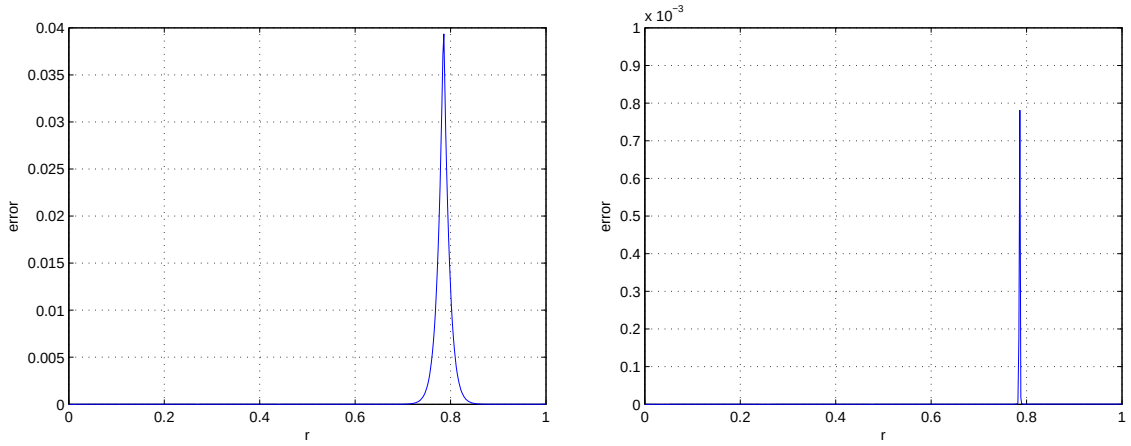

Figure 4.5: LEFT: Error of solution using smoothed, $\beta = \frac{1}{10}$, no r-stretching. RIGHT: Error of solution using smoothing plus r-stretching with $\beta = 2$.

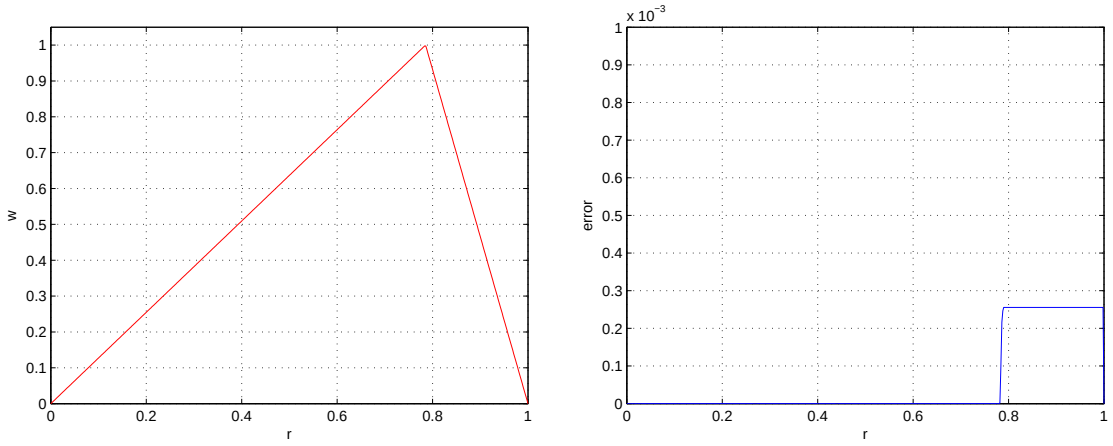

Figure 4.6: LEFT: Solution with steep σ, $\beta = 2$, no r-stretching. RIGHT: Significant error in the solution due to instability.

approximation to α

$$\alpha_h = \frac{4}{\pi} - \frac{16}{\pi(4-\pi)}\sigma_h(r)$$

and solve the corresponding boundary value problem

$$\frac{\partial u}{\partial r} = \alpha_h(r),$$

$$u(0) = 0, \quad u(1) = 0.$$

We first look at a smoothed solution with less steep approximated coefficient function, with steepness factor $\beta = \frac{1}{10}$. We see the that the sharp corner of the solution is rounded near the interface, resulting in high inaccuracy in a neighborhood of the interface. Next we use a much steeper σ function, with $\beta = 2$. The solution looks better, but examining the error compared to the analytic solution, we see significant error caused by instability. Finally, we use the same steepness factor $\beta = 2$, but this time with r-stretching to avoid instability. We obtain a solution that is very accurate, with a much smaller region of inaccuracy near the interface.

CHAPTER FIVE

The Immersed Interface Method

We extend the immersed interface method of Li to the numerical solution of the paraxial approximation of the Helmholtz equation as a comparison [43, 44, 45, 46]. From Maxwell's equations, the interface conditions are the continuity of the solution and the normal derivative of the solution [16].

As before, let $\eta(z)$ be the function which provides the position of the interface (the point of discontinuity of $k(z,r)$) with respect to the r axis. We will denote the z-position at propagation step k as z_k, and the r-position at $r = jh$ by r_j. At z_k, we have

$$k(r) = \begin{cases} k_1, & r \leq \eta(z_k), \\ k_2, & r > \eta(z_k). \end{cases}$$

We will utilize our two-level, six-point Crank-Nicholson scheme for regular points, which are points away from the interface. Here a point at (z_k, r_j) is determined to be regular if all of the points in our six-point stencil centered at $\left(z_{k-\frac{1}{2}}, r_j\right)$ are on the same side of the interface. Grid points where the corresponding stencil points straddle the interface are irregular, and schemes for those grid points must be derived according to how the stencil points are separated.

At any grid point (z_k, r_j) for which the corresponding stencil points on the right, *i.e.* at z_k lie on the same side of the interface, we simply substitute a four-point stencil consisting of a point (z_{k-1}, r_j) at the previous propagation level, and the three grid points (z_k, r_{j-1}), (z_k, r_j) and (z_k, r_{j+1}) on the right. We may do this because the interface conditions obtained from Maxwell's equations tell us that the derivative of the solution in the z-direction must be continuous, and therefore we may use points on opposite sides of the interface to approximate it, and also because the resulting four-point implicit scheme will be first-order accurate in both r and z, as are the

schemes derived using the immersed interface method.

Let $\eta = \eta(z_k)$. For grid points where the interface separates points of the corresponding stencil at the current propagation level z_k and the previous propagation level z_{k-1}, we employ the immersed interface method. First we derive our jump conditions. From Maxwell's equations (1.1)-(1.4), the first derivatives in both the r and z direction are continuous. Thus by examining the partial differential equation, we see that the second derivative in the r direction must have a jump discontinuity.

5.1 Jump Conditions

For a function $f(z, r)$ we will use the notation

$$f^+ = \lim_{r \to \eta^+} f(z, r), \quad f^- = \lim_{r \to \eta^-} f(z, r), \quad [f] = f^+ - f^-.$$

We now derive the jump conditions. We consider the interface as a function of z, $\eta(z)$. The solution is continuous across the interface, *i.e.* $u^-(z, \eta(z)) = u^+(z, \eta(z))$. Taking the derivative with respect to z gives us

$$u_z^- + u_r^- \eta' = u_z^+ + u_r^+ \eta'$$

$$[u_z] = -[u_r]\eta'.$$

Consider the interface as a function of r, $\chi(r)$ and taking the derivative with respect to r gives us

$$u_z^- \chi' + u_r^- = u_z^+ \chi' + u_r^+$$

$$[u_r] = -[u_z]\chi'.$$

We have

$$[u_r] = 0 \Leftrightarrow [u_z] = 0.$$

We see that the interface conditions implied by Maxwell's equations,

$$u^- = u^+, \quad u_r^- = u_r^+, \quad u_z^- = u_z^+,$$

remain applicable in the slowly varying approximation case. With the first derivative relations, we derive the jump relations for the second derivatives. We have

$$u_r^- \left(z, \eta(z)\right) = u_r^+ \left(z, \eta(z)\right),$$

$$u_{rz}^- + u_{rr}^- \eta' = u_{rz}^+ + u_{rr}^+ \eta',$$

$$u_{rz}^- = u_{rz}^+ + [u_{rr}]\eta',$$

thus we obtain

$$[u_{rz}] = -[u_{rr}]\eta'.$$

Next, we have

$$u_z^- \left(z, \eta(z)\right) = u_z^+ \left(z, \eta(z)\right),$$

$$u_{zz}^- + u_{zr}^- \eta' = u_{zz}^+ + u_{zr}^+ \eta',$$

$$u_{zz}^- = u_{zz}^+ + [u_{zr}]\eta',$$

thus we obtain

$$u_{zz}^- = u_{zz}^+ - [u_{rr}](\eta')^2.$$

To obtain the second derivative with respect to r jump relation, we use the one-sided version of the partial differential equation. At $\eta(z)$ we have

$$\begin{aligned}
u_{rr}^+ + (\frac{1}{r}u_r)^+ &= 2ik_1 u_z^-, \\
u_{rr}^- + (\frac{1}{r}u_r)^- &= 2ik_2 u_z^+, \\
u_{rr}^+ = 2ik_1 u_z^+ - \left(\frac{1}{r}u_r\right)^+ &= 2ik_1 u_z^- - 2ik_2 u_z^- + \left[2ik_2 u_z^- - \left(\frac{1}{r}u_r\right)^-\right] \\
&= 2i(k_1 - k_2)u_z^- + u_{rr}^- \\
u_{rr}^- &= 2i(k_2 - k_1)u_z^+ + u_{rr}^+.
\end{aligned}$$

We now have jump conditions for all second order derivatives

$$u_{rr}^- = u_{rr}^+ + 2i(k_2 - k_1)u_z,$$
$$u_{rz}^- = u_{rz}^+ + 2i(k_1 - k_2)\eta' u_z,$$
$$u_{zz}^- = u_{zz}^+ + 2i(k_2 - k_1)(\eta')^2 u_z,$$

where

$$\eta(z) = \sqrt{R^2 - (z-R)^2}, \quad \eta'(z) = \frac{R-z}{\eta(z)}.$$

5.2 Difference Schemes for Irregular Points

We next apply the techniques of the immersed interface method to derive difference schemes for irregular points depending upon how the stencil corresponding to the irregular point is divided by the interface.

Case 1: $\eta \geq r_{j+1}$

In this case the interface divides points in the six-point stencil, but it does not divide points in the right column, at $z = z_k$. Since u_z is continuous across the interface, we may substitute a four-point implicit scheme here which is first order accurate.

$$-u_{k-1,j} = \alpha(1 + \frac{1}{2j})u_{j,j+1} - (2\alpha + 1)u_{k,j} + \alpha(1 - \frac{1}{2j})u_{k,j-1}$$

where

$$\alpha = \frac{-\tau i}{2k_2 h^2}$$

Case 2: $j < M - 1$ and $r_{j-1} < \eta(z_k) \leq r_j$.

Let $\eta = \eta(z_k)$. We consider the Taylor expansions at (z_k, η), plugging in the jump relations across the interface. We have

$$u(z_k, r_{j+2}) = u^+(z_k, \eta) + (r_{j+2} - \eta)u_r^+(z_k, \eta) + \frac{1}{2}(r_{j+2} - \eta)^2 u_{rr}^+(z_k, \eta) + O\left(h^3\right),$$
$$u(z_k, r_{j+1}) = u^+(z_k, \eta) + (r_{j+1} - \eta)u_r^+(z_k, \eta) + \frac{1}{2}(r_{j+1} - \eta)^2 u_{rr}^+(z_k, \eta) + O\left(h^3\right),$$

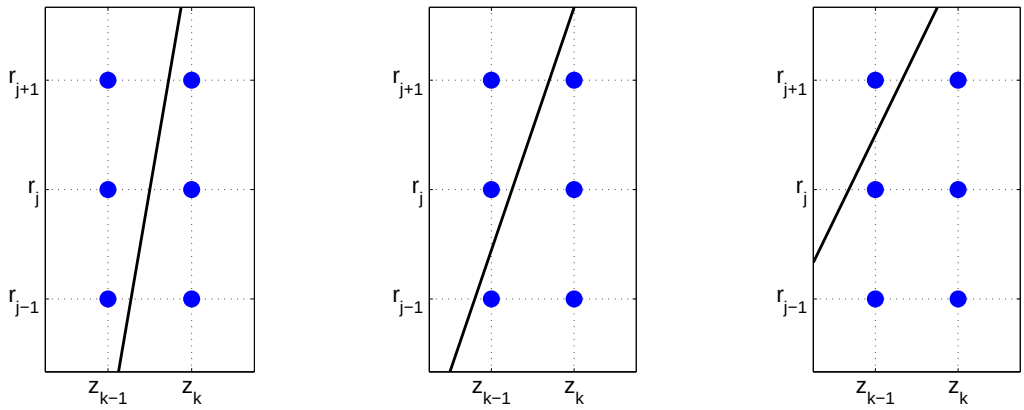

Figure 5.1: Case 1. The interface does not divide points on the right. An implicit four-point stencil will be used.

$$
\begin{aligned}
u(z_k, r_j) &= u^+(z_k, \eta) + (r_j - \eta) u_r^+(z_k, \eta) + \frac{1}{2}(r_j - \eta)^2 u_{rr}^+(z_k, \eta) + O\left(h^3\right), \\
u(z_k, r_{j-1}) &= u^-(z_k, \eta) + (r_{j-1} - \eta) u_r^-(z_k, \eta) + \frac{1}{2}(r_{j-1} - \eta)^2 u_{rr}^-(z_k, \eta) + O\left(h^3\right), \\
&= u^+(z_k, \eta) + (r_{j-1} - \eta) u_r^+(z_k, \eta) \\
&\quad + \frac{1}{2}(r_{j-1} - \eta)^2 \left[2i(k_2 - k_1) u_z^+(z_k, \eta) + u_{rr}^+(z_k, \eta)\right] + O\left(h^3\right).
\end{aligned}
$$

We would like to derive a difference equation of the form

$$\rho_{j,1} u(z_k, r_{j-1}) + \rho_{j,2} u(z_k, r_j) + \rho_{j,3} u(z_k, r_{j+1}) + \rho_{j,4} u(z_k, r_{j+2}) = 0$$

that is consistent with the paraxial Helmhotz equation in a radially symmetric domain, and is at least first order accurate. We examine the truncation error

$$
\begin{aligned}
T_j &= \rho_{j,1} u(z_k, r_{j-1}) + \rho_{j,2} u(z_k, r_j) + \rho_{j,3} u(z_k, r_{j+1}) + \rho_{j,4} u(z_k, r_{j+2}) \\
&\quad - 2ik_1 u_z^+ + u_{rr}^+ + \frac{1}{\eta} u_r^+ \\
&= \left(\rho_{j,1} + \rho_{j,2} + \rho_{j,3} + \rho_{j,4}\right) u^+(z_k, \eta) \\
&\quad + \left[\rho_{j,1}(r_{j-1} - \eta) + \rho_{j,2}(r_j - \eta) + \rho_{j,3}(r_{j+1} - \eta) + \rho_{j,4}(r_{j+2} - \eta) + \frac{1}{\eta}\right] u_r^+ \\
&\quad + \frac{1}{2}\left[\rho_{j,1}(r_{j-1} - \eta)^2 + \rho_{j,2}(r_j - \eta)^2 + \rho_{j,3}(r_{j+1} - \eta)^2 + \rho_{j,4}(r_{j+2} - \eta)^2 + 2\right] u_{rr}^+, \\
&\quad + \left[\rho_{j,1}(r_{j-1} - \eta)^2 i(k_2 - k_1) - 2ik_1\right] u_z^+ \\
&\quad + O\left(\rho_{j,1} h^2\right) + O\left(\rho_{j,2} h^2\right) + O\left(\rho_{j,3} h^2\right) + O\left(\rho_{j,4} h^2\right)
\end{aligned}
$$

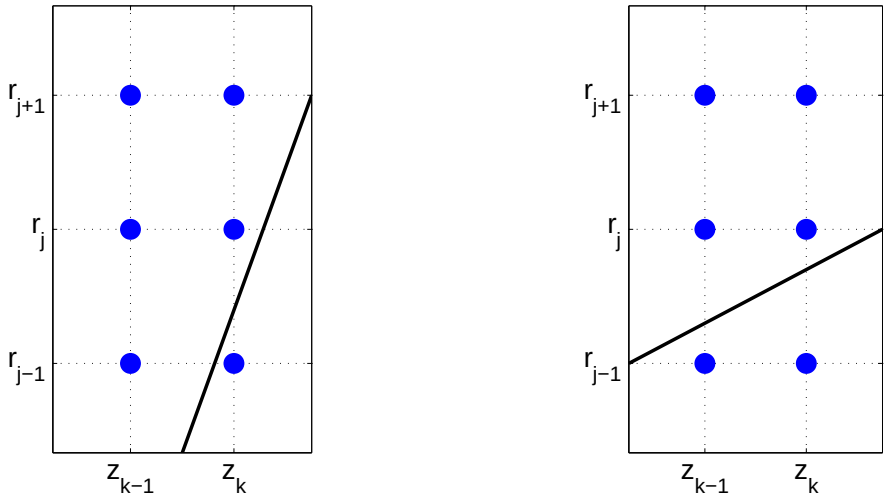

Figure 5.2. Case 2. Points on right column of stencil divided, with $r_{j-1} < \eta < r_j$.

We want the coefficients of $u^+(z_k, \eta)$ and each of the derivative terms in the truncation formula above to be zero. This gives us a system of four equations with four unknowns.

$$\rho_{j,1} + \rho_{j,2} + \rho_{j,3} + \rho_{j,4} = 0,$$
$$\rho_{j,1}(r_{j-1} - \eta) + \rho_{j,2}(r_j - \eta) + \rho_{j,3}(r_{j+1} - \eta) + \rho_{j,4}(r_{j+2} - \eta) + \frac{1}{\eta} = 0,$$
$$\rho_{j,1}(r_{j-1} - \eta)^2 + \rho_{j,2}(r_j - \eta)^2 + \rho_{j,3}(r_{j+1} - \eta)^2 + \rho_{j,4}(r_{j+2} - \eta)^2 + 2 = 0,$$
$$\rho_{j,1}(r_{j-1} - \eta)^2 i(k_2 - k_1) - 2ik_1 = 0$$

Solving for the $\rho_{j,k}$, $1 \le k \le 4$ values, we obtain the coefficients of the difference equation

$$\rho_{j,1} = -\alpha, \quad \rho_{j,2} = 3\alpha - \frac{2}{h^2} + \frac{3+2j}{2h\eta},$$
$$\rho_{j,3} = -3\alpha + \frac{4}{h^2} - \frac{2(j+1)}{h\eta}, \quad \rho_{j,4} = \alpha + \frac{h + 2hj - 4\eta}{2h^2\eta},$$

where

$$\alpha = \frac{2k_1}{[k](jh - h - \eta)^2}.$$

Since the coefficients $\rho_{j,k}$, $1 \le k \le 4$ are of order $O(h^{-2})$, the truncation error of the scheme will be $O(h)$.

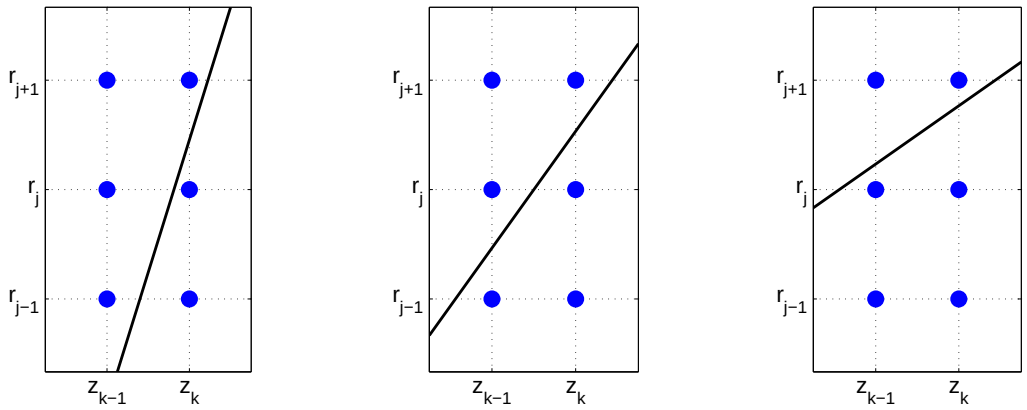

Figure 5.3. Case 3. Points on right column of stencil divided, with $r_j < \eta < r_{j+1}$.

Case 3: $j > 2$ and $r_{j-1} < \eta(z_k) \le r_j$.

$$
\begin{aligned}
u(z_k, r_{j+1}) &= u^+(z_k,\eta) + (r_{j+1}-\eta)u_r^+(z_k,\eta) + \frac{1}{2}(r_{j+1}-\eta)^2 u_{rr}^+(z_k,\eta) + O\left(h^3\right) \\
&= u^-(z_k,\eta) + (r_{j+1}-\eta)u_r^-(z_k,\eta) \\
&\quad + \frac{1}{2}(r_{j+1}-\eta)^2\left[2i(k_1-k_2)u_z^-(z_k,\eta) + u_{rr}^-(z_k,\eta)\right] + O\left(h^3\right) \\
u(z_k, r_j) &= u^-(z_k,\eta) + (r_j-\eta)u_r^-(z_k,\eta) + \frac{1}{2}(r_j-\eta)^2 u_{rr}^-(z_k,\eta) + O\left(h^3\right) \\
u(z_k, r_{j-1}) &= u^-(z_k,\eta) + (r_{j-1}-\eta)u_r^-(z_k,\eta) + \frac{1}{2}(r_{j-1}-\eta)^2 u_{rr}^-(z_k,\eta) + O\left(h^3\right) \\
u(z_k, r_{j-2}) &= u^-(z_k,\eta) + (r_{j-2}-\eta)u_r^-(z_k,\eta) + \frac{1}{2}(r_{j-2}-\eta)^2 u_{rr}^-(z_k,\eta) + O\left(h^3\right)
\end{aligned}
$$

We examine the truncation error

$$
\begin{aligned}
T_j &= \rho_{j,1}u(z_k, r_{j-2}) + \rho_{j,2}u(z_k, r_{j-1}) + \rho_{j,3}u(z_k, r_j) + \rho_{j,4}u(z_k, r_{j+1}) \\
&\quad - 2ik_1 u_z^+ + u_{rr}^+ + \frac{1}{\eta}u_r^+ \\
&= \left(\rho_{j,1} + \rho_{j,2} + \rho_{j,3} + \rho_{j,4}\right) u^+(z_k,\eta) \\
&\quad + \left[\rho_{j,1}(r_{j-2}-\eta) + \rho_{j,2}(r_{j-1}-\eta) + \rho_{j,3}(r_j-\eta) + \rho_{j,4}(r_{j+1}-\eta) + \frac{1}{\eta}\right] u_r^+ \\
&\quad + \frac{1}{2}\left[\rho_{j,1}(r_{j-2}-\eta)^2 + \rho_{j,2}(r_{j-1}-\eta)^2 + \rho_{j,3}(r_j-\eta)^2 + \rho_{j,4}(r_{j+1}-\eta)^2 + 2\right] u_{rr}^+, \\
&\quad + \left[\rho_{j,4}(r_{j+1}-\eta)^2 i(k_2-k_1) - 2ik_1\right] u_z^+ \\
&\quad + O\left(\rho_{j,1}h^2\right) + O\left(\rho_{j,2}h^2\right) + O\left(\rho_{j,3}h^2\right) + O\left(\rho_{j,4}h^2\right)
\end{aligned}
$$

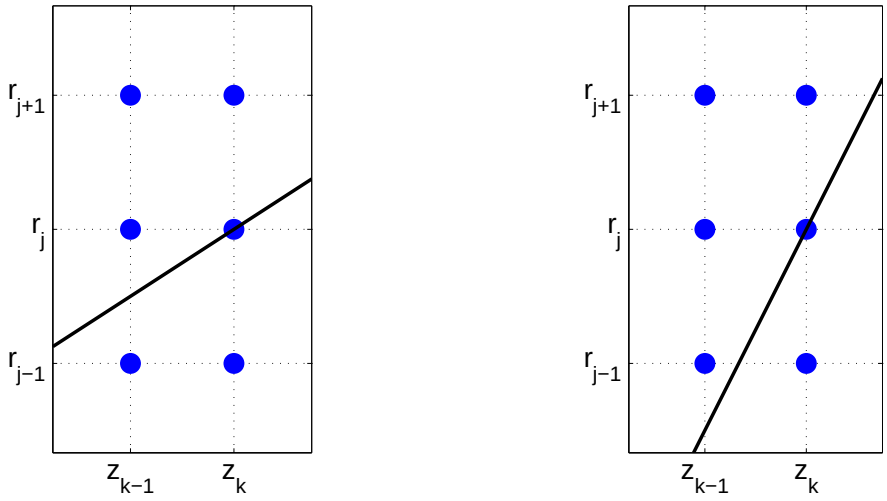

Figure 5.4. Case 4. Interface exactly divides right column of stencil, $\eta = r_j$.

As above, we solve a system of equations to obtain

$$\rho_{j,1} = -\alpha - \frac{h - 2hj + 4\eta}{2h^2\eta}, \quad \rho_{j,2} = 3\alpha + \frac{4}{h^2} - \frac{2(j-1)}{h\eta}$$
$$\rho_{j,3} = -3\alpha - \frac{2}{h^2} + \frac{-3 + 2j}{2h\eta}, \quad \rho_{j,4} = \alpha$$

where

$$\alpha = \frac{2k_2}{[k](jh + h - \eta)^2}$$

Case 4: $\eta(z_k) = r_j$.

Let $\eta = \eta(z_k)$. We examine the Taylor expansions at (z_k, η).

$$u(z_k, r_{j+1}) = u^+(z_k, \eta) + hu_r^+(z_k, \eta) + \frac{1}{2}h^2 u_{rr}^+(z_k, \eta) + O\left(h^3\right)$$
$$u(z_k, r_j) = u^+(z_k, \eta)$$
$$u(z_k, r_{j-1}) = u^-(z_k, \eta) - hu_r^-(z_k, \eta) + \frac{1}{2}h^2 u_{rr}^-(z_k, \eta) + O\left(h^3\right)$$
$$= u^+(z_k, \eta) - hu_r^+(z_k, \eta) + \frac{1}{2}h^2 \left[2i(k_2 - k_1)u_z^+ + u_{rr}^+\right](z_k, \eta) + O\left(h^3\right)$$

We can use two points above the interface:

$$\rho_{j,1} = \frac{2k_1}{[k]h^2}, \quad \rho_{j,2} = \frac{-2j[k] + 3[k] + 12jk_1}{2[k]h^2 j}, \quad \rho_{j,3} = \frac{2(j[k] - [k] - 3jk_1)}{[k]h^2 j}$$
$$\rho_{j,4} = \frac{-2j[k] + [k] + 4jk_1}{2[k]h^2 j}$$

or two points below the interface when necessary

$$\rho_{j,1} = \frac{-2j[k] - [k] - 4jk_2}{2[k]h^2 j}, \quad \rho_{j,2} = \frac{2(j[k] + [k] + 3jk_2)}{[k]h^2 j}$$
$$\rho_{j,3} = \frac{-2j[k] - 3[k] - 12jk_2}{2[k]h^2 j}, \quad \rho_{j,4} = \frac{2k_2}{[k]h^2}$$

Case 5: $j = M - 1$ and $\eta(z_{k-1}) \le r_{j-1}$ and $r_{j-1} < \eta(z_k) \le r_j$.

Let $\eta = \eta(z_k)$. We consider the Taylor expansions at (z_k, η).

$$u(z_k, r_{j+1}) = u^+(z_k, \eta) + (r_{j+1} - \eta)u_r^+ + \frac{1}{2}(r_{j+1} - \eta)^2 u_{rr}^+ + O\left(h^3\right)$$
$$u(z_k, r_j) = u^+(z_k, \eta) + (r_j - \eta)u_r^+ + \frac{1}{2}(r_j - \eta)^2 u_{rr}^+ + O\left(h^3\right)$$
$$u(z_k, r_{j-1}) = u^-(z_k, \eta) + (r_{j-1} - \eta)u_r^- + \frac{1}{2}(r_{j-1} - \eta)^2 u_{rr}^- + O\left(h^3\right)$$
$$= u^+(z_k, \eta) + (r_{j-1} - \eta)u_r^+ + \frac{1}{2}(r_{j-1} - \eta)^2 \left[2i(k_2 - k_1)u_z^+ + u_{rr}^+\right] + O\left(h^3\right)$$
$$u(z_{k-1}, r_{j+1}) = u^+(z_k, \eta) + (r_{j+1} - \eta)u_r^+ - \tau u_z^+ + \frac{1}{2}(r_{j+1} - \eta)^2 u_{rr}^+ + \frac{1}{2}\tau^2 u_{zz}^+ - \tau(r_{j+1} - \eta)u_{rz}^+ + O\left(h^3\right)$$
$$u(z_{k-1}, r_j) = u^+(z_k, \eta) + (r_j - \eta)u_r^+ - \tau u_z^+ + \frac{1}{2}(r_j - \eta)^2 u_{rr}^+ + \frac{1}{2}\tau^2 u_{zz}^+ - \tau(r_j - \eta)u_{rz}^+ + O\left(h^3\right)$$
$$u(z_{k-1}, r_{j-1}) = u^+(z_k, \eta) + (r_{j-1} - \eta)u_r^+ - \tau u_z^+ + \frac{1}{2}(r_{j-1} - \eta)^2 u_{rr}^+ + \frac{1}{2}\tau^2 u_{zz}^+ - \tau(r_{j-1} - \eta)u_{rz}^+ + O\left(h^3\right)$$

and examine the truncation error

$$
\begin{aligned}
T_j &= \rho_{j,1}u(z_k, r_{j-1}) + \rho_{j,2}u(z_k, r_j) + \rho_{j,3}u(z_k, r_{j+1}) - \rho_{j,4}u(z_{k-1}, r_{j-1}) - \rho_{j,5}u(z_{k-1}, r_j \\
&\quad - \rho_{j,6}u(z_{k-1}, r_{j+1}) - 2ik_1u_z^- + u_{rr}^+ + \frac{1}{\eta}u_r^+ + O(h) \\
&= \left(\rho_{j,1} + \rho_{j,2} + \rho_{j,3} - \rho_{j,4} - \rho_{j,5} - \rho_{j,6}\right) u^+(z_k, \eta) \\
&\quad + \left[\left(\rho_{j,1} - \rho_{j,4}\right)(r_{j-1} - \eta) + \left(\rho_{j,2} - \rho_{j,5}\right)(r_j - \eta) + \left(\rho_{j,3} - \rho_{j,6}\right)(r_{j+1} - \eta) + \frac{1}{\eta}\right] u_r^+ \\
&\quad + \frac{1}{2}\left[\left(\rho_{j,1} - \rho_{j,4}\right)(r_{j-1} - \eta)^2 + \left(\rho_{j,2} - \rho_{j,5}\right)(r_j - \eta)^2 + \left(\rho_{j,3} - \rho_{j,6}\right)(r_{j+1} - \eta)^2 + 2\right] u_{rr}^+ \\
&\quad + \left[\rho_{j,1}(r_{j-1} - \eta)^2 i(k_2 - k_1) + \left(\rho_{j,4} + \rho_{j,5} + \rho_{j,6}\right)\tau - 2ik_1\right] u_z^+ \\
&\quad - \frac{1}{2}\tau^2\left(\rho_{j,4} + \rho_{j,5} + \rho_{j,6}\right) u_{zz}^+ \\
&\quad + \tau\left[\rho_{j,4}(r_{j-1} - \eta) + \rho_{j,5}(r_j - \eta) + \rho_{j,6}(r_{j+1} - \eta)\right] u_{rz}^+.
\end{aligned}
$$

We solve for the scheme coefficients

$$
\begin{aligned}
&\rho_{j,1} = -\alpha, \quad \rho_{j,2} = 2\alpha + \frac{1}{h\eta}, \quad \rho_{j,3} = -\alpha - \frac{1}{h\eta} \\
&\rho_{j,4} = -\alpha - \frac{1}{2}\beta, \quad \rho_{j,5} = 2\alpha + \beta, \qquad \rho_{j,6} = -\alpha - \frac{1}{2}\beta,
\end{aligned}
$$

where

$$
\alpha = \frac{2k_1}{(k_1 - k_2)(h - hj + \eta)^2}, \quad \beta = \frac{h + 2hj - 4\eta}{h^2\eta}.
$$

Case 6: $j = M - 1$ and $r_{j-1} \le \eta(z_k) < r_j$, or $j = 1$ and $r_j \le \eta(z_k) < r_{j+1}$.

We solve for the scheme coefficients

$$
\rho_{j,1} = \frac{\alpha_1}{\beta}, \quad \rho_{j,2} = \frac{\alpha_2}{\beta}, \quad \rho_{j,3} = \frac{\alpha_3}{\beta}, \quad \rho_{j,4} = \frac{\alpha_4}{\beta},
$$

where

$$
\begin{aligned}
\alpha_1 &= -2[k]j^3h^3 - 3[k]j^2h^3 + 8[k]j^2\eta h^2 + 6[k]j\eta h^2 - 4k_2\eta h^2 - 3[k]\eta^2 h - 10[k]jn^2 h \\
&\quad + 4[k]\eta^3,
\end{aligned}
$$

$$\alpha_2 = -2[k]j^3h^3 + [k]j^2h^3 - 3[k]h^3 + 4[k]jh^3 + 8[k]j^2\eta h^2 - 2[k]\eta h^2 - 6[k]j\eta h^2$$
$$- 12k_2\eta h^2 + 5[k]\eta^2 h - 10[k]j\eta^2 h + 4[k]\eta^3,$$
$$\alpha_3 = -2[k]j^3h^3 - 7[k]j^2h^3 + 4[k]h^3 - 4[k]jh^3 + 8[k]j^2\eta h^2 + 22[k]j\eta h^2 + 12k_2\eta h^2$$
$$- 15[k]\eta^2 h - 10[k]j\eta^2 h + 4[k]\eta^3,$$
$$\alpha_4 = 2[k]j^3h^3 + 3[k]j^2h^3 - [k]h^3 - 8[k]j^2\eta h^2 + 2[k]\eta h^2 - 10[k]j\eta h^2 - 4k_2\eta h^2$$
$$+ 7[k]\eta^2 h + 10[k]j\eta^2 h - 4[k]\eta^3,$$
$$\beta = 2[k]h^2\eta(-h^2 + 2h^2 j + 2h^2 j^2 - 2h\eta - 4hj\eta + 2\eta^2),$$
$$[k] = k_1 - k_2.$$

We now have difference equations for all grid points. We proceed to simulate beam propagation within the rectangular domain segment consisting of the pre-lens and lens regions. Grid points with corresponding stencils completely within the pre-lens region use the homogeneous scheme with wavenumber $k = k_1$, while grid points with corresponding stencils completely within the lens segment use the homogeneous scheme with wavenumber $k = k_2$, and irregular points use the difference schemes derived above according to how the corresponding stencil is divided by the interface. The computed solution at the right edge of the combined pre-lens/lens region becomes the initial solution for the post-lens region, again using the homogeneous scheme with wavenumber $k = k_1$.

CHAPTER SIX

Summary

6.1 Thesis Contribution

In this dissertation we proposed and examined several new methods for the Helmholtz equation with coefficients that are discontinuous at an interface. In Chapter Two we derived a general formula by which a six-point, two-level difference scheme can be derived for any partial differential equation of the form

$$c_4 u_{rr} + c_3 u_r + c_2 u_z + c_1 u + c_0 = 0,$$

simply by plugging in the specific coefficient values. Further, we established consistency of a scheme so derived for any equation of the above form, eliminating the need for a new consistency proof for each specific scheme and demonstrating the potential usefulness of our results beyond our model problem. In addition, we demonstrated that if we replace the discontinuous coefficient functions with continuous functions that are dependent on the grid spacing, h, and which approach the discontinuous function as $h \to 0$, we maintain consistency.

Also in Chapter Two, we introduced a matrix method for stability analysis which is applicable to a broad class of schemes, and particularly effective for schemes which employ stencils that are symmetric around a reference point, such as Crank-Nicholson type two-level schemes. Using that matrix method, we established the stability of our six-point, two-level scheme both in the homogeneous case, and in the "smoothed coefficient" case, where we approximate the discontinuous wavenumber function with a continuous function.

In Chapter Three, we derived and implemented the z-stretching method. Here we decompose the domain into pre-lens, lens and post-lens regions, and stretch the coordinates in the direction of propagation to obtain a rectangular lens domain, in

which we can apply finite difference methods for a homogeneous wavenumber coefficient value. Using the principles of the slow-varying envelope approximation, we demonstrated that a useful approximation could be obtained for the paraxial case using a two-level difference scheme. Our matrix method was applied to demonstrate stability of the scheme. The scheme was efficiently implemented with less than 50 lines of Matlab code in the simulation loops.

In Chapter Four, we introduced the r-stretching method, which uses domain transformation to minimize the region of inaccuracy resulting from coefficient smoothing. This allowed us to solve the equation numerically without treating grid points near the interface as a special case. Also, while the position of the interface must be known, the method can be applied to an interface of arbitrary shape and smoothness.

The mesh generator we derived for the r-stretching method is highly efficient, and provides an excellent distribution of grid points in the physical space. We demonstrated the technique for several simple cases, and implemented the method in Matlab for the paraxial Helmholtz equation in a radially symmetric domain.

In Chapter Five, we derived the precise jump conditions for the solution and first and second solution derivatives for the paraxial Helmholtz equation in a radially symmetric domain in the case of a smooth interface. We utilized the immersed interface method to derive specialized difference equations for "irregular points," which are points adjacent to the interface.

6.2 Future Research

6.2.1 The Matrix Analysis Method

The matrix analysis method we introduced relies on examining tridiagonal matrices to determine positive semistability. The method would benefit greatly from improved techniques for determining semistability. A constructive technique utilizing the generalized Lyapunov Theorem below, should be possible.

Theorem 6.1 (Generalized Lyapunov). *Let $A \in \mathbb{C}^{N\times N}$ be given. Then A is positive semistable if there is a positive definite matrix G and a positive semidefinite matrix H satisfying the equation*

$$GA + A^*G = H.$$

We will give an example on one such constructive approach. As a special case of the above, we have the following lemma.

Lemma 6.1. *Let $A \in \mathbb{C}^{N\times N}$ be given. Then the eigenvalues of A are pure imaginary if there is a positive definite matrix G satisfying the equation*

$$GA = -A^*G.$$

Proof. Let $A \in \mathbb{C}^{N\times N}$ be given. Assume $G \in \mathbb{C}^{N\times N}$ is positive definite with $GA = -A^*G$, and let $x \in \mathbb{C}^n$ be an eigenvector of A with corresponding eigenvalue λ. Then

$$-\overline{\lambda}x^*Gx = x^*\left(-A^*G\right)x = x^*GAx = \lambda x^*Gx.$$

Since $x^*GAx > 0$ for all $x \in \mathbb{C}^n$, we have $\lambda = -\overline{\lambda}$. Thus λ is pure imaginary. □

We seek to construct appropriate matrices H and G that will satisfy the conditions of Lemma (6.1). We first assume the G is diagonal, and see what constraints are induced upon A.

For the theorems to follow, matrix $A \in \mathbb{C}^{N\times N}$ is of the form

$$A = \begin{bmatrix} a_1 & c_1 & 0 & \cdots & 0 \\ b_2 & a_2 & c_2 & 0 & \cdots \\ 0 & b_3 & a_3 & c_3 & 0 \\ & \cdots & & & \\ & & \cdots & & \\ & & & \cdots & \\ \cdots & 0 & b_{N-1} & a_{N-1} & c_{N-1} \\ 0 & \cdots & 0 & b_N & a_N \end{bmatrix}$$

Theorem 6.2. *If $A \in \mathbb{C}^{N\times N}$ is a tridiagonal matrix such that*

$$Re(a_i) = 0,\ 1 \le i \le N$$

and

$$\frac{c_{i-1}}{\overline{b_i}} = -d_i \text{ for some real } d_i > 0,\ 2 \le i \le N$$

then A has pure imaginary eigenvalues.

Proof. Let matrix $G \in \mathbb{C}^{N\times N}$ be diagonal, i.e.,

$$G = diag\,\{g_1, g_2, ..., g_N\}$$

then

$$GA + A^*G = \begin{bmatrix} \overline{a_1}g_1+a_1g_1 & c_1g_1+\overline{b_2}g_2 & 0 & \cdots & 0 \\ \overline{c_1}g_1+b_2g_2 & \overline{a_2}g_2+a_2g_2 & c_2g_2+\overline{b_3}g_3 & 0 & \cdots \\ 0 & \overline{c_2}g_2+b_3g_3 & \overline{a_3}g_3+a_3g_3 & c_3g_3+\overline{b_4}g_4 & 0 \\ & \cdots & \cdots & & \\ & & & \cdots & \\ \cdots & 0 & \overline{c_{N-2}}g_{N-2}+b_{N-1}g_{N-1} & \overline{a_{N-1}}g_{N-1}+a_{N-1}g_{N-1} & c_{N-1}g_{N-1}+\overline{b_N}g_N \\ 0 & \cdots & 0 & \overline{c_{N-1}}g_{N-1}+b_Ng_N & \overline{a_N}g_N+a_Ng_N \end{bmatrix}$$

We assume $\mathrm{Re}(a_i) = 0,\ 1 \le i \le N$. We then have

$$GA + A^*G = \begin{bmatrix} 0 & c_1g_1+\overline{b_2}g_2 & 0 & \cdots & 0 \\ \overline{c_1}g_1+b_2g_2 & 0 & c_2g_2+\overline{b_3}g_3 & 0 & \cdots \\ 0 & \overline{c_2}g_2+b_3g_3 & 0 & c_3g_3+\overline{b_4}g_4 & 0 \\ & \cdots & \cdots & & \\ & & & \cdots & \\ \cdots & 0 & \overline{c_{N-2}}g_{N-2}+b_{N-1}g_{N-1} & 0 & c_{N-1}g_{N-1}+\overline{b_N}g_N \\ 0 & \cdots & 0 & \overline{c_{N-1}}g_{N-1}+b_Ng_N & 0 \end{bmatrix}$$

Set $g_1 = 1$ and

$$g_i = -\frac{c_{i-1}}{\overline{b_i}}g_{i-1} = d_ig_{i-1}.$$

Then G is positive definite and $GA = -A^*G$. By Lemma (6.1), A has only pure imaginary eigenvalues. □

More powerful constructive techniques appear possible.

6.2.2 A Moving Mesh Method for Higher Spatial Dimensions

Our stretching functions are defined only along the grid lines, and we only need to know the position of the interface at each grid. We do not need the interface to be

smooth, or even to be defined by a parameterized function. Therefore, it should be straightforward to extend the method to higher spatial dimensions, with stretching along grid lines in each coordinate direction occurring at alternating time steps. The computational expense should scale proportionately with the dimension.

6.2.3 A Solution Adaptive Moving Mesh Method

A solution adaptive version of our method would allow us to apply it to general interface problems regardless of the properties of the interface, even if the location of the interface is unknown. An iterative method would likely need to be utilized to determine the transformation at the initial propagation step. However, this should add only a fixed amount of time to the simulation.

Unlike the stretching mesh generator based on a smooth sigma function, the mesh generator for a solution adaptive method will be based on the current computed solution, of which we will have only discrete sample points. We will have to formulate systems of difference equations that ensure sufficient smoothness and orthogonality of the transformed coordinates, rather than using numerical ODE methods.

APPENDICES

APPENDIX A

Derivative and Antiderivative Approximations on Nonuniform Grids

An advantage of the adaptive methods we have discussed is the use of grids that are nonuniform in the physical space. A grid that is nonuniform, even if some of the local regions of the grid become "dense", that is, a significantly large number of points are concentrated in a particular region as compared to the other local regions, can be considered a so-called *hybrid grid,* or *time scale* in the physical space[12, 20]. The novel theory of time scales has been established for the study and analysis of generalized "dynamic equations," on hybrid grids [3, 13, 63]. In this Appendix, we wish to answer certain fundamental questions before an application: does the theory of timescales give us a tool by which we can approximate dynamic equations on hybrid grids without transformation to a uniform grid in computational space? Is it possible to derive a dynamic derivative on timescales that is accurate as an derivative approximation and has an antiderivative such that a calculus may be formed? By investigating these questions we seek insight as to whether or not boundary value problems such as our optical wave equations be solved accurately via a hybrid grid using time scales generalization techniques.

Much of the development of time scales theory has focused on the unification of continuous and discrete analytical methods. Recent discussions have suggested that the theory and methods of time scales might also provide a means of integrating difference and differential methods for modeling nonlinear systems of dynamic equations on domains that are arbitrary nonempty closed subsets of the reals. To this end, the usefulness of various dynamic derivative formulae, including the standard Δ and ∇ derivatives, in approximating functions and solutions of nonlinear differential equations has been explored [12, 13, 20, 63]. It has been demonstrated in several recent papers [58, 59, 60, 63] that a proposed dynamic derivative formula, called the

$\diamondsuit_\alpha$ derivative and defined as a linear combination, or the Broyden's formula [15, 68], of the Δ and the ∇ dynamic derivatives, provides a more accurate approximation to the conventional derivative. The question remains, however, as to whether the $\diamondsuit_\alpha$ derivative is a well-defined dynamic derivative upon which a calculus on time scales can be built. Many recent discussions can be found, for instance, see [52] and references there in.

This study redefines the $\diamondsuit_\alpha$ derivative independently of the standard Δ and ∇ dynamic derivatives, and further examines its properties and relationship with the Δ and the ∇ formulae. In addition, we examine the feasibility of formulating a corresponding $\diamondsuit_\alpha$ integral. Finally, we implement several computational experiments and compare the performance of various dynamic derivatives as approximation formulae.

Our discussions are be organized as follows: Section A.1 contains basic definitions and theorems of time scales theory and of the Δ and ∇ dynamic derivatives. In Section A.2, we define the $\diamondsuit_\alpha$ derivative without reference to the Δ and ∇ derivatives, and show that this new function is well-defined and equivalent to a linear combination of the Δ and ∇ derivatives at points where those derivatives exist. We present several theorems concerning the properties of the $\diamondsuit_\alpha$ derivative. In Section A.3, we consider two counterexamples that demonstrate that a $\diamondsuit_\alpha$ antiderivative does not exist for some continuous functions on a time scale in the case of a fixed α value strictly between 0 and 1.

Finally, in Section A.4, we discuss computational experiments where nonuniform time scales resulting from adaptive computations of the numerical solution of a solitary wave equation are employed [64, 65]. Numerical errors will be computed and compared between different first order dynamic derivative approximates over an interval which includes a singularity in the conventional derivative. The simulation results confirm the computational superiority of the diamond-α as an approximation formula. The combined dynamic derivatives can be used in various nonlinear dynamic

equations generated via adaptive or hybrid approximations [20, 65].

A.1 The Delta and Nabla Derivatives

An one-dimensional time scale $\mathbb{T}$ is an arbitrary nonempty closed subset of $\mathbb{R}$ and has the inherited topology. Let $a = \inf \mathbb{T}$ and $b = \sup \mathbb{T}$. For $t \in \mathbb{T}$ such that $a < t < b$, we define the *forward-jump operator*, σ, and *backward-jump operator*, ρ, as

$$\sigma(t) = \inf\{s \in \mathbb{T} : s > t\}, \quad \rho(t) = \sup\{s \in \mathbb{T} : s < t\},$$

respectively, and

$$\sigma(b) = b, \quad \rho(a) = a,$$

if $\mathbb{T}$ is bounded. The corresponding *forward-step* and *backward-step functions* μ, η are defined as as

$$\mu(t) = \sigma(t) - t, \quad \eta(t) = t - \rho(t),$$

respectively. For a function f defined on $\mathbb{T}$, to provide a shorthand notation we let

$$f^{\sigma}(t) = f(\sigma(t)), \ f^{\rho}(t) = f(\rho(t)).$$

We say that a point $t \in \mathbb{T}$ is *right-scattered* if $\sigma(t) > t$ and *left-scattered* if $\rho(t) < t$. A point $t \in \mathbb{T}$ that is both right-scattered and left-scattered is called *scattered*. Also, we say that a point $t \in \mathbb{T}$ is *right-dense* if $\sigma(t) = t$, *left-dense* if $\rho(t) = t$, and *dense* if it is both right-dense and left-dense.

We define $\mathbb{T}^{\kappa} = \mathbb{T} \setminus \{b\}$ if $\mathbb{T}$ is bounded above and b is left-scattered; otherwise $\mathbb{T}^{\kappa} = \mathbb{T}$. Similarly, we define $\mathbb{T}_{\kappa} = \mathbb{T} \setminus \{a\}$ if $\mathbb{T}$ is bounded below and a is right-scattered; otherwise $\mathbb{T}_{\kappa} = \mathbb{T}$. We denote $\mathbb{T}^{\kappa} \cap \mathbb{T}_{\kappa}$ by $\mathbb{T}_{\kappa}^{\kappa}$. We say a time scale $\mathbb{T}$ is *uniform* if for all $t \in \mathbb{T}_{\kappa}^{\kappa}$, $\mu(t) = \eta(t)$. A uniform time scale is an interval if $\mu(t) = 0$, and is a uniform difference grid if $\mu(t) > 0$.

We say a function f defined on $\mathbb{T}$ is right continuous at $t \in \mathbb{T}$ if for all $\epsilon > 0$ there is some $\delta > 0$ such that for all $s \in [t, t + \delta)$, $|f(t) - f(s)| < \epsilon$. Similarly, we say

that f is left continuous at $t \in \mathbb{T}$ if for all $\epsilon > 0$ there is some $\delta > 0$ such that for all $s \in (t-\delta, t]$, $|f(t) - f(s)| < \epsilon$. The function $f(t)$ is said to be continuous if it is both right and left continuous.

For the sake of readability of subsequent formulas, we introduce the following notation. Let $t, s \in \mathbb{T}$ and define

$$\mu_{ts} = \sigma(t) - s, \qquad \eta_{ts} = \rho(t) - s.$$

Let $f : \mathbb{T} \to \mathbb{R}$ be a function on a timescale. Then for $t \in \mathbb{T}^\kappa$ we define $f^\Delta(t)$ to be the value, if one exists, such that for all $\epsilon > 0$ there is a neighborhood U of t (i.e. $U = (t-\delta, t+\delta) \cap \mathbb{T}$ for some $\delta > 0$) such that for all $s \in U$

$$\left|[f^\sigma(t) - f(s)] - f^\Delta(t)(\sigma(t) - s)\right| < \epsilon|\sigma(t) - s|.$$

We say that f is *delta differentiable* on $\mathbb{T}^\kappa$ provided $f^\Delta(t)$ exists for all $t \in \mathbb{T}^\kappa$. Similarly, for $t \in \mathbb{T}_\kappa$ we define $f^\nabla(t)$ to be the number, if one exists, such that for all $\epsilon > 0$ there is a neighborhood V of t such that for all $s \in V$

$$\left|[f^\rho(t) - f(s)] - f^\nabla(t)(\rho(t) - s)\right| < \epsilon|\rho(t) - s|.$$

We say that f is *nabla differentiable* on $\mathbb{T}_\kappa$ provided $f^\nabla(t)$ exists for all $t \in \mathbb{T}_\kappa$.

In subsequent proofs, we will wish to make use of the following theorem due to Hilger [34], and the analogous theorem for the nabla case, which can be found in [3, 12]:

Theorem A.1.1. *Assume $f : \mathbb{T} \to \mathbb{R}$ is a function and let $t \in \mathbb{T}^\kappa$. Then we have the following:*

(*i*) *If f is delta differentiable at t, then f is continuous at t.*

(*ii*) *If f is left continuous at t and t is right-scattered, then f is delta differentiable at t with*

$$f^\Delta(t) = \frac{f^\sigma(t) - f(t)}{\sigma(t) - t}.$$

(*iii*) *If t is right-dense, then f is delta differentiable at t iff the limit*

$$\lim_{s\to t}\frac{f(t)-f(s)}{t-s}$$

exists as a finite number. In this case

$$f^{\Delta}(t)=\lim_{s\to t}\frac{f(t)-f(s)}{t-s}.$$

Theorem A.1.2. *Assume $f:\mathbb{T}\to\mathbb{R}$ is a function and let $t\in\mathbb{T}_{\kappa}$. Then we have the following:*

(*i*) *If f is nabla differentiable at t, then f is continuous at t.*

(*ii*) *If f is right continuous at t and t is left-scattered, then f is nabla differentiable at t with*

$$f^{\nabla}(t)=\frac{f(t)-f^{\rho}(t)}{t-\rho(t)}.$$

(*iii*) *If t is left-dense, then f is nabla differentiable at t iff the limit*

$$\lim_{s\to t}\frac{f(t)-f(s)}{t-s}$$

exists as a finite number. In this case

$$f^{\nabla}(t)=\lim_{s\to t}\frac{f(t)-f(s)}{t-s}.$$

With the above theorems in hand we can establish the following

Corollary A.1.3. *Assume $f:\mathbb{T}\to\mathbb{R}$ is a function and let $t\in\mathbb{T}^{\kappa}_{\kappa}$. The existence of the delta derivative of f at t does not imply the existence of the nabla derivative at t, and visa-versa.*

Proof. Consider the function

$$f(t)=\begin{cases} t\sin(1/t), & x\neq 0\\ 0, & x=0\end{cases}$$

on a timescale $\mathbb{T}=[-2,-1]\cup[0,1]$. The function f is continuous at 0, and the point $0\in\mathbb{T}$ is right-dense, left-scattered. By A.1.2(ii), f is nabla differentiable at 0. But a finite limit

$$\lim_{s\to t}\frac{f(t)-f(s)}{t-s}$$

does not exist at 0. Thus by Theorem A.1.1 (iii), f is not delta differentiable at 0. To show the existence of the delta derivative does not imply the existence nabla derivative, we may consider the same function f at point 0 on a timescale $\mathbb{T} = [-1, 0] \cup [1, 2]$. □

A.2 The Diamond-α Dynamic Derivative

Definition A.2.1. *Let $\mathbb{T}$ be a time scale. We define $f^{\diamond_\alpha}(t)$ to be the value, if one exists, such that for all $\epsilon > 0$ there is a neighborhood U of t (i.e. $U = (t-\delta, t+\delta) \cap \mathbb{T}$ for some $\delta > 0$) such that for all $s \in U$*

$$\left|\alpha[f^\sigma(t) - f(s)]\eta_{ts} + (1-\alpha)[f^\rho(t) - f(s)]\mu_{ts} - f^{\diamond_\alpha}(t)\mu_{ts}\eta_{ts}\right| < \epsilon|\mu_{ts}\eta_{ts}|.$$

We say that f is diamond-α differentiable on $\mathbb{T}_\kappa^\kappa$ provided $f^{\diamond_\alpha}(t)$ exists for all $t \in \mathbb{T}^\kappa$.

Remark. It is clear that $f^{\diamond_\alpha}(t)$ reduces to $f^\Delta(t)$ for $\alpha = 1$ and $f^\nabla(t)$ for $\alpha = 0$. The idea of such a formula can be traced back to Broyden's method in which combinations of different formulae are utilized. The new formula takes advantage of each individual method and provides a far more effective formula [15].

We show that the function described above is well-defined. Let each of $\Phi_1(t)$ and $\Phi_2(t)$ be values such that $\forall\epsilon > 0$ there exist neighborhoods U_1 and U_2 of t such that $\forall s \in U_1$

$$|\alpha[f^\sigma(t) - f(s)]\eta_{ts} + (1-\alpha)[f^\rho(t) - f(s)]\mu_{ts} - \Phi_1(t)\mu_{ts}\eta_{ts}| < \epsilon|\mu_{ts}\eta_{ts}|$$

and $\forall s \in U_2$

$$|\alpha[f^\sigma(t) - f(s)]\eta_{ts} + (1-\alpha)[f^\rho(t) - f(s)]\mu_{ts} - \Phi_2(t)\mu_{ts}\eta_{ts}| < \epsilon|\mu_{ts}\eta_{ts}|.$$

Let $\epsilon > 0$ be given and set $\epsilon_* = \epsilon/2$. Then $\forall s \in U = U_1 \cap U_2$ and

$$\begin{aligned}
&|\Phi_1(t) - \Phi_2(t)||\mu_{ts}\eta_{ts}| \\
=&|\Phi_1(t)\mu_{ts}\eta_{ts} - \Phi_2(t)\mu_{ts}\eta_{ts}| \\
=&\big|-\alpha[f^\sigma(t) - f(s)]\eta_{ts} - (1-\alpha)[f^\rho(t) - f(s)]\mu_{ts} + \Phi_1(t)\mu_{ts}\eta_{ts} \\
&+ \alpha[f^\sigma(t) - f(s)]\eta_{ts} + (1-\alpha)[f^\rho(t) - f(s)]\mu_{ts} - \Phi_2(t)\mu_{ts}\eta_{ts}\big| \\
<&\big|\alpha[f^\sigma(t) - f(s)]\eta_{ts} + (1-\alpha)[f^\rho(t) - f(s)]\mu_{ts} - \Phi_1(t)\mu_{ts}\eta_{ts}\big| \\
&+ \big|\alpha[f^\sigma(t) - f(s)]\eta_{ts} + (1-\alpha)[f^\rho(t) - f(s)]\mu_{ts} - \Phi_2(t)\mu_{ts}\eta_{ts}\big| \\
<&\epsilon_*|\mu_{ts}\eta_{ts}| + \epsilon_*|\mu_{ts}\eta_{ts}| \\
=&\epsilon|\mu_{ts}\eta_{ts}|.
\end{aligned}$$

Thus $|\Phi_1(t) - \Phi_2(t)| < \epsilon$ and letting ϵ go to zero, we see $\Phi_1(t) = \Phi_2(t)$. □

Theorem A.2.2. *Let $0 \le \alpha \le 1$. If f is both Δ and ∇ differentiable at $t \in \mathbb{T}$, then f is $\diamondsuit_\alpha$ differentiable at t and $f^{\diamondsuit_\alpha}(t) = \alpha f^\Delta(t) + (1-\alpha)f^\nabla(t)$.*

Proof. Assume $f^\Delta(t)$ and $f^\nabla(t)$ exist. Then $\forall \epsilon > 0$, $\exists$ neighborhoods U_1 and U_2 such that $\forall s \in U_1$

$$\big|[f^\sigma(t) - f(s)] - f^\Delta(t)\mu_{ts}\big| < \epsilon|\mu_{ts}|$$

and $\forall s \in U_2$

$$\big|[f^\rho(t) - f(s)] - f^\nabla(t)\eta_{ts}\big| < \epsilon|\eta_{ts}|.$$

Then $\forall s \in U_1$

$$\big|\alpha[f^\sigma(t) - f(s)]\eta_(ts) - \alpha f^\Delta(t)\mu_{ts}\eta_{ts}\big| < \alpha\epsilon|\mu_{ts}\eta_{ts}|$$

and $\forall s \in U_2$

$$\big|(1-\alpha)[f^\rho(t) - f(s)]\mu_{ts} - (1-\alpha)f^\nabla(t)\mu_{ts}\eta_{ts}\big| < (1-\alpha)\epsilon|\mu_{ts}\eta_{ts}|.$$

Thus $\forall s \in U = U_1 \cap U_2$ we have

$$\big|\alpha[f^\sigma(t) - f(s)]\eta_{ts} + (1-\alpha)[f^\rho(t) - f(s)]\mu_{ts} - [\alpha f^\Delta(t) + (1-\alpha)f^\nabla(t)]\mu_{ts}\eta_{ts}\big|$$

$$\leq \left|\alpha[f^{\sigma}(t) - f(s)]\eta_{ts} - \alpha f^{\Delta}(t)\mu_{ts}\eta_{ts}\right| + \left|(1-\alpha)[f^{\rho}(t) - f(s)]\mu_{ts} - (1-\alpha)f^{\nabla}(t)\mu_{ts}\eta_{ts}\right|$$

$$< \alpha\epsilon|\mu_{ts}\eta_{ts}| + (1-\alpha)\epsilon|\mu_{ts}\eta_{ts}| = \epsilon|\mu_{ts}\eta_{ts}|.$$

Thus $f^{\diamondsuit_\alpha}(t)$ exists and $f^{\diamondsuit_\alpha}(t) = \alpha f^{\Delta}(t) + (1-\alpha)f^{\nabla}(t)$. □

Corollary A.2.3. *Let $t \in \mathbb{T}$ be dense. Then if $f'(t)$ exists we have*

$$f^{\diamondsuit_\alpha}(t) = f^{\Delta}(t) = f^{\nabla}(t) = f'(t).$$

Proof. Let the point t be dense and $f'(t) = \lim_{h\to 0} \dfrac{f(t+h) - f(t)}{h}$ exist as a finite value. For a sufficiently small neighborhood U of t, $\forall s, t \in U$ we may substitute $h = s - t$ to see $f'(t) = \lim_{h\to 0} \dfrac{f(t+h) - f(t)}{h} = \lim_{s\to t} \dfrac{f(t) - f(s)}{t - s}$. Then by Theorem A.1.1 (iii), $f^{\Delta}(t) = f'(t)$, and by Theorem A.1.2 (iii), $f^{\nabla}(t) = f'(t)$. Thus by Theorem A.2.6,

$$f^{\diamondsuit_\alpha}(t) = \alpha f^{\Delta}(t) + (1-\alpha)f^{\nabla}(t) = \alpha f'(t) + (1-\alpha)f'(t) = f'(t).$$

□

Lemma A.2.4. *Let $t \in \mathbb{T}$ be scattered. Then f is continuous at t.*

Proof. Assume $t \in \mathbb{T}$ is scattered. Then $\mu(t) > 0$ and $\eta(t) > 0$. Let $0 < \delta < min(\mu(t), \eta(t))$. Then $\forall \epsilon > 0$ there is a neighborhood $U = (t-\delta, t+\delta) \cap \mathbb{T}$ of t such that $\forall s \in U$, $s = t$ and thus $|f(t) - f(s)| = 0 < \epsilon$. □

Corollary A.2.5. *Let $t \in \mathbb{T}$ be scattered. Then*

(i) $f^{\Delta}(t)$ exists and

$$f^{\Delta}(t) = \frac{f^{\sigma}(t) - f(t)}{\sigma(t) - t};$$

(ii) $f^{\nabla}(t)$ exists and

$$f^{\nabla}(t) = \frac{f^{\rho}(t) - f(t)}{\rho(t) - t};$$

(*iii*) $f^{\diamondsuit_\alpha}(t)$ *exists and*

$$f^{\diamondsuit_\alpha}(t) = \alpha \frac{f^\sigma(t) - f(t)}{\sigma(t) - t} + (1-\alpha)\frac{f^\rho(t) - f(t)}{\rho(t) - t}$$

Proof. By Lemma A.2.4, f is continuous at t. Then (ii) follows from Theorem A.1.1(ii), and (iii) follows from Theorem A.1.2(ii). Then by Theorem A.2.2,

$$f^{\diamondsuit_\alpha}(t) = \alpha f^\Delta(t) + (1-\alpha) f^\nabla(t) = \alpha \frac{f^\sigma(t) - f(t)}{\sigma(t) - t} + (1-\alpha)\frac{f^\rho(t) - f(t)}{\rho(t) - t}.$$

□

Corollary A.2.6. *Let $t \in \mathbb{T} \subset \mathbb{R}$ be left-scattered, right-dense, and assume*

$$f'(t^+) = \lim_{h \to 0^+} \frac{f(t+h) - f(t)}{h}$$

exists. Then

(*i*) $f^\Delta(t) = f'(t^+)$;
(*ii*) $f^\nabla(t) = \dfrac{f^\rho(t) - f(t)}{\rho(t) - t}$;
(*iii*) $f^{\diamondsuit_\alpha}(t) = \alpha f'(t^+) + (1-\alpha)\dfrac{f^\rho(t) - f(t)}{\rho(t) - t}$

Proof. For all neighborhoods $U = (t-\delta, t+\delta)$ of t such that $\delta < t - \rho(t)$, we have $s - t > 0$. Thus $\forall s, t \in U$ we can substitute $h = s - t$ in the limit from the right to see

$$\lim_{h \to 0^+} \frac{f(t+h) - f(t)}{h} = \lim_{s \to t} \frac{f(t) - f(s)}{t - s}$$

Then by Theorem A.1.1(iii),

$$f^\Delta(t) = \lim_{s \to t} \frac{f(t) - f(s)}{t - s} = f'(t^+).$$

Since $f'(t^+)$ exists, (ii) follows from Theorem A.1.2(ii). Then by Theorem A.2.2,

$$f^{\diamondsuit_\alpha}(t) = \alpha f^\Delta(t) + (1-\alpha) f^\nabla(t) = \alpha f'(t^+) + (1-\alpha)\frac{f^\rho(t) - f(t)}{\rho(t) - t}.$$

□

The proof of the following corollary is similar.

Corollary A.2.7. *Let $t \in \mathbb{T} \subset \mathbb{R}$ be left-dense, right-scattered, and assume*

$$f'(t^-) = \lim_{h \to 0^-} \frac{f(t+h) - f(t)}{h}$$

exists. Then

(i) $f^{\Delta}(t) = \dfrac{f^{\sigma}(t) - f(t)}{\sigma(t) - t}$;

(ii) $f^{\nabla}(t) = f'(t^-)$;

(iii) $f^{\diamondsuit_\alpha}(t) = \alpha \dfrac{f^{\sigma}(t) - f(t)}{\sigma(t) - t} + (1-\alpha) f'(t^-)$.

Theorem A.2.8. *Let $\mathbb{T}$ be a time scale and $0 \leq \alpha \leq 1$. If f is $\diamondsuit_\alpha$ differentiable at t, then f is continuous at t.*

Proof. Assume f is $\diamondsuit_\alpha$ differentiable at $t \in \mathbb{T}$. If t is a dense or scattered point, the result follows from Corollary A.2.3 and A.2.5 respectively. It remains to consider the two cases where t is right-dense and left-scattered, or t is right-scattered and left-dense.

Assume t right-dense and left-scattered. Thus $\sigma(t) = t$ and $\rho(t) < t$.

Let $\epsilon \in (0,1)$ and

$$\epsilon_* = \frac{\epsilon\alpha|\rho(t) - t|}{(1-\alpha)\big|[f^{\rho}(t) - f(t)] - f^{\diamondsuit_\alpha}(t)[\alpha(\rho(t) - t) - 1]\big| + |\rho(t) - t| + 1}.$$

Thus $0 < \epsilon_* < 1$. Then there is a neighborhood U_1 of t such that for all $s \in U_1$

$$\begin{aligned}
&\big|\alpha[f^{\sigma}(t) - f(s)]\eta_{ts} + (1-\alpha)[f^{\rho}(t) - f(s)]\mu_{ts} - f^{\diamondsuit_\alpha}(t)\mu_{ts}\eta_{ts}\big| \\
&= \big|\alpha[f(t) - f(s)][(\rho(t) - t) + (t - s)] \\
&+ (1-\alpha)[(f^{\rho}(t) - f(t)) + (f(t) - f(s))](t - s) \\
&- f^{\diamondsuit_\alpha}(t)(t - s)[(\rho(t) - t) + (t - s)]\big|
\end{aligned}$$

$$
\begin{aligned}
&= \big|\alpha[f(t)-f(s)](\rho(t)-t)+(1-\alpha)[f^{\rho}(t)-f(t)](t-s)\\
&\quad +[f(t)-f(s)](t-s)-f^{\diamondsuit_\alpha}(t)(t-s)[(\rho(t)-t)+(t-s)]\big|\\
&= \big|[f(t)-f(s)][\alpha(\rho(t)-t)+(t-s)]\\
&\quad +[(1-\alpha)[f^{\rho}(t)-f(t)]-f^{\diamondsuit_\alpha}(t)[\alpha(\rho(t)-t)+(t-s)]](t-s)\big|\\
&< \epsilon_*|\mu_{ts}\eta_{ts}|\\
&= \epsilon_*|(t-s)||[(\rho(t)-t)+(t-s)]|
\end{aligned}
$$

Thus

$$
\begin{aligned}
&\big||[f(t)-f(s)]\omega|-|[(1-\alpha)[f^{\rho}(t)-f(t)]-f^{\diamondsuit_\alpha}(t)\omega](t-s)|\big|\\
&<\epsilon_*|(t-s)||[(\rho(t)-t)+(t-s)]|
\end{aligned}
$$

where $\omega=\alpha(\rho(t)-t)+(t-s)$. Since t is left-scattered, right-dense we have for all $s\in U_1$, $\rho(t)<t\le s$. Thus for all $s\in U=U_1\cap(t-\epsilon_*,t+\epsilon_*)$

$$
|[f(t)-f(s)]\alpha(\rho(t)-t)|<|[f(t)-f(s)][\alpha(\rho(t)-t)+(t-s)]|
$$

$$
<\big|(1-\alpha)[f^{\rho}(t)-f(t)]-f^{\diamondsuit_\alpha}(t)[\alpha(\rho(t)-t)+(t-s)]\big|\,|t-s|+\epsilon_*|t-s||(\rho(t)-t)+(t-s)|
$$

$$
<\epsilon_*\big|(1-\alpha)[f^{\rho}(t)-f(t)]-f^{\diamondsuit_\alpha}(t)[\alpha(\rho(t)-t)-1]\big|+\epsilon_*[|\rho(t)-t|+1]
$$

Thus

$$
|f(t)-f(s)|<\frac{\epsilon_*\left[\big|(1-\alpha)[f^{\rho}(t)-f(t)]-f^{\diamondsuit_\alpha}(t)[\alpha(\rho(t)-t)-1]\big|+|\rho(t)-t|+1\right]}{\alpha|\rho(t)-t|}
$$

$$
=\epsilon.
$$

□

Theorem A.2.9. *Let $\mathbb{T}$ be a time scale and $0<\alpha<1$. If f is $\diamondsuit_\alpha$ differentiable at t, then f is both Δ and ∇ differentiable at t.*

Proof. Let $\mathbb{T}$ be a time scale and $0<\alpha<1$. Let $\epsilon>0$ be given, and set $\epsilon_*=\epsilon\frac{1-\alpha}{1+\alpha}>0$. Assume f is $\diamondsuit_\alpha$ differentiable at $t\in\mathbb{T}$. Thus by Theorem A.2.8, f is continuous at

t. If t is a dense or scattered point, the result follows from Corollaries A.2.3 and A.2.5 respectively. It remains to consider the two cases where t is right-dense and left-scattered, or t is right-scattered and left-dense.

Assume t right-scattered and left-dense. Thus $\sigma(t) > t$ and $\rho(t) = t$. Also, since f is continuous at t, by Theorem A.1.1(ii), f is Δ differentiable at t. Then for all $\epsilon_* > 0$ there is a neighborhood U_1 of t such that for all $s \in U_1$

$$|\alpha[f^\sigma(t) - f(s)]\eta_{ts} + (1-\alpha)[f^\rho(t) - f(s)]\mu_{ts} - f^{\diamondsuit_\alpha}(t)\mu_{ts}\eta_{ts}| < \epsilon_*|\mu_{ts}\eta_{ts}|$$

and neighborhood U_2 of t such that for all $s \in U_2$

$$\left|[f^\sigma(t) - f(s)] - f^\Delta(t)\mu_{ts}\right| < \epsilon_*|\mu_{ts}|.$$

Choose γ such that $f^{\diamondsuit_\alpha}(t) = \alpha f^\Delta(t) + (1-\alpha)\gamma$. Then there exists neighborhood $U = U_1 \cap U_2$ of t such that for all $s \in U$

$$\begin{aligned}
&\left|\alpha[f^\sigma(t) - f(s)]\eta_{ts} + (1-\alpha)[f^\rho(t) - f(s)]\mu_{ts} - [\alpha f^\Delta(t) + (1-\alpha)\gamma]\mu_{ts}\eta_{ts}\right| \\
&= \left|\alpha[f^\sigma(t) - f(s) - f^\Delta(t)\mu_{ts}]\eta_{ts} + (1-\alpha)[f^\rho(t) - f(s) - \gamma\eta_{ts}]\mu_{ts}\right| \\
&< \epsilon_*|\mu_{ts}\eta_{ts}|.
\end{aligned}$$

Thus

$$\begin{aligned}
|(1-\alpha)[f^\rho(t) - f(s) - \gamma\eta_{ts}]\mu_{ts}| &\le \epsilon|\mu_{ts}\eta_{ts}| + \left|\alpha[f^\sigma(t) - f(s) - f^\Delta(t)\mu_{ts}]\eta_{ts}\right| \\
&< \epsilon_*|\mu_{ts}\eta_{ts}| + \alpha\epsilon_*|\mu_{ts}\eta_{ts}| = (1+\alpha)\epsilon_*|\mu_{ts}\eta_{ts}|
\end{aligned}$$

Then

$$\left|[f^\rho(t) - f(s)] - \gamma\eta_{ts}\right| < \epsilon_*\frac{1+\alpha}{1-\alpha}|\eta_{ts}| = \epsilon|\eta_{ts}|.$$

Thus $f^\nabla(t) = \gamma$ exists.

The case t right-dense, left-scattered is similar. □

Remark. Note that the strict inequalities in $0 < \alpha < 1$ are necessary for the results above. In the case $\alpha = 1$, the $\diamondsuit_\alpha$ derivative reduces to the Δ derivative, which by Corollary A.1.3, does not imply the existence of the ∇. Similarly for $\alpha = 0$.

A.3 A Diamond-α Integral

We present two problematic cases that arise when we attempt to determine a corresponding $\diamondsuit_\alpha$ integral.

First, let $\alpha = \frac{1}{2}$ and $\mathbb{T}$ be the set $\{0, 1, 2, 3\}$. Then the $\diamondsuit_\alpha$ derivative for a function on $\mathbb{T}$ is defined on the set $\mathbb{T}_\kappa^\kappa$ which is $\{1, 2\}$. Define the function $f(t) \equiv 0$. Next define functions F and G as follows:

$$F(0) = 0, \qquad G(0) = 1;$$
$$F(1) = 5, \qquad G(1) = -3;$$
$$F(2) = 0, \qquad G(2) = 1;$$
$$F(3) = 5, \qquad G(3) = -3.$$

Then

$$F^{\diamondsuit_\alpha}(1) = \frac{1}{2}\frac{F(2) - F(1)}{2 - 1} + \frac{1}{2}\frac{F(1) - F(0)}{1 - 0} = \frac{1}{2}(0 - 5) + \frac{1}{2}(5 - 0) = 0 = f(1)$$

and

$$F^{\diamondsuit_\alpha}(2) = \frac{1}{2}\frac{F(3) - F(2)}{3 - 2} + \frac{1}{2}\frac{F(2) - F(1)}{2 - 1} = \frac{1}{2}(5 - 0) + \frac{1}{2}(0 - 5) = 0 = f(2).$$

Also

$$G^{\diamondsuit_\alpha}(1) = \frac{1}{2}\frac{G(2) - G(1)}{2 - 1} + \frac{1}{2}\frac{G(1) - G(0)}{1 - 0} = \frac{1}{2}(1 - (-3)) + \frac{1}{2}(-3 - 1) = 0 = f(1)$$

and

$$G^{\diamondsuit_\alpha}(2) = \frac{1}{2}\frac{G(3) - G(2)}{3 - 2} + \frac{1}{2}\frac{G(2) - G(1)}{2 - 1} = \frac{1}{2}(-3 - 1) + \frac{1}{2}(1 - (-3)) = 0 = f(2).$$

Thus $F^{\diamondsuit_\alpha}(t) = G^{\diamondsuit_\alpha}(t) = f(t)$ on $\mathbb{T}_\kappa^\kappa$. We see that both F and G are $\diamondsuit_\alpha$ antiderivatives of f on $\mathbb{T}_\kappa^\kappa$. However,

$$\int_1^2 f(t)\diamondsuit_\alpha t = F(2) - F(1) = -5 \neq 4 = G(2) - G(1) = \int_1^2 f(t)\diamondsuit_\alpha t$$

and we have arrived at a contradiction.

The above counterexample can be generalized for any fixed α strictly between 0 and 1, and for any purely discrete time scale, such as $\mathbb{T} = \mathbb{Z}$.

Next, we present an example where no $\diamondsuit_\alpha$ antiderivative exists. Again let $\alpha = \frac{1}{2}$. Let $\mathbb{T}$ be $(-\infty, 1] \cup [2, \infty)$. Set

$$f(t) = \begin{cases} -1 & x \leq 1 \\ 5 & x \geq 2. \end{cases}$$

Assume a $\diamondsuit_\alpha$ antiderivative F of f exists on $\mathbb{T}_\kappa^\kappa$. On $(-\infty, 1]$, F must be of the form $-t + C_1$ where C_1 is a constant. On $[2, \infty)$, F must be of the form $5t + C_2$

We have

$$F^{\diamondsuit_\alpha}(1) = \frac{1}{2}F^{\Delta}(1) + \frac{1}{2}F^{\nabla}(1) = f(1).$$

Thus

$$\frac{1}{2}[(5(2) + C_2) - (-1(1) + C_1)] + \frac{1}{2}(-1) = -1. \tag{A.1}$$

Also,

$$F^{\diamondsuit_\alpha}(2) = \frac{1}{2}F^{\Delta}(2) + \frac{1}{2}F^{\nabla}(2) = f(2).$$

Thus

$$\frac{1}{2}(5) + \frac{1}{2}[(5(2) + C_2) - (-1(1) + C_1)] = 5. \tag{A.2}$$

From $(A.1)$ and $(A.2)$ we obtain a system of equations

$$C_1 - C_2 = 12,$$

$$C_1 - C_2 = 6$$

with no solution. Thus for function f, which is continuous on $\mathbb{T}$, no $\diamondsuit_\alpha$ antiderivative exists on $\mathbb{T}_\kappa^\kappa$. Therefore it cannot be used for solving the optical wave equations, including the Helmholtz equation, on hybrid grids.

A.4 Numerical Examples

We consider adaptive approximations of the kink function,

$$u(x,y) = \alpha \arctan \exp\left\{\beta - \sqrt{x^2+y^2}\right\}, \tag{A.3}$$

for initializing a sequence of circular ring solitons from the sine-Gordon equation,

$$w_{rr} = w_{xx} + w_{yy} - \phi(x,y)\sin w, \quad r > 0,$$

in the spacial domain $\Omega = \{(x,y)| -a < x < a, \ -b < y < b\}$, where the function ϕ is often interpreted as a Josephson current density of the solitary wave [1, 65].

For the sake of simplicity in our one-dimensional experiments, we set $\alpha = \beta = \pi$, $a = 14$ and $y \equiv 0$. Replace the notation x by t, from $(A.3)$ we have

$$u(t) = \pi \arctan \exp\{\pi - |t|\}, \quad -14 \le t \le 14.$$

The function value changes rapidly while $-7 < t < 7$, and u is not smooth throughout the interval [-14, 14] due to the fact that

$$u'(t) = \begin{cases} \pi/\left[1+(\pi+t)^2\right], & t < 0, \\ -\pi/\left[1+(\pi-t)^2\right], & t > 0, \end{cases}$$

and $u'(0)$ does not exist. The change of the derivative function value is more violent throughout the domain, and introduces substantial difficulties in approximating u' over the interval [-14, 14] using one formula. This motivates our numerical investigations targeted at the approximations of u'.

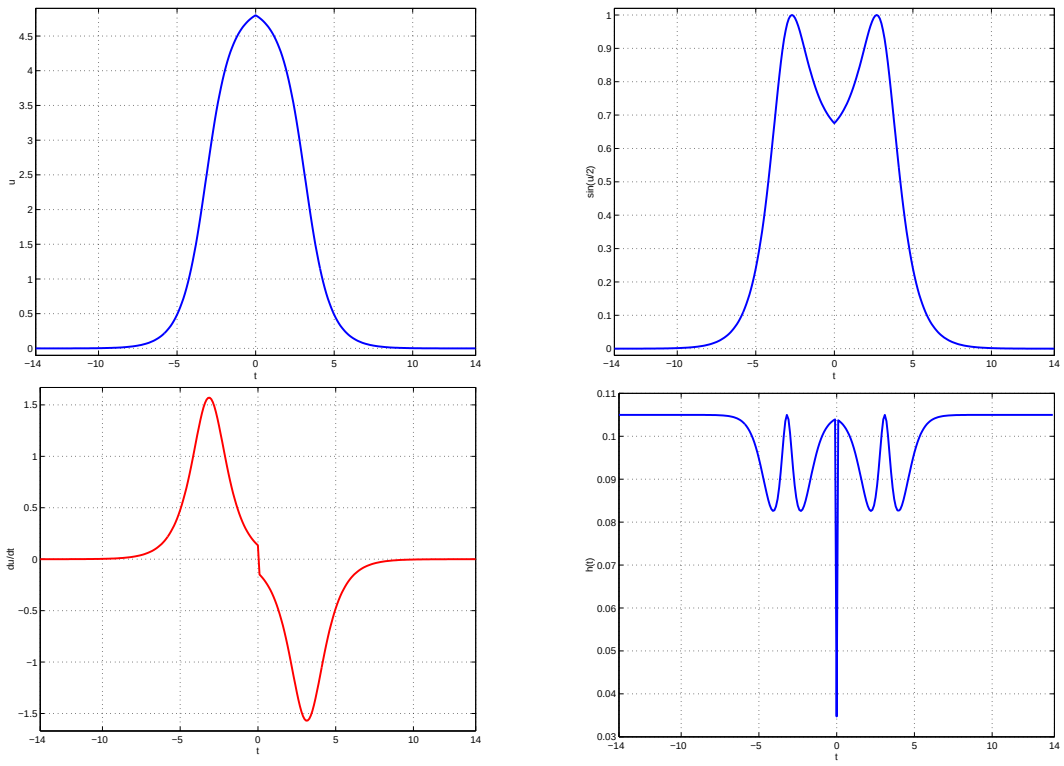

FIGURE A.4.1. The kink function u (top-left); its sine mode representation $\sin(u/2)$ (top-right); derivative u' (bottom-left); and distribution of the adaptive step sizes based on the derivative function (bottom-right).

In Figure A.4.1, we show the solitary kink function, its sine mode representation $s = \sin(u/2)$, the velocity of the kink, that is, $v = u'$, and an arc-length adaptive step (equivalent to μ or η) distribution generated based on the derivative function [64, 65]. Note that the sudden decrease of the step sizes as t approaches 0 is due to the singularity involved. The adaptive mechanism established offers a nonuniform time scale $\mathbb{T}$ superimposed over the interval [-14, 14] for a possibly more accurate approximation to the derivative function u' from the data u. The number of grids used, n, is 280, with the minimal step size $h_{\min} \approx 0.03473491$ and maximal step size $h_{\max} \approx 0.10497856$. Since the nonuniform grids obtained are symmetric about $t = 0$, anti-symmetric properties of the Δ and ∇ dynamic derivatives are expected [20, 58, 59].

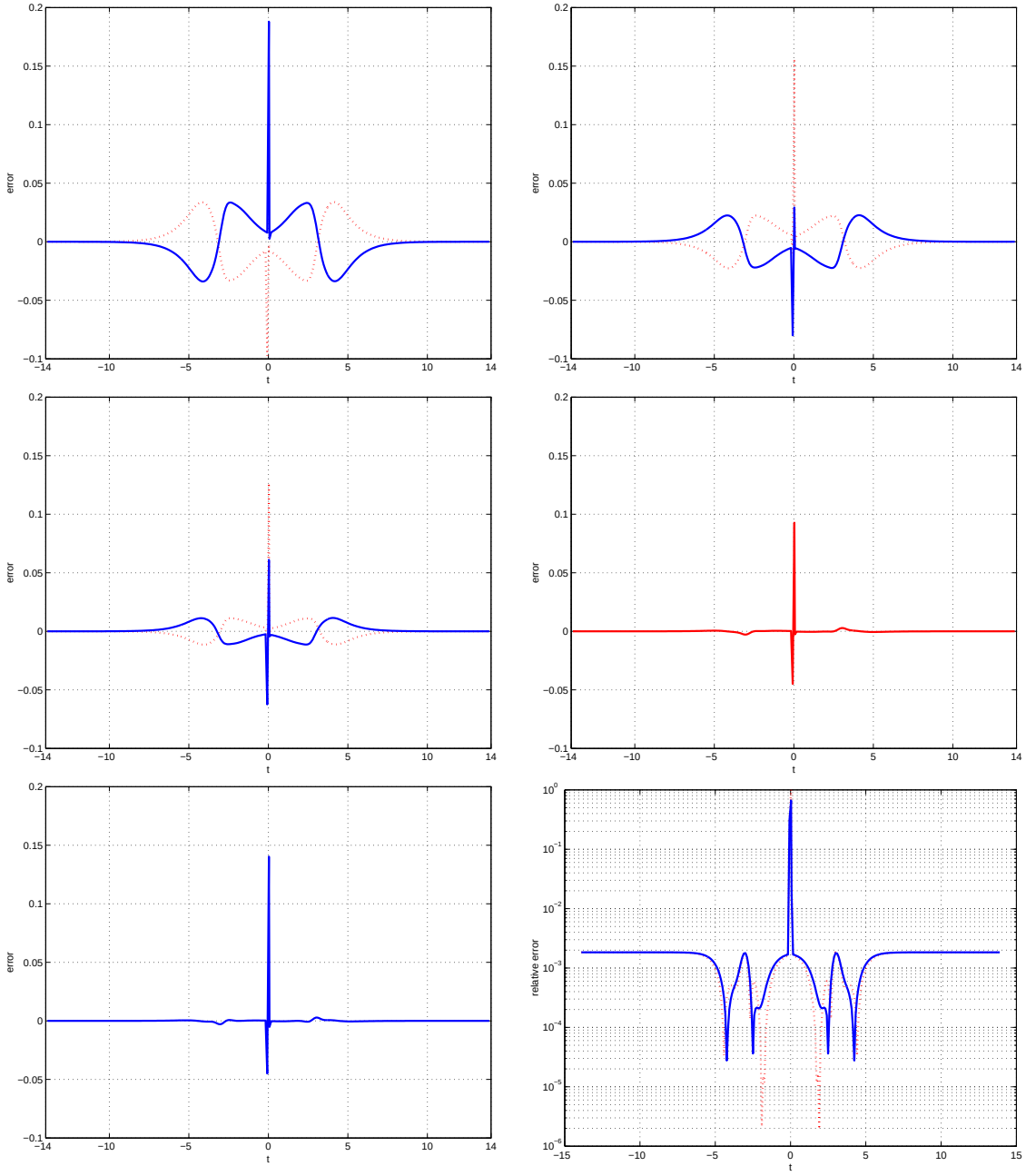

FIGURE A.4.2. Numerical errors of the different approximations of u' on the discrete time scale $\mathbb{T}$. TOP-LEFT: ϵ_{Δ} (dotted curve) and ϵ_{∇} (solid curve); TOP-RIGHT: $\epsilon_{\diamondsuit_{1/6}}$ (dotted curve) and $\epsilon_{\diamondsuit_{5/6}}$ (solid curve); CENTER-LEFT: $\epsilon_{\diamondsuit_{1/3}}$ (dotted curve) and $\epsilon_{\diamondsuit_{2/3}}$ (solid curve); CENTER-RIGHT: $\epsilon_{\diamondsuit_{1/2}}$; BOTTOM-LEFT: ϵ_{D}; BOTTOM-RIGHT: relative errors of the $\diamondsuit_{1/2}$ (solid curve) and modified central difference formula $(A.4)$ (dotted curve). Logarithmic y-scale is used to show details of the error distributions.

Numerical errors of approximations of u' on $\mathbb{T}$ via different dynamic derivative

$$\begin{aligned} \epsilon_{\Delta} &= u^{\Delta} - u', \\ \epsilon_{\nabla} &= u^{\nabla} - u', \\ \epsilon_{\diamondsuit_\alpha} &= u^{\diamondsuit_\alpha} - u' \end{aligned}$$

are presented in Figure A.4.2. A modified finite difference formula,

$$u^{\mathrm{D}} = 2\frac{u^{\Delta}(t) - u^{\nabla}(t)}{\mu(t) + \eta(t)}, \tag{A.4}$$

is introduced for comparison purposes on the nonuniform discrete time scale $\mathbb{T}$. For it, we denote $u^{\mathrm{D}} - u' = \epsilon_{\mathrm{D}},\ t \in \mathbb{T}$. Further, to see more precisely the superior quality of the $\diamondsuit_{1/2}$ approximation, we also plot the point-wise relative errors,

$$\mathcal{E}_{\diamondsuit_{1/2}} = \left\{ \frac{|\epsilon_{\diamondsuit_{1/2}}|_i}{|u'|_i} \right\}_{i=1}^{n}, \quad \mathcal{E}_{\mathrm{D}} = \left\{ \frac{|\epsilon_{\mathrm{D}}|_i}{|u'|_i} \right\}_{i=1}^{n},$$

in Figure A.4.2. Logarithmic y-scale is used to give a better view of the details. All computations are implemented based on the u on the nonuniform discrete time scale $\mathbb{T}$.

It is observed in Figure A.4.2 that the $\diamondsuit_\alpha$ dynamic derivative provides better overall approximation results than traditional Δ and ∇ dynamic derivatives with the α values used. When $\alpha = 1/2$, the $\diamondsuit_\alpha$ derivative not only indicates a comparable quality as compared with the modified finite difference formula which is used in most adaptive algorithms, but also demonstrates a superior tolerance around the singular point. The latter property implies that the $\diamondsuit_\alpha$ dynamic derivative is perhaps a better approximation formula to be used in numerical problems involving possible singularities. This is important in many adaptive and hybrid computational applications.

For each point t, it is possible to calculate a value of α that minimizes $|\epsilon_{\diamondsuit_\alpha}|$. When t is scattered, we have

$$\epsilon_{\diamondsuit_\alpha} = u^{\diamondsuit_\alpha}(t) - u'(t) = u^{\diamondsuit_\alpha}(t) = \alpha\frac{u^{\sigma}(t) - u(t)}{\sigma(t) - t} + (1-\alpha)\frac{u^{\rho}(t) - u(t)}{\rho(t) - t} - u'(t).$$

We find that the error is minimized when

$$\alpha = \frac{\mu(t)[\eta(t)u'(t) - u(t) + u^{\rho}(t)]}{\eta(t)[u^{\sigma} - u(t)] - \mu(t)[u(t) - u^{\rho}(t)]}.$$

Figure A.4.3 below presents the best α values for the grid points used in the domain of our kink function example.

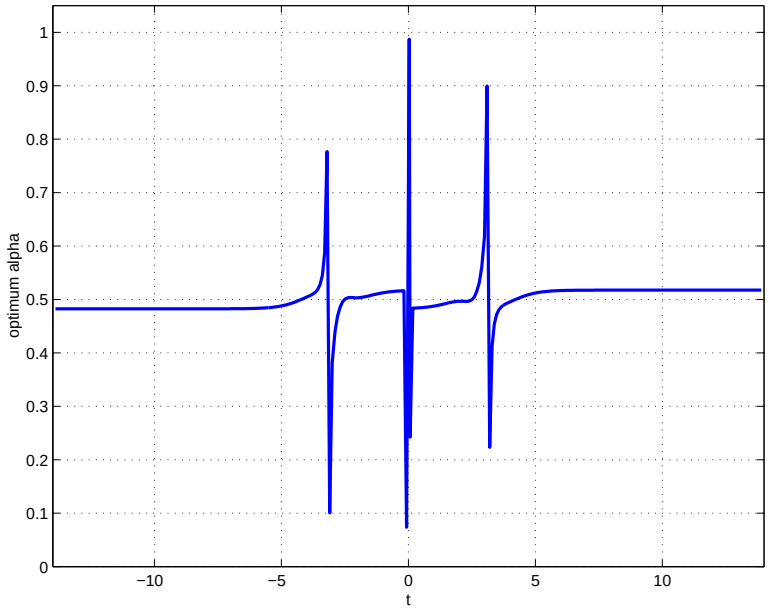

FIGURE A.4.3. Alpha values minimizing $|\epsilon_{\diamondsuit_\alpha}|$

Numerical experiments were carried out using MATLAB and SIMULINK subroutines on dual-processor DELL Precision workstations.

APPENDIX B

Matlab Code

B.1 Example r-Stretching Transformations

```
% toy problem for r-stretching proof of principle
function f = example()

clear;
R1 = 1;

M = 500;          % number of steps in y direction
h = R1/M;         % spatial step size

eta = pi/4;       % interface position
bta = 1;        % steepness factor

%-- Calculate initial r transform

xfrm(1) = 0;
q = h/2;
for j = 2:2*M+1
  p1 = q*stretch_factor(xfrm(j-1),eta,bta,R1,h);
  p2 = q*(stretch_factor(xfrm(j-1) + (p1/2),eta,bta,R1,h));
  p3 = q*(stretch_factor(xfrm(j-1) + (p2/2),eta,bta,R1,h));
  p4 = q*(stretch_factor(xfrm(j-1) + p3,eta,bta,R1,h));
  xfrm(j) = xfrm(j-1) + p1/6 + p2/3 + p3/3 + p4/6;
end

%-- Calculate r transform derivatives

r_val(1) = xfrm(1);
half_r(1) = xfrm(2);
for j = 2:M
  r_val(j) = xfrm(2*j - 1);
  half_r(j) = xfrm(2*j);
  r_y(j-1) = (xfrm(2*j-1) - xfrm(2*j-3))/h;
  r_yy(j) = (xfrm(2*j) - 2*xfrm(2*j-1) + xfrm(2*j-2))/(q^2);
end
r_val(M+1) = xfrm(2*M + 1);
r_yy(1) = 0;
r_y(M) = (xfrm(2*M+1) - xfrm(2*M-1))/h;
r_y(M+1) = r_y(M);
r_yy(M+1) = 0;
```

```
% set coefficient matrix

lhs_mtx(1,1:M+1) = -1;
lhs_mtx(2,1:M+1) = 1;
lhs_mtx(3,1:M+1) = 0;

lhs_mtx(3,1) = 0;
lhs_mtx(3,M+1) = 0;
lhs_mtx(2,1) = 1;
lhs_mtx(2,M+1) = 1;
lhs_mtx(1,1) = 0;
lhs_mtx(1,M+1) = -1;

u1(1) = 0;
u1(2:M+1) = h*r_y(1:M).*(f_func(half_r(1:M),eta,bta,R1,h));

% solve system of linear equations with Thomas algorithm
d(1) = lhs_mtx(3,1)/lhs_mtx(2,1);
v(1) = u1(1)/lhs_mtx(2,1);
for k=2:M+1
  c1 = lhs_mtx(1,k);
  p = lhs_mtx(2,k) - c1*d(k-1);
  d(k) = lhs_mtx(3,k)/p;
  v(k) = (u1(k) - c1*v(k-1))/p;
end
u1(M+1) = v(M+1);
for k=M:-1:1
  u1(k) = v(k)-d(k)*u1(k+1);
end

ygrid = 0:h:M*h;
rgrid = 0:h:M*h;

%% plotting figures <==========

figure(1)
plot(ygrid,r_y,'b')
xlabel('y');
ylabel('r_y');
grid on
axis([0 R1 -0.05 2.05]);
title('r derivative')

figure(2)
plot(ygrid,r_val,'b')
xlabel('y');
ylabel('r_val');
```

```
grid on
axis([0 R1 0 R1+0.01]);
title('r transform')

figure(3)
plot(ygrid,u1,'b')
xlabel('y');
ylabel('u');
grid on
axis([0 R1 0 R1+0.05]);
title('stretched solution')

v = interp1(r_val,u1,rgrid,'spline');

figure(4)
plot(rgrid,v,'r')
xlabel('r');
ylabel('v');
grid on
axis([0 R1 0 R1+0.05]);
title('solution in r')

% analytic piecewise linear solution
for k=1:M+1
  r = (k-1)*h;
  if (r < pi/4)
    a_u(k) = (4/pi)*r;
  else
    a_u(k) = 1 - (4/(4-pi))*(r-(pi/4));
  end
end

figure(5)
plot(rgrid,a_u,'b')
xlabel('r');
ylabel('error');
grid on
axis([0 R1 0 1.05]);
title('analytic solution')

figure(6)
plot(rgrid,abs(v-a_u),'b')
xlabel('r');
ylabel('error');
grid on
axis([0 R1 0 0.003]);
title('error of solution post transform')
```

```
% the sigma function
function a1 = sigma_func(r,eta,bta,R1,h)
  a1 = (tanh(bta*(r-eta)/h)...
    - tanh(bta*(-eta)/h))/(tanh(bta*(R1-eta)/h)...
    - tanh(bta*(-eta)/h));

% sigma function first derivative w/respect to r
function a2 = sigma_r(r,eta,bta,R1,h)
  a2 = bta*((sech(bta*(r-eta)/h)).^2)./(h*(tanh(bta*(R1-eta)/h)...
    - tanh(bta*(-eta)/h)));

% simple mesh generator dr/dy = stretch_factor(y,r)
function a4 = stretch_factor(r,eta,bta,R1,h)
  s_r = sigma_r(r,eta,bta,R1,h);
  a4 = 2./(1 + R1*s_r);

% the differential equation: du/dr = f_func(r,eta,bta,R1,h)
function a5 = f_func(r,eta,bta,R1,h)
  a5 = 4/pi - (16/((4-pi)*pi))*sigma_func(r,eta,bta,R1,h);
```

B.2 Moving Mesh Method

```
%% Helmholtz paraxial, radially symmetric domain
function f = movmesh()

clear;
R = 1.969;
lens = 0.7643;
Z1 = lens;
R1 = 1.5574;

N = 32000;    % number of steps in x direction
M = 5000;    % number of steps in y direction

tau = Z1/N;  % propagation step size
h = R1/M    % spatial step size

z = 0;
eta = interface_r_position(z,R);
etam = max(eta,h);
etam = min(etam,R1-h);
bta = 1/20;
alph = tau/(2*(h^2));

tic
```

```
%-- Calculate initial r transform
fine_r(1) = 0;
omega = h/2;
for j = 2:2*M+1
  p1 = omega*stretch_factr(fine_r(j-1),etam,bta,R1,h);
  p2 = omega*(stretch_factr(fine_r(j-1) + (p1/2),etam,bta,R1,h));
  p3 = omega*(stretch_factr(fine_r(j-1) + (p2/2),etam,bta,R1,h));
  p4 = omega*(stretch_factr(fine_r(j-1) + p3,etam,bta,R1,h));
  fine_r(j) = fine_r(j-1) + p1/6 + p2/3 + p3/3 + p4/6;
end

%-- Calculate r transform derivatives

new_r(1:M+1) = fine_r(1:2:2*M+1);
new_r_y(2:M) = (new_r(3:M+1) - new_r(1:M-1))/(2*h);
new_r_y(1) = new_r_y(2);
new_r_y(M+1) = new_r_y(M);
new_r_yy(2:M) = (new_r(3:M+1)-2*new_r(2:M)+new_r(1:M-1))/(h*h);
new_r_yy(1) = 0;
new_r_yy(M+1) = 0;

init_r = new_r;
old_r = new_r;
old_r_y = new_r_y;
old_r_yy = new_r_yy;

k2 = 9.97e+03;
k1 = (2/3)*k2;

m_cnt(1:M+1) = 0:1:M;
rgrid = 0:h:M*h;

init_soln = gaussian(0,old_r,k1);
u0 = init_soln;
soln_near_axis(1) = init_soln(2);

ygrid = 0:h:M*h;
figure(1)
plot(ygrid,old_r,'y')
axis([0 R1 0 R1]);
xlabel('y');
ylabel('r(y)');
grid on;
title('initial r transform')

for kk=1:N

  %% we need to reset matrices for each z
```

```
z = z + tau;
eta = interface_r_position(z,R);
etam = max(eta,h);
etam = min(etam,R1-h);

%-- Calculate r transform for current propagation step
fine_r(1) = 0;
omega = h/2;
for j = 2:2*M+1
  p1 = omega*stretch_factr(fine_r(j-1),etam,bta,R1,h);
  p2 = omega*(stretch_factr(fine_r(j-1) + (p1/2),etam,bta,R1,h));
  p3 = omega*(stretch_factr(fine_r(j-1) + (p2/2),etam,bta,R1,h));
  p4 = omega*(stretch_factr(fine_r(j-1) + p3,etam,bta,R1,h));
  fine_r(j) = fine_r(j-1) + p1/6 + p2/3 + p3/3 + p4/6;
end

%-- Calculate r transform derivatives

new_r(1:M+1) = fine_r(1:2:2*M+1);
new_r_y(2:M) = (new_r(3:M+1) - new_r(1:M-1))/(2*h);
new_r_y(1) = new_r_y(2);
new_r_y(M+1) = new_r_y(M);
new_r_yy(2:M) = (new_r(3:M+1)-2*new_r(2:M)+new_r(1:M-1))/(h*h);
new_r_yy(1) = 0;
new_r_yy(M+1) = 0;

%-- Calculate the mid-step transform, derivative
%-- and coefficient values
r_val = (old_r + new_r)/2;
r_x = (new_r - old_r)/tau;
r_y = (old_r_y + new_r_y)/2;
r_yy = (old_r_yy + new_r_yy)/2;
eta = interface_r_position(z-(tau/2),R);
k_val = wave_number(r_val,eta,bta,R1,h);

%% mtx(1,*) is the left subdiagonal line; index starts at 2
%% mtx(2,*) is the main diagonal line; index starts at 1
%% mtx(3,*) is the right subdiagonal line; index starts at 1

gam(1:M+1) = i*alph./(k_val.*(r_y.^2));
phi(2:M) = (h*r_y(2:M)/2).*(2*i*k_val(2:M).*r_x(2:M)...
  - r_yy(2:M)./(r_y(2:M).^2) + 1./r_val(2:M));
phi(1) = 1;
phi(M+1) = 1;

lhs_mtx(1,:) = gam.*(1-phi);
lhs_mtx(2,:) = 2 - 2*gam;
lhs_mtx(3,:) = gam.*(1+phi);
```

```
   lhs_mtx(3,1) = 2*gam(1);
   lhs_mtx(3,M+1) = 0;
   lhs_mtx(1,1) = 0;
   lhs_mtx(1,M+1) = 2*gam(M+1);

   rhs_mtx(1,:) = -gam.*(1-phi);
   rhs_mtx(2,:) = 2 + 2*gam;
   rhs_mtx(3,:) = -gam.*(1+phi);

   rhs_mtx(3,1) = -2*gam(1);
   rhs_mtx(3,M+1) = 0;
   rhs_mtx(1,1) = 0;
   rhs_mtx(1,M+1) = -2*gam(M+1);

%% solution of the system:
%% right-hand-side of the system:

   u1(1) = rhs_mtx(2,1)*u0(1) + rhs_mtx(3,1)*u0(2);
   u1(2:M) = rhs_mtx(1,2:M).*u0(1:M-1) + rhs_mtx(2,2:M).*u0(2:M)...
     + rhs_mtx(3,2:M).*u0(3:M+1) ;
   u1(M+1) = rhs_mtx(1,M+1)*u0(M) + rhs_mtx(2,M+1)*u0(M+1);

% solution of the tridiagonal system:
% Thomas algorithm

   u1 = thomas_solve(u1,lhs_mtx,M);
   u0 = u1;

   old_r = new_r;
   old_r_y = new_r_y;
   old_r_yy = new_r_yy;

   soln_near_axis(kk+1) = u1(2);
end

toc

% boundary values for next domain segment
u0 = u1;
last_r = new_r;

%% plotting figures <==========

real_near_axis = real(soln_near_axis);
imag_near_axis = imag(soln_near_axis);
intensity_near_axis = (real_near_axis.^2)+(imag_near_axis.^2);
max_real_near_axis = max(real_near_axis);
min_real_near_axis = min(real_near_axis);
```

```
max_imag_near_axis = max(imag_near_axis);
min_imag_near_axis = min(imag_near_axis);
max_intensity_near_axis = max(intensity_near_axis);
min_intensity_near_axis = min(intensity_near_axis);

x = 0:tau:N*tau;

u_real = real(init_soln);
u_imag = imag(init_soln);
u_intensity = u_real.^2 + u_imag.^2;

v = interp1(init_r,init_soln,rgrid,'spline');
u_real = real(v);
u_imag = imag(v);
u_intensity = u_real.^2 + u_imag.^2;

figure(3)
plot(rgrid,u_real,'r')
axis([0 R1 -1.02 1.05]);
xlabel('r');
ylabel('u');
grid on;
hold on;
plot(rgrid,u_imag,'k')
plot(rgrid,u_intensity,'--b','linewidth',2)
title('initial value: r-real, k-imaginary, b-intensity')
hold off

u_real = real(u0);
u_imag = imag(u0);
u_intensity = u_real.^2 + u_imag.^2;
max_real_u = max(u_real);
min_real_u = min(u_real);
max_imag_u = max(u_imag);
min_imag_u = min(u_imag);
max_intensity_u = max(u_intensity);
min_intensity_u = min(u_intensity);
u_max = max([max_real_u,max_imag_u,max_intensity_u]);
u_min = min([min_real_u,min_imag_u,min_intensity_u]);

figure(7)
plot(rgrid,u_real,'r')
axis([0 R1 u_min u_max]);
xlabel('r');
ylabel('u');
grid on;
hold on;
plot(rgrid,u_imag,'k')
```

```
plot(rgrid,u_intensity,'--b','linewidth',2)
title('soln exiting lens: r-real, k-imaginary, b-intensity')
hold off


%%-------------------------------------
%%-------------------------------------
% domain segment past lens
%%-------------------------------------
%%-------------------------------------

Z2 = 6*Z1;
lensN = N;
N = 5*N;

tau = (Z2-Z1)/N;
h = R1/M;
courant = tau/(h*h)
lam = tau/(2*i*h*h*k1)

%% ------------------------

lhs_mtx(1,2:M) = -lam*(1-(1./(2*m_cnt(2:M))));
lhs_mtx(2,:) = 2 + 2*lam;
lhs_mtx(3,2:M) = -lam*(1+(1./(2*m_cnt(2:M))));

lhs_mtx(3,1) = -2*lam;
lhs_mtx(3,M+1) = 0;
lhs_mtx(1,1) = 0;
lhs_mtx(1,M+1) = -2*lam;

rhs_mtx(1,2:M) = lam*(1-(1./(2*m_cnt(2:M))));
rhs_mtx(2,:) = 2 - 2*lam;
rhs_mtx(3,2:M) = lam*(1+(1./(2*m_cnt(2:M))));

rhs_mtx(3,1) = 2*lam;
rhs_mtx(3,M+1) = 0;
rhs_mtx(1,1) = 0;
rhs_mtx(1,M+1) = 2*lam;

%% now, advancement in z-direction:

%% we will save the solution at max intensity
u_max = u0;
intensity = 0.0;
max_intensity = 0.0;
max_intense_index = 0;
```

```
for kk=1:N

%% solution of the system:
%% right-hand-side of the system:

  u1(1) = rhs_mtx(2,1)*u0(1) + rhs_mtx(3,1)*u0(2);
  u1(2:M) = rhs_mtx(1,2:M).*u0(1:M-1) + rhs_mtx(2,2:M).*u0(2:M)...
    + rhs_mtx(3,2:M).*u0(3:M+1) ;
  u1(M+1) = rhs_mtx(1,M+1)*u0(M) + rhs_mtx(2,M+1)*u0(M+1);

  u0=u1;

  u1 = thomas_solve(u1,lhs_mtx,M);
  u0 = u1;

  if (intensity > max_intensity)
    max_intensity = intensity;
    max_intense_index = N+kk;
    u_max = u1;
  end;
  soln_near_axis(lensN+kk+1) = u1(2);
end


%% plotting figures <==========


real_near_axis = real(soln_near_axis);
imag_near_axis = imag(soln_near_axis);
intensity_near_axis = (real_near_axis.^2) + (imag_near_axis.^2);
max_real_near_axis = max(real_near_axis);
min_real_near_axis = min(real_near_axis);
max_imag_near_axis = max(imag_near_axis);
min_imag_near_axis = min(imag_near_axis);
max_intensity_near_axis = max(intensity_near_axis);
min_intensity_near_axis = min(intensity_near_axis);

x = 0:tau:(lensN + N)*tau;

u_real = real(u_max);
u_imag = imag(u_max);
u_intensity = u_real.^2 + u_imag.^2;
max_real_u = max(u_real);
min_real_u = min(u_real);
max_imag_u = max(u_imag);
min_imag_u = min(u_imag);
max_intensity_u = max(u_intensity);
min_intensity_u = min(u_intensity);
```

```
u_max = max([max_real_u,max_imag_u,max_intensity_u]);
u_min = min([max_real_u,max_imag_u,max_intensity_u]);
max_t = max([max_real_u max_imag_u max_intensity_u]);
min_t = min([min_real_u min_imag_u min_intensity_u]);

figure(8)
plot(rgrid,u_real,'r')
axis([0 R1 min_t max_t]);
xlabel('r');
ylabel('u');
grid on;
hold on;
plot(rgrid,u_imag,'k')
plot(rgrid,u_intensity,'--b','linewidth',2)
title('soln at focus: r-real, k-imaginary, b-intensity')
hold off

figure(9)
plot(x,real_near_axis,'r')
xlabel('z');
ylabel('real(u)');
grid on
axis([0 Z2 min_real_near_axis max_real_near_axis]);
title('real component of solution near z-axis')

figure(10)
plot(x,imag_near_axis,'r')
xlabel('z');
ylabel('imag(u)');
grid on
axis([0 Z2 min_imag_near_axis max_imag_near_axis]);
title('imag component of solution near z-axis')

figure(11)
plot(x,intensity_near_axis,'r')
xlabel('z');
ylabel('real(u)*real(u)+imag(u)*imag(u)');
grid on
axis([0 Z2 min_intensity_near_axis max_intensity_near_axis]);
title('intensity of solution near z-axis')


% the sigma function
function a1 = sigma_func(r,eta,bta,R1,h)
  a1 = (tanh(bta*(r-eta)/h)...
    - tanh(bta*(-eta)/h))/(tanh(bta*(R1-eta)/h)...
    - tanh(bta*(-eta)/h));
```

```
% sigma function first derivative w/respect to r
function a2 = sigma_r(r,eta,bta,R1,h)
  a2 = bta*((sech(bta*(r-eta)/h)).^2)./(h*(tanh(bta*(R1-eta)/h)...
    - tanh(bta*(-eta)/h)));

% simple mesh generator dr/dy = stretch_factr(y,r)
function a4 = stretch_factr(r,eta,bta,R1,h)
  s_r = sigma_r(r,eta,bta,R1,h);
  a4 = 2./(1 + R1*s_r);

function a5 = wave_number(r,eta,bta,R1,h)
  k = 9.97e+03;
  a5 = k*(1 - (1/3)*sigma_func(r,eta,0.5,R1,h));

function a6 = interface_r_position(z,R)
  a6 = sqrt(R^2 - (z-R).^2);

function a7 = thomas_solve(u,lhs_mtx,M)

  w = u;
  d(1) = lhs_mtx(3,1)/lhs_mtx(2,1);
  v(1) = w(1)/lhs_mtx(2,1);
  for k=2:M+1
    c1 = lhs_mtx(1,k);
    p = lhs_mtx(2,k) - c1*d(k-1);
    d(k) = lhs_mtx(3,k)/p;
    v(k) = (w(k) - c1*v(k-1))/p;
  end
  w(M+1) = v(M+1);
  for k=M:-1:1
    w(k) = v(k)-d(k)*w(k+1);
  end
  a7 = w;

function a8 = gaussian(z,r,k)

  B0 = 0.5;
  z0 = 100;
  A = exp(i*k*z0);
  B = sqrt(1/((1/(B0^2))+(i*k/(2*z0))));
  Z = 2*z/((B^2)*k);
  a8 = (A./(1+i*Z)).*exp(i*k*z - ((r.^2)./((B^2).*(1+i*Z))));
```

BIBLIOGRAPHY

[1] M. J. Ablowitz, B. M. Herbst and C. Schober, On the numerical solution of the sine-Gordon equation, *J. Comput. Phys,* **126** (1996), 299-314.

[2] R. E. Alcouffe, A. Brandt, J. E. Dendy and J. W. Painter, The multi-grid method for the diffusion equation with strongly discontinuous coefficients, *J. Sci. Stat. Comput.,* **2** (1981), 430–454.

[3] F. M. Atıcı and G. Sh. Guseinov, On Green's functions and positive solutions for boundary value problems on time scales, *J. Comput. Appl. Math.,* **18** (2002), 75-99.

[4] A. Bamberger, B. Engquist, L. Halpern and P. Joly, Parabolic wave equation approximations in heterogeneous media, *SIAM J. Applied Math.,* **48** (1988), 99-128.

[5] A. Bamberger, B. Engquist, L. Halpern and P. Joly, Higher order paraxial wave equation approximations in heterogeneous media, *SIAM J. Applied Math.,* **48** (1988), 129-154.

[6] Y. B. Band, *Light and Matter: Electromagnetism, Optics, Spectroscopy and Lasers,* John Wiley & Sons, West Sussex, 2006.

[7] J. T. Beale and A. T. Layton, On the accuracy of finite difference methods for elliptic problems with interfaces, *Commun. Appl. Math. Comput. Sci.,* **1** (2006), 91–119.

[8] M. J. Berger and J. Oliger, Adaptive mesh refinement for hyperbolic partial differential equations, *J. Comp. Physics,* **53** (1984) 484–512.

[9] M. J. Berger, Local adaptive mesh refinement for shock hydrodynamics, *J. Comp. Physics,* **82** (1989) 64–84.

[10] M. J. Berger and R. J. LeVeque, Adaptive mesh refinement using wave-propagation algorithms for hyperbolic systems, *SIAM J. Numer. Anal.,* **35** (1998) 2298–2316.

[11] G. Beylkin, On the Fast Fourier Transform of functions with singularities, *Applied and Comp. Harmonic Anal.,* **2** (1995) 363–381.

[12] M. Bohner and A. Peterson, *Dynamic Equations on Time Scales: An Introduction with Applications*, Birkhäuser, Boston and Berlin, 2001.

[13] M. Bohner and A. Peterson, *Advances in Dynamic Equations on Time Scales*, Birkhäuser, Boston and Berlin, 2003.

[14] D. L. Brown, A note on the numerical solution of the wave equation with piecewise smooth coefficients, *Math. Comput.* **42** (1984), 369–391.

[15] C. G. Broyden, A Class of Methods for Solving Nonlinear Simultaneous Equations, *Math. Comput.* **19** (1965), 577–593.

[16] W. S. C. Chang, *Principles of Lasers and Optics,* Cambridge University Press, 2005

[17] K. H. Craig, Propagation modelling in the troposphere: parabolic equation technique, *Electronics Letters,* **24** (1988) 1136–1139.

[18] C. de Boor, Good approximation by splines with variable knots II, *Conf. on the Numerical Solution of Differential Equations, Lecture Notes in Math. 363,* Springer-Verlag, Berlin, 1973, 12–20.

[19] E. A. Dorfi and L. O'C. Drury, Simple adaptive grids for 1-D initial value problems, *J. Comp. Physics,* **69** (1987) 175–195.

[20] P. W. Eloe, S. Hilger and Q. Sheng, A qualitative analysis on nonconstant graininess of the adaptive grid via time scales, *Rocky Mountain J. Math.,* in press.

[21] H. J. Eom, *Electromagnetic Wave Theory for Boundary-Value Problems - An Advanced Course on Analytical Methods,* Springer-Verlag, Berlin Heidelberg, 2004.

[22] B. G. Ersland, M.S. Espedal, R. Nybo, Numerical methods for flow in a porous medium with internal boundaries, *Comp. Geosciences,* **2** (1998) 217-240.

[23] G. X. Fan, Q. H. Lui, Fast Fourier transform of functions with jump discontinuities, *Antennas and Propagation Soc. Intl. Symp.,* **1** (2000) 148-151.

[24] M. Farrashkhalvat and J. P. Miles, *Basic structured grid generation with an introduction to unstructured grid generation,* Butterworth-Heinemann, Oxford, 2003.

[25] B. Fornberg and R. Meyer-Spasche, A finite difference procedure for a class of free boundary problems, *J. Comp. Physics,* **102** (1992) 72–77.

[26] G. T. Gilbert, Positive definite matrices and Sylvester's Criterion, *Amer. Math. Monthly,* **98** (1991) 44–46.

[27] G. D. Gillen and S. Guha, Modeling and propagation of near-field diffraction patterns: a more complete approach, *Amer. J. Phys.,* **72** (2004), 1195-1201.

[28] L. Gonzalez, S. Guha, J. W. Rogers and Q. Sheng, An interface adaptive method for light beam propagation simulations, Submitted, 2007.

[29] J. W. Goodman, *Introduction to Fourier Optics,* Third Edition, Roberts&Company Publishers, Denver, 2004

[30] S. Guha, Validity of the paraxial approximation in the focal region of a small-f-number lens, *Optical Lett.,* **26** (2001), 1598-1600.

[31] S. Guha and G. D. Gillen, Description of light propagation through a circular aperture using non-paraxial vector diffraction theory, *Optics Express,* **13** (2005), 1424-1447.

[32] S. Guha, L. P. Gonzalez and Q. Sheng, Description of light focusing by a spherical lens using diffraction integral method, *Proc. Appl. Math. Mech.,* **7** (2007), 1086-1088.

[33] E. Haber, U. M. Ascher, Fast finite volume simulation of 3D electromagnetic problems with highly discontinuous coefficients, *J. Sci. Comput.,* **22** (2001), 1943-1961.

[34] S. Hilger, Analysis on measure chains - a unified approach to continuous and discrete calculus, *Results Math.,* **18** (1990), 18-56.

[35] H. H. Hopkins, Canonical and real-space coordinates used in the theory of image formation, *Applied Optics and Optical Engineering,* **IX** Academic Press, New York, 1983

[36] R. A. Horn and C. R. Johnson, *Matrix Analysis,* Cambridge University Press, 1985

[37] R. A. Horn and C. R. Johnson, *Topics in Matrix Analysis,* Cambridge University Press, 1991

[38] W. M. Kays, B. Weigand, M. E. Crawford, *Convective Heat and Mass Transfer,* 4th Ed., McGraw-Hill, 2004

[39] P. Knupp and S. Steinberg, *The fundamentals of grid generation,* CRC Press, Boca Raton, 1993

[40] H.-O. Kreiss, N. A. Petersson, An embedded boundary method for the wave equation with discontinuous coefficients, *SIAM J. Sci. Comput.,*, **28** (2006) 2054–2074

[41] E. Larsson, A domain decomposition method for the Helmholtz equation in a multilayer domain, *SIAM J. Sci. Comput.,* **20** (1999) 1713-1731.

[42] P. D. Lax and R. D. Richtmeyer, Survey of the stability of linear finite difference equations, *Comm. Pure Appl. Math,* **9** (1956) 267–294.

[43] R. J. LeVeque and Z. Li, The immersed interface method for elliptic equations with discontinuous coefficients and singular sources, *SIAM J. Num. Anal.,* **31** (1994), 1019–1044.

[44] Z. Li, Immersed interface methods for moving interface problems, *Num. Algorithms,* **14** (1997), 269–293.

[45] Z. Li, An overview of the immersed interface method and its applications, *Taiwanese J. Math.,* **7** (2003), 1–49.

[46] Z. Li, *The Immersed Interface Method – A Numerical Approach for Partial Differential Equations with Interfaces,* Ph.D. thesis, University of Washington, 1994.

[47] R. J. MacKinnon and G. F. Carey, Analysis of material interface discontinuities and superconvergent fluxes in finite difference theory, *J. Comp. Physics,* **75** (1988) 151–167.

[48] A. Mayo, The fast solution of Poisson's and the biharmonic equations on irregular regions, *J. Num. Anal.* **21** No. 2 (1984) 285-299.

[49] A. Mayo and A. Greenbaum, Fast parallel iterative solution of Poisson's and the biharmonic equations on irregular regions, *J. Sci. Stat. Comput.* **21** No. 1 (1992) 101-118.

[50] K. W. Morton and D. F. Mayers, *Numerical Solution of Partial Differential Equations,* 2nd Edition, Cambridge University Press, 2005, Cambridge

[51] K. W. Morton, Stability of finite difference approximations to a diffusion-convection equation, *Int. J. Num. Meth. Eng.,* **15** (1980), 677–683.

[52] U. M. Özkan, M. Z. Sarikaya and H. Yildirim, Extensions of certain inequalities on time scales, *Appl. Math. Lett.,* to appear.

[53] C. S. Peskin, Numerical analysis of blood flow in the heart, *J. Comp. Physics,* **25** (1977) 220–252.

[54] T. Poon and T. Kim, *Engineering Optics with Matlab,* World Scientific Publishing, 2006, Singapore

[55] J. W. Rogers, Jr. and Q. Sheng, Notes on the diamond-α dynamic derivative on time scales, *J. Math. Anal. Appl.,* **326** (2007), 228-241.

[56] M. N. O. Sadiku, *Numerical Techniques in Electromagnetics,* 2nd Edition, CRC Press, 2001

[57] B. E. A. Saleh and M. C. Teich, *Fundamentals of Photonics,* John Wiley & Sons, 1991.

[58] Q. Sheng, A view of dynamic derivatives on time scales from approximations, *J. Difference Eqn. Appl.,* **11** (2005) 63–82.

[59] Q. Sheng, A second view of dynamic derivatives on time scales from approximations, preprint.

[60] Q. Sheng, A paradoxical consistency between dynamic and conventional derivatives on hybrid grids, *Comm. Numer. Math.,* (2007), in press.

[61] Q. Sheng and H. Cheng, An adaptive grid method for degenerate semilinear quenching problems, *Computers Math. Appl.,* **39** (2000), 57–71.

[62] Q. Sheng, S. Guha and L. Gonzalez, Fast computer simulations of the Helmhloltz equation solutions in multi-layer medians with high wavenumbers, *Technical Report,* AFRL/MLPJ-0804 (2006).

[63] Q. Sheng, M. Fadag, J. Henderson and J. M. Davis, An exploration of combined dynamic derivatives on time scales and their applications, *Nonlinear Anal.,* **7** (2006), 395–413.

[64] Q. Sheng and A. Khaliq, Modified arc-length adaptive algorithms for degenerate reaction-diffusion equations, *Appl. Math. Comput.,* **126** (2002), 279-297.

[65] Q. Sheng, A. Khaliq and D. Voss, Numerical simulation of two-dimensional sine-Gordon solitons via a split cosine scheme, *Math. Comput. Simulations,* **68** (2005), 947–956.

[66] J. Shibayama, K. Matsubara M. Sekiguchi, J. Yamauchi and H. Nakano, Efficient nonuniform schemes for paraxial and wide-angle finite-difference beam propagation methods, *J. Lightwave. Tech.,* **17** (1999), 677-683.

[67] G. D. Smith, *Numerical Solution of Partial Differential Equations: Finite Difference Methods,* Oxford University Press, Oxford, 1990.

[68] G. P. Srivastava, Broyden's method for self-consistent field convergence acceleration, *J. Phys. A.* **17** (1984), L/317-321.

[69] J. C. Strikwerda, *Finite Difference Schemes and Partial Differential Equations,* SIAM, Philadelphia, 2004.

[70] V. Thomée, From finite differences to finite elements A short history of numerical analysis of partial differential equations, *J. of Comp. and Appl. Math.,* **128** (2001) 1-54

[71] J. F. Thompson, Z.U.A. Warsi, and C.W. Mastin, *Numerical Grid Generation,* North-Holland, New York, 1985.

[72] A. N. Tikhonov and A. A. Samarskii, Homogeneous difference schemes, *USSR Comp. Math. and Math. Phys.* **1** (1961) 5-63.

[73] W. T. Welford, *Useful Optics,* The University of Chicago Press, Chicago, 1991

[74] J. Yamauchi, J. Shibayama, and H. Nakano, Modified finite-difference beam propagation method based on the generalized Douglas scheme for variable coefficients, *IEEE Photon. Tech. Lett.,* **7** (1995), 661-663.

[75] J. Yamauchi, J. Shibayama, O. Saito, O. Uchiyama and H. Nakano, Improved finite-difference beam-propagation method based on the generalized Douglas scheme and its application to semivectorial analysis, *J. Lightwave. Tech.,* **14** (1996), 2401-2406.

[76] N. K. Yamaleev and M. H. Carpenter, On accuracy of adaptive grid methods for captured shocks, *J. Comp. Physics,* **181** (2002) 280–316.

[77] K. S. Yee, Numerical solution of initial boundary value problems involving Maxwell's Equations in isotropic media, *IEEE Trans. Antennas and Propagation,* **14** (1966) 302–307.

[78] C. Zhang, *Immersed Interface Methods for Hyperbolic Systems of Partial Differential Equations with Discontinuous Coeffcients,* Ph.D. thesis, University of Washington, 1996.